



UNIVERSIDADE ESTADUAL DE CAMPINAS

INSTITUTO DE BIOLOGIA

HELOÍSA MONTEIRO DO AMARAL PRADO

CHARACTERIZING THE INTERACTOME OF THE RNA-  
BINDING PROTEIN BICC1

CARACTERIZAÇÃO DO INTERACTOMA DA PROTEÍNA DE  
LIGAÇÃO A RNA BICC1

CAMPINAS  
2023

**HELOÍSA MONTEIRO DO AMARAL PRADO**

**CHARACTERIZING THE INTERACTOME OF THE RNA-BINDING  
PROTEIN BICC1**

**CARACTERIZAÇÃO DO INTERACTOMA DA PROTEÍNA DE  
LIGAÇÃO A RNA BICC1**

*Dissertação apresentada ao  
Instituto de Biologia da Universidade  
Estadual de Campinas como parte dos  
requisitos exigidos para a obtenção do  
Título de Mestra em Genética e Biologia  
Molecular, na área de Genética Animal e  
Evolução.*

*Dissertation presented to the  
Institute of Biology of the State University of  
Campinas in partial fulfillment of the  
requirements for the degree of Master in  
Genetics and Molecular Biology, in the area  
of Genetics and Animal Evolution.*

*Orientadora: Prof<sup>ª</sup>. Dr<sup>ª</sup>. Katlin Brauer Massirer*

ESTE ARQUIVO DIGITAL  
CORRESPONDE À VERSÃO FINAL DA  
DISSERTAÇÃO DEFENDIDA PELA ALUNA HELOÍSA  
MONTEIRO DO AMARAL PRADO E ORIENTADA  
PELA PROF<sup>ª</sup>. DR<sup>ª</sup>. KATLIN BRAUER MASSIRER.

Ficha catalográfica  
Universidade Estadual de Campinas  
Biblioteca do Instituto de Biologia  
Mara Janaina de Oliveira - CRB 8/6972

Am13c Amaral-Prado, Heloísa Monteiro, 07/1-  
Characterizing the Interactome of the RNA-binding protein BICC1 / Heloísa Monteiro do Amaral Prado. – Campinas, SP : [s.n.], 2023.

Orientador: Katlin Brauer Massirer.  
Dissertação (mestrado) – Universidade Estadual de Campinas, Instituto de Biologia.

1. Interatoma. 2. Proteína bicaudal C homóloga 1. 3. RNA. 4. Splicing de RNA. 5. Condensados biomoleculares. I. Massirer, Katlin Brauer, 1975-. II. Universidade Estadual de Campinas. Instituto de Biologia. III. Título.

Informações Complementares

**Título em outro idioma:** Caracterização do interactoma da proteína de ligação a RNA BICC1

**Palavras-chave em inglês:**

Interactome

Protein bicaudal C homolog 1

RNA

RNA splicing

Biomolecular condensates

**Área de concentração:** Genética Animal e Evolução

**Titulação:** Mestra em Genética e Biologia Molecular

**Banca examinadora:**

Katlin Brauer Massirer [Orientador]

Aline Mara dos Santos

Ivan Rosa e Silva

**Data de defesa:** 22-11-2023

**Programa de Pós-Graduação:** Genética e Biologia Molecular

**Identificação e informações acadêmicas do(a) aluno(a)**

- ORCID do autor: <https://orcid.org/0000-0001-6324-0579>

- Currículo Lattes do autor: <http://lattes.cnpq.br/7680266883667931>

Campinas, 22 de novembro de 2023

**COMISSÃO EXAMINADORA**

**Prof<sup>a</sup>. Dr<sup>a</sup>. Katlin Brauer Massirer (orientadora)**

**Prof<sup>a</sup>. Dr<sup>a</sup>. Aline Mara dos Santos**

**Prof. Dr. Ivan Rosa e Silva**

A Ata da defesa com as respectivas assinaturas dos membros encontra-se no SIGA/Sistema de Fluxo de Dissertação/Tese e na Secretaria do Programa de Pós-Graduação em Genética e Biologia Molecular do Instituto de Biologia da Universidade Estadual de Campinas.



## **Dedicatória**

Aos meus pais. Sem o amor e carinho deles por mim, nada teria feito sentido durante esse período.

# Agradecimentos

Agradeço a Deus pela vida que me deu e pelas oportunidades que tem me dado ao longo de meu caminhar.

À minha orientadora, Dra. Katlin Brauer Massirer, por acreditar em mim, ter me dado a oportunidade de realizar esse estudo, aberto as portas de seu laboratório para mim e por ter me passado tanto conhecimento.

Ao Prof. Dr. Mario Henrique Bengston por todos os conselhos, auxílio na execução de experimentos e por ter permitido eu realizar parte de meus experimentos em seu laboratório.

À Fundação de Amparo à Pesquisa do Estado de São Paulo (processo nº 21/04867-5, Fundação de Amparo à Pesquisa do Estado de São Paulo (FAPESP)) e ao Conselho Nacional de Desenvolvimento Científico e Tecnológico (CNPq) pela concessão de bolsas de estudo e apoio financeiro para realização desse projeto.

Agradeço também à CAPES. O presente trabalho foi realizado com apoio da Coordenação de Aperfeiçoamento de Pessoal de Nível Superior - Brasil (CAPES) - Código de Financiamento 001.

Aos meus pais, Fernanda e Emídio, e minha irmã, Gabriela, por sempre me incentivarem nos estudos desde muito pequena e não medirem esforços para cuidar de mim e me proporcionar o melhor.

Ao meu namorado, Luciano, por todo apoio emocional, companheirismo e auxílios na parte computacional. Obrigada por sempre estar presente em minha vida, me apoiar e incentivar, e por ser essa pessoa tão gentil e amável.

Aos meus colegas de laboratório do Centro de Química Medicinal e Centro de Biologia Molecular e Engenharia Genética, por todas as conversas, desabafos, risadas, e auxílios científicos. Em especial, gostaria de agradecer a minha primeira parceira de bancada em laboratório, Gabriela Alves, por todos seus ensinamentos, conselhos, e paciência comigo, e ao Guilherme Barbosa pelos auxílios com os experimentos de imunofluorescência e microscopia.

Aos meus colegas da Unicamp que tocam percussão comigo na bateria, por terem feito minhas semanas mais leves, alegres e cheias de ritmo.

Ao Professor Fernando Moreira Simabuco pelos conselhos experimentais dados durante a minha banca de qualificação e por ter cedido gentilmente as alíquotas de anticorpos para a execução de experimentos fundamentais para este estudo. A Professora Adriana Franco Paes Leme pelos conselhos experimentais fornecidos também durante minha banca de qualificação. Aos professores Ivan Rosa e Silva e Aline Mara dos Santos, que foram da minha banca de defesa do Mestrado, pelos conselhos e correções finais do projeto.

Gostaria também de agradecer à equipe de Proteômica da Fiocruz Paraná - Instituto Carlos Chagas que preparou as amostras para análise de espectrometria de massas e executou a análise dos dados brutos da espectrometria de massas, e à equipe de Biologia Celular e Genômica do Laboratório Central de Tecnologias de Alto Desempenho em Ciências da Vida (LaCTAD), parte da Universidade Estadual de Campinas (UNICAMP), pelas contribuições nas etapas de sequenciamento, microscopia confocal e citometria de fluxo.

Por fim, agradeço o acesso aos equipamentos e assistência do Instituto Nacional de Ciência e Tecnologia em Fotônica Aplicada à Biologia Celular (INFABIC) da Universidade Estadual de Campinas; O INFABIC é cofinanciado pela Fundação de Amparo à Pesquisa do Estado de São Paulo (FAPESP) (2014/50938-8) e pelo Conselho Nacional de Desenvolvimento Científico e Tecnológico (CNPq) (465699/2014-6).

## RESUMO

Bicaudal C Homóloga 1 (BICC1) é uma proteína de ligação a RNA (RBP) conservada em diversos organismos e, neste estudo, a proteína humana BICC1 foi investigada. Estudos iniciais mostraram que mutações em BICC1 estão associadas com a doença do rim policístico e que a via de sinalização de Wnt/ $\beta$ -catenina é hiperativada quando BICC1 está ausente ou mutada em camundongos. Pesquisas também apontam a desregulação da expressão de BICC1 em diferentes tipos de câncer, como a sua maior expressão em câncer gástrico e pancreático. Estruturalmente, essa RBP é composta por três domínios do tipo KH (K homólogos) em sua porção N-terminal, que são importantes para a ligação com RNAs mensageiros. Em sua porção C-terminal, há o domínio SAM (motivo alfa estéril), que é principalmente envolvido com interações proteína-proteína, polimerização proteica, localização de RNAs mensageiros, e importante para localização de BICC1 em corpos de processamento de RNA. Este estudo teve como principal objetivo caracterizar o interactoma de BICC1 na dependência de RNA e do domínio SAM, resultando na seleção e validação de proteínas parceiras de BICC1 e, portanto, contribuindo para a descoberta de novos processos biológicos em que BICC1 pode ter um papel regulador. Ensaios celulares foram conduzidos em linhagem celular HEK293T, que foi submetida a superexpressão das construções de BICC1, as quais incluí a construção de BICC1 em seu comprimento total, bem como com o domínio SAM deletado, e do gene GFP, como controle experimental. De acordo com as análises de interação proteína-proteína e anotações de ontologia genética, processos biológicos relacionados com splicing e componentes celulares relacionados com o complexo de metilação e condensados biomoleculares (como corpos cajais, corpos-P e grânulos de estresse) foram enriquecidos. A interação de BICC1 com algumas proteínas (PRMT5, STK38, IGF2BP1 e PARP1) foi confirmada por ensaios complementares (western blotting e imunofluorescência), entre as quais a interação com a proteína IGF2BP1 foi identificada como dependente de RNA. Em resumo, este estudo contribuiu para a caracterização do interactoma proteico de BICC1, identificando novas proteínas parceiras de BICC1 e processos biológicos relacionados com a expressão de BICC1 na células, como o splicing e a regulação de condensados biomoleculares.

**Palavras-chave:** Interactoma, BICC1, RNA, splicing, condensados biomoleculares.

## ABSTRACT

Bicaudal C Homolog 1 (BICC1) is a conserved RNA-binding protein (RBP) found in diverse organisms, and in this study, the human BICC1 protein was investigated. Initial studies revealed that mutations in BICC1 are associated with polycystic kidney disease and that the Wnt/ $\beta$ -catenin signaling pathway is hyperactivated when BICC1 is absent or mutated in mice. Research also indicates the dysregulation of BICC1 expression in different types of cancer, such as high expression in gastric and pancreatic cancer. Structurally, this RBP is composed of three KH (K homology) domains in the N-terminal portion that are important for mRNA binding. In its C-terminal region, there is a SAM domain (sterile alpha motif), mainly involved in protein-protein interactions, protein polymerization, localization of target mRNAs, and important for the localization of BICC1 in RNA processing bodies. This study had as main objective to characterize the BICC1 interactome in RNA and SAM domain dependence, resulting in the selection and validation of BICC1 protein partners, thus contributing to the discovery of new biological processes in which BICC1 may play a regulatory role. Cellular assays were conducted in HEK293T cell line subjected to overexpression of BICC1 constructs, including full-length, BICC1 with SAM domain deletion, and GFP gene as an experimental control. According to protein-protein interaction analyses and genetic ontology annotation, biological processes related to splicing and cellular components related to the methylosome complex and biomolecular condensates (such as Cajal bodies, P-bodies, and stress granules) were enriched. The interaction of BICC1 with some proteins (PRMT5, STK38, IGF2BP1, and PARP1) was confirmed by complementary assays (western blotting and immunofluorescence), among which the interaction with IGF2BP1 was identified as RNA-dependent. In summary, this study contributed to the characterization of the BICC1 protein interactome, identifying new BICC1 protein partners and biological processes related to BICC1 expression in the cell, such as splicing and regulation of biomolecular condensates.

**Keywords:** Interactome, BICC1, RNA, splicing, biomolecular condensates.

## FIGURES SUMMARY

Figure 1.....	17
Figure 2.....	18
Figure 3.....	20
Figure 4.....	21
Figure 5.....	24
Figure 6.....	25
Figure 7.....	32
Figure 8.....	34
Figure 9.....	38
Figure 10.....	39
Figure 11.....	40
Figure 12.....	40
Figure 13.....	41
Figure 14.....	42
Figure 15.....	46
Figure 16.....	47
Figure 17.....	49
Figure 18.....	51
Figure 19.....	53
Figure 20.....	54
Figure 21.....	56
Figure 22.....	57
Figure 23.....	58
Figure 24.....	59
Figure 25.....	60
Figure 26.....	63
Figure 27.....	70

## TABLE SUMMARY

Table 1.....	29
Table 2.....	35
Table 3.....	44
Table 4.....	60

## **ABBREVIATION LIST**

(+) – Treatment with RNase A

(-) – No treatment with RNase A

BICC1 – Bicaudal C Homolog 1

CCT2 – T-complex protein 1 subunit beta

Co-IP-MS – Co-immunoprecipitation followed by mass spectrometry

CSD – cold shock domain

DAPI – 4',6-diamidino-2-phenylindole

dsRBD - Double-stranded RNA-binding domain

Dvl – Dishevelled

FL – Construct of the full-length sequence of BICC1 in pcDNA.3.1 vector backbone

Fzd –Frizzled receptor

GFP – Green fluorescent protein

GO – Gene ontology

GSK3- $\beta$  – Glycogen synthase kinase-3

HEK293T – Human embryonic kidney cell line

IGF2BP1 – Insulin-like growth factor 2 mRNA-binding protein 1

IF – Immunofluorescence

KH – K-homology domain

LLPS – Liquid-liquid phase separation

LRP – Lipoprotein receptor-related protein

miR-17 – microRNA 17



MLO – Membrane-less organelles

MS – Mass spectrometry

P-body – RNA-processing bodies

PARP1 – Poly [ADP-ribose] polymerase 1

PAZ - Piwi/Argonaute/Zwille domain

PC – Pearson’s correlation

PKD – Polycystic kidney disease

PKD2 – Polycystin 2

PPI – Protein-protein interaction

PPIN – Protein-protein interaction network

PRMT5 – Protein arginine methyltransferase 5

PRMTs – Protein arginine methyltransferases

PTM - Post-translational modifications

RBD – RNA-binding domain

RBP – RNA-binding protein

RGG – Glycine-arginine-rich (GAR) domain

RRM – RNA-recognition motif

RT – Room temperature

SAM – Sterile alpha motif domain

SDMA – Monomethylarginine and/or symmetric dimethylarginine

SG – Stress granules

STK38 – Serine/threonine kinase 38

TCF – T-cell factors

WDR77 – Methylosome protein WDR77

Wnt – Wingless-related integration site

WB – Western blotting

ZF – Zinc fingers

$\Delta$ SAM – Deletion of the sterile alpha motif domain

## SUMMARY

1. INTRODUCTION .....	17
1.1. RNA-BINDING PROTEINS (RBPs) .....	17
1.2. THE RBP BICAUDAL C-HOMOLOG 1 (BICC1) .....	19
1.3. EXPLORING THE PROTEIN INTERACTOME OF BICC1 .....	22
1.4. THE PRMT5 METHYLOSOME COMPLEX .....	23
2. OBJECTIVES .....	26
2.1. GENERAL OBJECTIVE .....	26
2.2. SPECIFIC OBJECTIVES .....	26
3. DETAILED METHODOLOGIES .....	27
3.1. CELL CULTURE .....	27
3.2. PLASMID CONSTRUCTS AND DNA PURIFICATION .....	27
3.4. WESTERN BLOTTING .....	28
3.5. SILVER NITRATE IMPREGNATION OF PROTEINS IN POLYACRYLAMIDE GELS .....	30
3.6. PROTEOMIC ANALYSIS .....	30
3.6.1. CO-IMMUNOPRECIPITATION FOR MASS SPECTROMETRY (MS) ANALYSES AND WESTERN BLOTTING .....	30
3.6.2. SAMPLES DIGESTION WITH TRYPSIN .....	32
3.6.3. SAMPLES DESALTING AND PEPTIDES PURIFICATION .....	32
3.6.4. LIQUID CHROMATOGRAPHY AND MASS SPECTROMETRY ANALYSES (LC-MS/MS) .....	33
3.7. BIOINFORMATIC ANALYSES .....	33
3.8. IMMUNOFLUORESCENCE .....	34
3.9. IMAGES PROCESSING AND CALCULATION OF CO- LOCALIZATION COEFFICIENT .....	36
3.10. CELL VIABILITY AND CYTOTOXICITY .....	36
3.11. REPORTER GENE OF WNT- $\beta$ CATENIN SIGNALING PATHWAY .....	37
3.12. REPLICATES AND STATISTICAL ANALYSIS .....	37
4. RESULTS .....	38
4.1. CONFIRMATION OF THE BICC1 RECOMBINANT VECTORS OVEREXPRESSION IN HEK293T HUMAN CELLS .....	38
4.2. INTERACTOME DETERMINATION BY CO- IMMUNOPRECIPITATION FOLLOWED BY MASS SPECTROMETRY (CO-IP-MS) .....	39
4.3. PROTEIN-PROTEIN INTERACTION NETWORKS (PPIN) OF BICC1 INTERACTOME SHOWS ENRICHMENT OF SPLICING, METHYLOSOME AND INTRACELLULAR MEMBRANELLER ORGANELLES PROTEINS .....	44

4.4. CONFIRMATION THAT BICC1-FLAG CO-IMMUNOPRECIPITATES WITH PRMT5, IGF2BP1, PARP1 AND STK38 THROUGH WESTERN BLOTTING ...	50
4.5. INVESTIGATION OF CELLULAR LOCALIZATION OF BICC1 WITH PROTEIN PARTNERS VALIDATED BY CO-IP-MS AND CO-IP-WB .....	52
4.5.1. <i>BICC1</i> ANTIBODY EFFICIENCY FOR IF AND IDENTIFICATION OF STRUCTURES LIKE BIOMOLECULAR CONDENSATES WHEN <i>BICC1</i> WAS OVEREXPRESSED: .....	52
4.5.2. <i>BICC1</i> AND PRMT5 CELLULAR LOCALIZATION: .....	53
4.5.3. <i>BICC1</i> AND PARP1 CELLULAR LOCALIZATION: .....	55
4.6. CONFIRMATION OF PRMT5 RECOMBINANT VECTOR OVEREXPRESSION AND PRMT5 INHIBITION COMPOUNDS ACTIVITY IN HEK293T CELLS .....	57
4.7. INVESTIGATION OF METHYLATION SITES IN BICC1 CO-IMMUNOPRECIPITATED IN CONDITIONS OF PRMT5 INHIBITION WITH GSK591 .....	59
4.8. INVESTIGATION OF THE CANONICAL WNT/ $\beta$ -CATENIN SIGNALING ACTIVITY IN CONDITIONS OF PRMT5 INHIBITION WITH GSK591 AND PRMT5 OVEREXPRESSED TOGETHER WITH BICC1 CONSTRUCTS (FL AND $\Delta$ SAM) .....	61
5. DISCUSSION AND PERSPECTIVES .....	64
6. CONCLUSIONS .....	71
7. REFERENCES .....	72
ATTACHMENT 1 .....	80
ATTACHMENT 2 .....	82
ATTACHMENT 3 .....	84
ATTACHMENT 4 .....	86
ATTACHMENT 5 .....	88
ATTACHMENT 6 .....	90
ATTACHMENT 7 .....	92
ATTACHMENT 8 .....	95
ATTACHMENT 9 .....	96
ATTACHMENT 10 .....	97
ATTACHMENT 11 .....	98
ATTACHMENT 12 .....	100

## 1. INTRODUCTION

### 1.1. RNA-BINDING PROTEINS (RBPs)

The RNA-binding proteins (RBPs) are a group with more than 2,000 proteins responsible for interacting with the RNA transcripts which drive many cellular processes in RNA regulation (CORLEY; BURNS; YEO, 2020). This protein class guides RNA fate and function in the cell by binding to double or single-stranded RNA and forming ribonucleoprotein particles (RNPs) which are dynamic according to the cellular context (GEBAUER et al., 2021). These proteins have crucial roles in various cellular processes, illustrated in Figure 1, as RNAs post-transcriptional control like export, localization, degradation, stabilization, translation, and alternative splicing (CORLEY; BURNS; YEO, 2020).

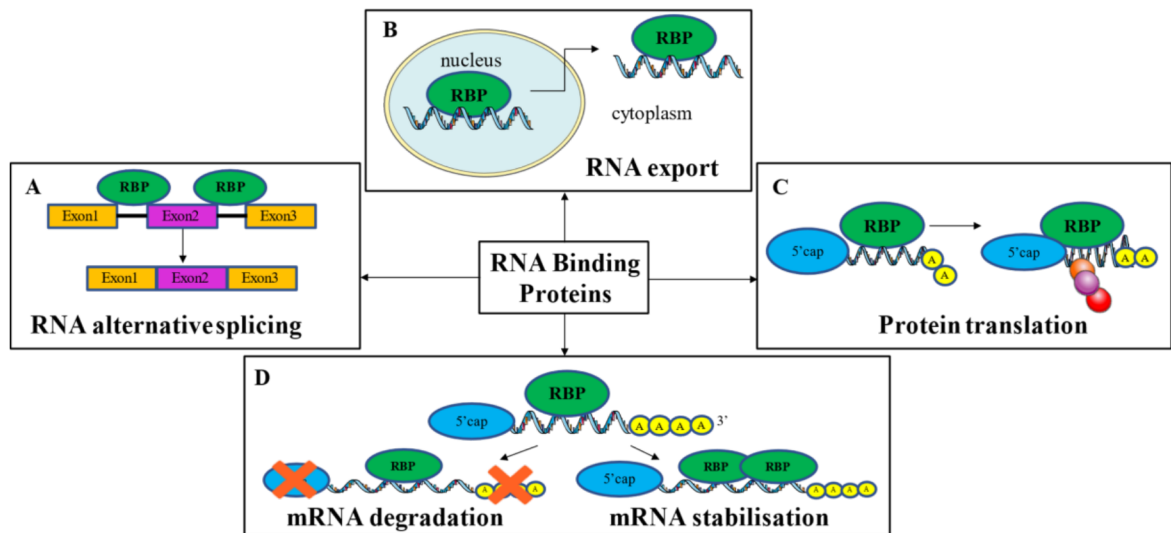


Figure 1. Main post-transcriptional control mechanisms that are controlled by RNA-binding proteins (RBPs). A) RNA alternative splicing (remotion of introns and junction of exons); B) RNA export from nucleus to cytoplasm; C) Protein translation supporting, and D) mRNA degradation or mRNA stabilisation according to the cellular condition. Figure elaborated by the author.

The RBPs bind to the RNAs through one or more RNA-binding domains (RBDs), which are usually conserved within protein classes (GEBAUER et al., 2021). In the literature is reported that more than 50 different RBDs are characterized in RBPs, which the most common are: KH (K-homology domain); RRM (RNA-recognition motif); CSD (cold shock domain); RGG (glycine-arginine-rich (GAR) domains); ZF (zinc fingers); dsRBD (double-stranded RNA-binding domain), La motif (La) and PAZ (Piwi/Argonaute/Zwille) domain (ZHAO et al., 2022). Figure 2 shows some examples of RBPs with the most common domains.

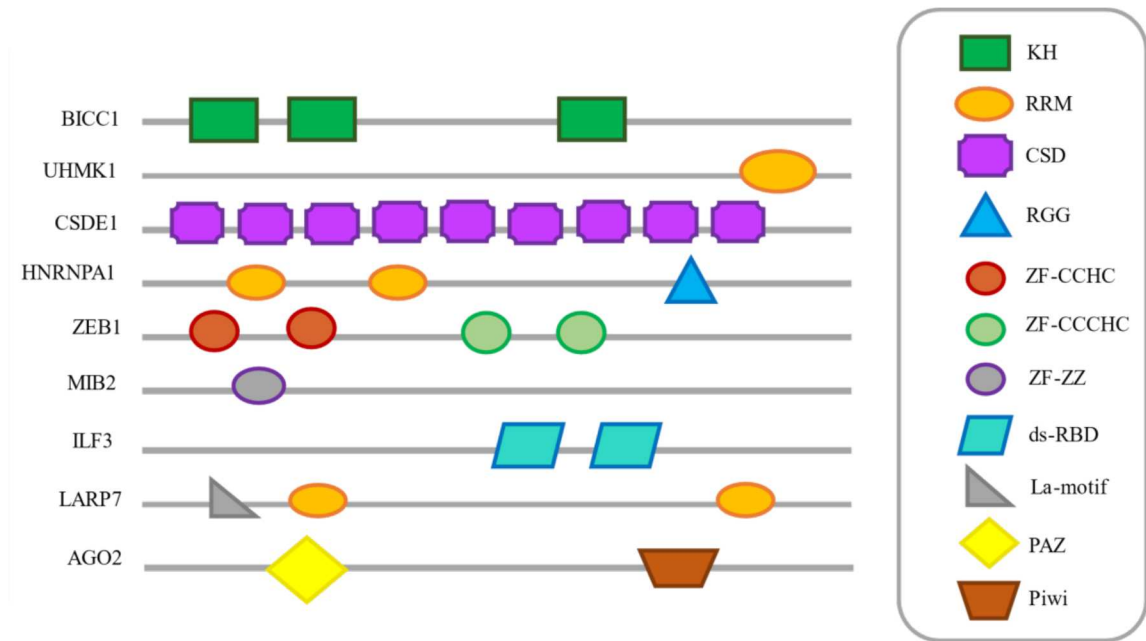


Figure 2. Illustrative and representative examples of different RBDs from different RBPs: RRM (RNA-recognition motif); KH (K-homology domain); CSD (cold shock domain); RGG (glycine-arginine-rich (GAR) domains); ZF (zinc fingers); dsRBD (double-stranded RNA-binding domain); La motif (La); PAZ (Piwi/Argonaute/Zwille) domain, and Piwi domain. Figure elaborated by the author.

Many diseases have been related to functional defects of RBPs and dysregulation in their expression levels, including neurological disorders, muscular atrophy, and cancers (SEUFERT et al., 2021). Studies about tumorigenesis, for example, have shown how this protein class impacts the prognosis and diagnosis of cancer (ZHAO et al., 2022). Neurodegenerative diseases, such as amyotrophic lateral sclerosis (ALS) and frontotemporal dementia (FTD), also have been associated with alterations of RBP expression (STERNBURG; GRUIJS DA SILVA; DORMANN, 2022), as well as polycystic kidney disease (PKD) (SEUFERT et al., 2021). Therefore, it is possible to conclude that this protein class has crucial roles in the cellular activity and development of diseases.

Advancements in new methods in molecular biology integrated with bioinformatics, such as transcriptome-wide experimental and sequencing methods, have allowed the identification of the RBPs and their target mRNAs (STERNBURG; KARGINOV, 2020). This brought new perceptions about the function of many proteins in the regulatory cell process and their roles in disease development (STERNBURG; KARGINOV, 2020). The study of RBPs has been the subject of study in our group and more recently we are focusing on its role as drug targets.

## 1.2. THE RBP BICAUDAL C-HOMOLOG 1 (BICC1)

The Bicaudal C Homolog 1 (BICC1) is an RNA-binding protein conserved between organisms (alignment showed in [Attachment 1](#)), however, is still understudied in the context of disease. The origin of its name is due to mutations of the BicC locus in *Drosophila* that caused phenotypes of mirror image duplications of anterior-posterior structures during the development of these organisms (double-abdomen or “bicaudal” phenotype) (BULL, 1966; DOWDLE et al., 2022). Among mammals, studies started taking place when mutations in this RBP were related to PKD and renal organogenesis in mice and human patients (FU et al., 2010; KRAUS et al., 2012; LIAN et al., 2014). Studies have also been pointing to differential expression levels of BICC1 in cancer, such as the downregulation in samples from patients with glioblastoma (SUN et al., 2021) and upregulation in gastric and pancreatic cancer (MENG et al., 2023; ZHAO et al., 2020), and in neurology, with serum of patients with mood disorders showing differential expression levels of BICC1 (CHEN et al., 2019).

Although the exact mechanisms by which BICC1 contributes to cancer development are not fully understood, its dysregulation in cancer suggests that it may be a potential therapeutic target for the treatment of cancers. In addition, BICC1 could be a biomarker for the determination of different types of mood disorders.

Structurally, BICC1 is composed of three KH domains at the N-terminus with the conserved hallmark “GXXG” loops, important for binding to RNA (VALVERDE; EDWARDS; REGAN, 2008), and two KH-like domains, which lack the “GXXG” motifs, in which the “G” corresponds to glycine and one or both “X” are a positively charged amino acid residue (“R” - arginine, “K” - lysine or “H” - histidine). The KH domains are composed of approximately 70 amino acid residues. In its C-terminus region, there is a sterile alpha motif (SAM domain, displayed using the SMART database ((SCHULTZ et al., 1998), see Figure 3), which has been related to protein-protein interactions, self-association architecture, and even to RNA binding activities (KIM; BOWIE, 2003). The SAM domains are also composed of approximately 70 amino acid residues and this domain class is generally described as important for protein–protein interactions and oligomerization, and even RNA-binding activity and BICC1 recruitment to RNA-processing bodies (P-bodies) (ESTRADA MALLARINO et al., 2020; MAISONNEUVE et al., 2009).

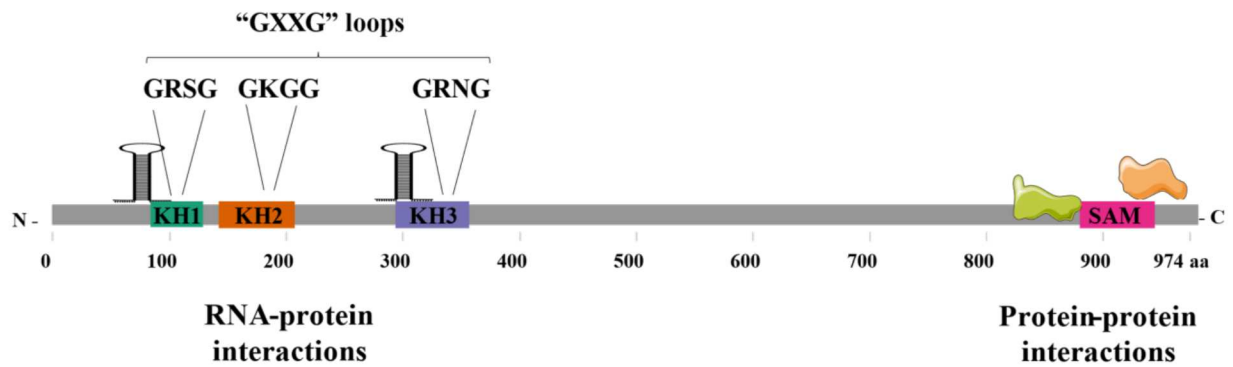


Figure 3. Schematic illustration of the human BICC1 protein (NP\_001073981.1) with its three KH (RNA-binding activity) and SAM (protein-protein interaction) domains identified using the SMART database. Each domain has the respective amino acid residue range position and E-value: KH1 (45-127, E-value: 2.69); KH2 (131-204, E-value: 5.43E-18), KH3 (283-353, E-value: 3.85E-9) and SAM (871-936, E-value: 2.29E-12). Figure elaborated by the author.

Studies have pointed to the importance of the SAM domain for the BICC1 function *in vivo*, being essential for the localization and silencing of target mRNAs (ROTHÉ et al., 2018). The SAM domain is also associated with this negative role of the BICC1 Wnt/ $\beta$ -catenin pathway, which is described as important in cell cytogenesis regulation and embryonic development (DOWDLE et al., 2022; KRAUS et al., 2012), as well as disease development when this pathway is dysregulated (NUSSE; CLEVERS, 2017).

Briefly, the Wnt/ $\beta$ -catenin is a conserved pathway including the Wnt glycoproteins group, responsible for the activation of the cell membrane receptor Frizzled (Fzd) and/or (LRP) 5/6, generating a cascade of signaling that controls the amount of  $\beta$ -catenin protein in the cytoplasm through a proteasome complex formation via phosphorylation of  $\beta$ -catenin (E.g., by the kinase GSK3- $\beta$ ) (PFISTER; KÜHL, 2018). When Wnt proteins are bound to the membrane receptors, the protein Dishevelled (Dvl) is activated and promotes the downstream inactivation of the GSK3- $\beta$  (PFISTER; KÜHL, 2018). This will allow the  $\beta$ -catenin accumulation in the cytoplasm and its translocation to the nucleus, promoting the activation of transcription factors (E.g., T-cell factor (TCF)) responsible for cell growth and proliferation through activation of  $\beta$ -catenin target genes (E.g, PDK1, cMYC, CYCLIN D1, and AXIN- 2) (PFISTER; KÜHL, 2018). Figure 4 shows a schematic illustration of the Wnt/ $\beta$ -catenin signaling pathway in a normal cell.



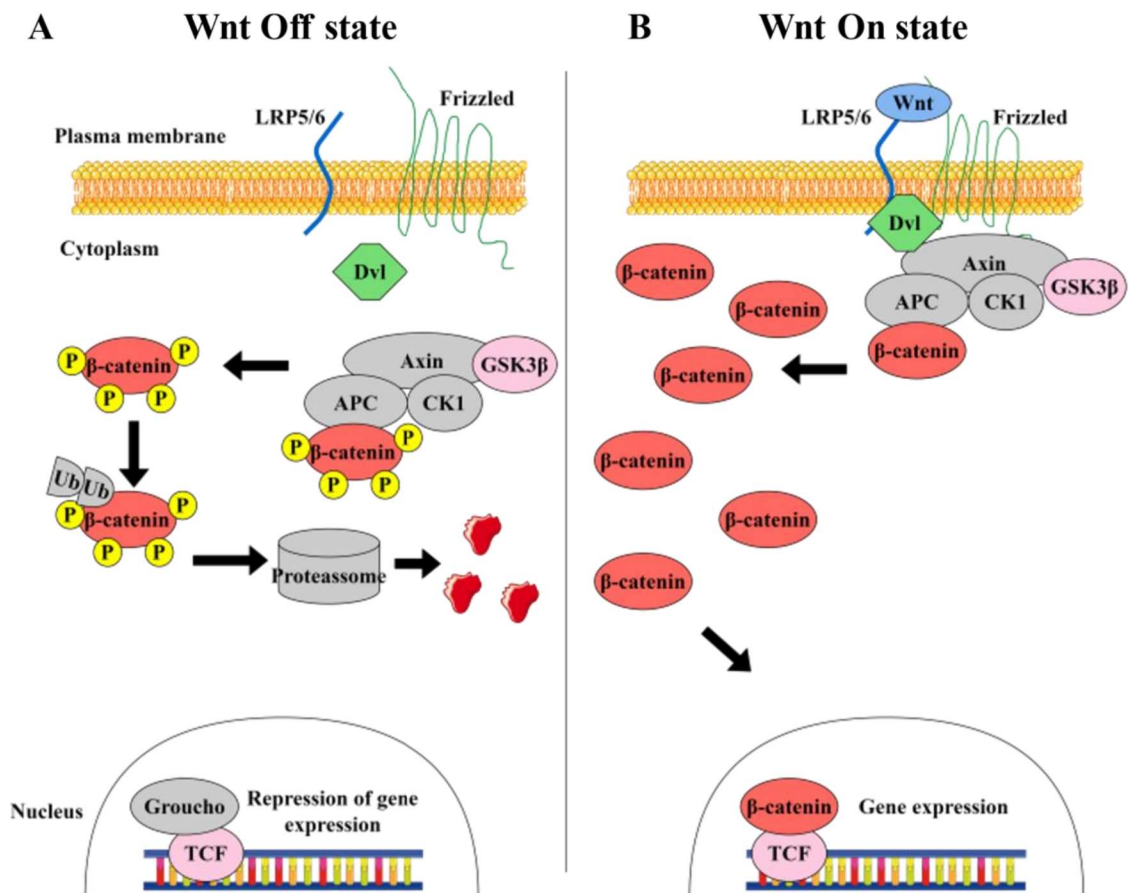


Figure 4. Schematic illustration of the Wnt/β-catenin signaling pathway in a normal cell. A) Wnt off state: β-catenin is phosphorylated by the kinase GSK3β and marked to degradation through a proteasome complex; B) Wnt on state: GSK3β is inhibited by the Dvl protein activation through the signaling cascade of Wnt proteins that were bound to the membrane receptors, and β-catenin is accumulated in the cytoplasm and translocated to the nucleus, promoting the expression of Wnt target genes (E.g, MYC and cyclin D1). Figure elaborated by the author.

The negative regulation of the Wnt pathway by BICC1 was reported at the level of Dishevelled (Dvl), which was sequestered to P-bodies together with BICC1 overexpressed in HEK293T cells, and measured through a luciferase reporter system of the Wnt/β-catenin pathway signaling (KRAUS et al., 2012; MAISONNEUVE et al., 2009), showing a direct role of BICC1 in this pathway.

The role of BICC1 in the development of PKD is already well established. The loss-of-function mutations of this RBP in mice caused similar aspects of the cytogenesis-related disease PKD in Humans, such as fluid-filled cysts and expansion of epithelial ducts, through destabilization of the Pkd2 mRNA (TRAN et al., 2010). According to the literature, PKD2 patients, when compared to patients with PKD1 mutations, have fewer complications of PKD (HATEBOER et al., 1999). However, both conditions of PKD (autosomal dominant polycystic

disease type 1 – *PKD1* mutant, and 2 – *PKD2* mutant), are considered deleterious and cannot be addressed as a benign disease. In addition, the presence of BICC1 in stress granules is reported in a study about ciliopathies, and BICC1 was reported as important to the localization of nephronophthisis family proteins (ANKS3, ANKS6, and INVERSIN) during the induction of stress granules (ESTRADA MALLARINO et al., 2020). The RNA granule database (MILLAR et al., 2023) also shows evidence of BICC1 presence in stress granules and P-bodies, suggesting a role of this RBP in liquid-liquid phase separation (LLPS), which is an important mechanism for cellular compartmentalization (LIU et al., 2023).

In summary, further studies may help to establish BICC1 as a promising therapeutic target for the treatment of PKD, which is a kind of nephronophthisis (WOLF; HILDEBRANDT, 2011), as well as other diseases, such as cancer. Therefore, in this study we proposed to investigate the BICC1 interactome in different conditions (in RNA and SAM domain dependence), aiming to contribute to new insights about BICC1 function in cells.

### 1.3. EXPLORING THE PROTEIN INTERACTOME OF BICC1

Few studies have elucidated the BICC1 protein interactome. To date, BICC1 is well described as a protein partner of ANKS3 and ANKS6 by co-immunoprecipitation in kidney extracts and structural analyses, and this interaction may be important to the cilia signaling pathway (ROTHÉ et al., 2018; STAGNER et al., 2009). In addition, there is no study yet reporting enzymes interacting with BICC1 and post-translationally modifying this RBP, which could be important information for future studies establishing BICC1 as a therapeutic target, since post-translational regions are essential for the expression and localization of proteins in cells (LOVCI; BENGTSON; MASSIRER, 2016).

The development of high-throughput experimental methods, such as yeast two-hybrid screening and mass spectrometry, has enabled the identification and characterization of large-scale protein-protein interactions (PPI) (CHUA; WONG, 2008). The interactome can be visualized as a protein-protein interaction network (PPIN), where each node represents a protein and the edges represent the interactions between them. Network analysis can be used to identify clusters within the network, as well as to predict new protein-protein interactions and functional relationships (DE LAS RIVAS; FONTANILLO, 2010). The STRING is an important platform used to generate PPI that integrates data from other databases, such as BIND, BioGRID, DIP, HPRD, IntAct, and MINT (DE LAS RIVAS; FONTANILLO, 2010). Overall, the protein interactome is a powerful tool for understanding the complexity of cellular processes and

developing new therapeutic strategies for diseases that arise from perturbations in protein-protein interactions.

In this work, **our main aim was to characterize the BICC1 protein interactome.** There are a few described BICC1 protein partners in databases of protein interactions, such as the BioGRID, however, most of these interactors come from high-throughput studies, especially studies about stress granules (SG) formation. **Therefore, a better understanding of the interactome of this RBP will allow the identification of new molecular mechanisms and disease pathways involved with BICC1 expression.** The next section of the introduction will cover the PRMT5 protein, a protein partner of BICC1 that was identified in this present study and the interaction was chosen to be further investigated.

#### 1.4. THE PRMT5 METHYLOSOME COMPLEX

The methylation complex, also known as the methyltransferase complex or methylosome complex, is a protein complex that includes a group of enzymes that add a methyl group to specific molecules in cells (MULVANEY et al., 2021). Methylation is an important post-translational modification that can regulate transcription, protein-protein interactions, protein transport, protein stability, and other processes in cells (LOVCI; BENGTON; MASSIRER, 2016). The methylation complex typically consists of several subunits that work together to recognize target molecules and catalyze the transfer of a methyl group to them (RENGASAMY et al., 2017).

The methylation complex also includes various cofactors and regulators that modulate its activity and specificity. The methylosome complex which includes PRMT5 and MEP50/WDR77 with substrate adaptors (E.g., CLNS1A and RIOK1) is involved in the methylation of arginine residues in many proteins, such as some histones and splicing proteins (ANTONYSAMY et al., 2012a; MULVANEY et al., 2021; PESIRIDIS; DIAMOND; VAN DUYNE, 2009).

PRMT5 (Protein Arginine Methyltransferase 5) is a nuclear and cytoplasmic enzyme that belongs to the family of protein arginine methyltransferases (PRMTs) and is classified as a type II of PRMT. Structurally, it is characterized by the presence of three protein domains: TIM barrel, Rossmann-fold, and  $\beta$ -barrel (SUN et al., 2011) (see illustration in Figure 5). In general, PRMTs exhibit a preference for arginine-glycine (RGG) rich motifs, which are commonly enriched in intrinsically unstructured regions of proteins and implicated in RNA

binding and biomolecular liquid-liquid phase separation (CHONG; VERNON; FORMAN-KAY, 2018).

The enzymatic action of PRMT5 is due to its catalytic action of transferring a methyl group from S-adenosyl-L-methionine (SAM) to the guanidine nitrogen atom of arginine residues in target proteins, resulting in the formation of monomethylarginine and/or symmetric dimethylarginine (SDMA) residues (see illustration in Figure 6) (MOTOLANI et al., 2021). In proteins, the guanidinium side chain of arginine residues carries a positive charge and this side chain can undergo a monomethylation process, which is catalyzed by the type I, II, and III PRMTs enzyme family (SUN et al., 2011). In summary, the methylation of proteins increases the hydrophobicity and the arginine side chains, impacting the interaction between proteins (LI et al., 2021; ZHU et al., 2019)

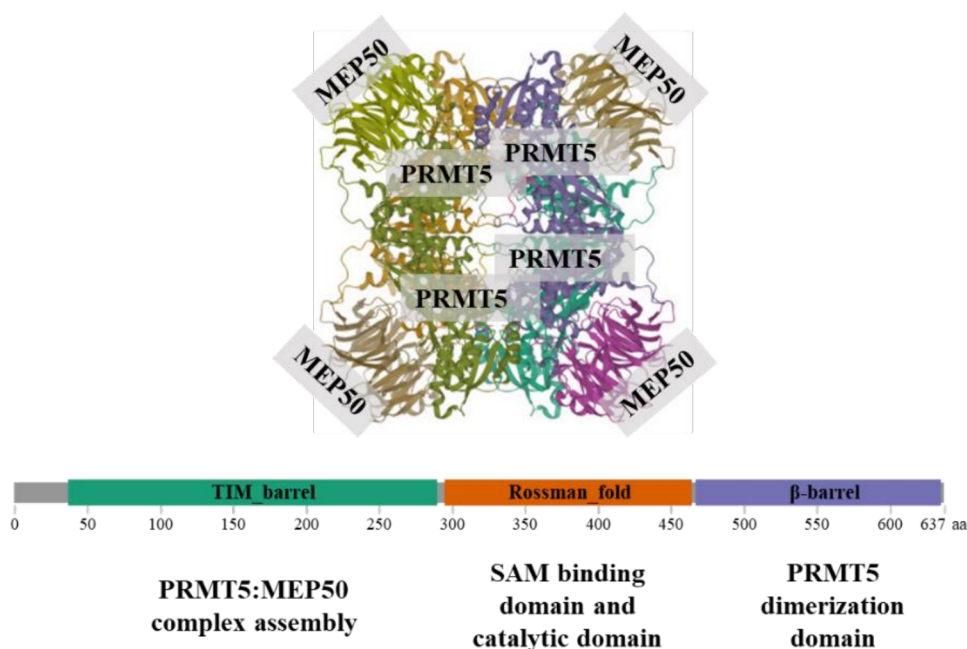


Figure 5. Crystal structure of the human protein arginine methyltransferase 5 (PRMT5) in a heterooctameric complex with the methylosome protein 50 (MEP50), as reported under the Protein Data Bank identification code 4GQB, and schematic illustration of the human PRMT5 protein (NP\_001034708.1) with its three domains identified with SMART database and the respective function (MOTOLANI et al., 2021). Each domain has the respective amino acid residue range position and E-value: TIM barrel (37-290, E-value: 1.1E-79), Rossman fold 295-464, E-value: 1.9E-75) and β-barrel (467-635, E-value: 9.9E-63). Figure elaborated by the author.

PRMT5 is involved in various biological processes, including gene expression regulation, RNA processing, DNA damage response, cell signaling, splicing, and even protein-protein interactions (MOTOLANI et al., 2021). Some of its substrates are histones (E.g., H3R8,

and H4R3), spliceosomal proteins (SmD1 and SmD3), and transcription factors (E.g., SPT5) (BRANSCOMBE et al., 2001; KWAK et al., 2003; PAL; SIF, 2007; SUN et al., 2011). When dysregulated it is also involved in the development and progression of various diseases, such as cancer, neurodegeneration, and viral infections (MOTOLANI et al., 2021).

As a modulator of splicing, PRMT5 leads to SDMA of the spliceosome Sm proteins (SmB, SmB0, SmN, SmD1, SmD2, SmD3, SmE, SmF, and SmG), that are capable of binding small RNAs and to form small nuclear ribonucleoproteins (snRNPs) (LIANG et al., 2021; RATOVITSKI et al., 2015).

There are also studies reporting the methylation by PRMTs (PRMT1 and PRMT5) in the Ras GTPase-activating protein-binding protein (G3BP1), which is an important protein in stress granules formation. The methylation in the G3BP1 was proved to occur in its RGG domain, and the demethylation of G3BP1, through PRMT1 and PRMT5 knockout, was linked to the stress granules assembly (TSAI et al., 2016, 2017).

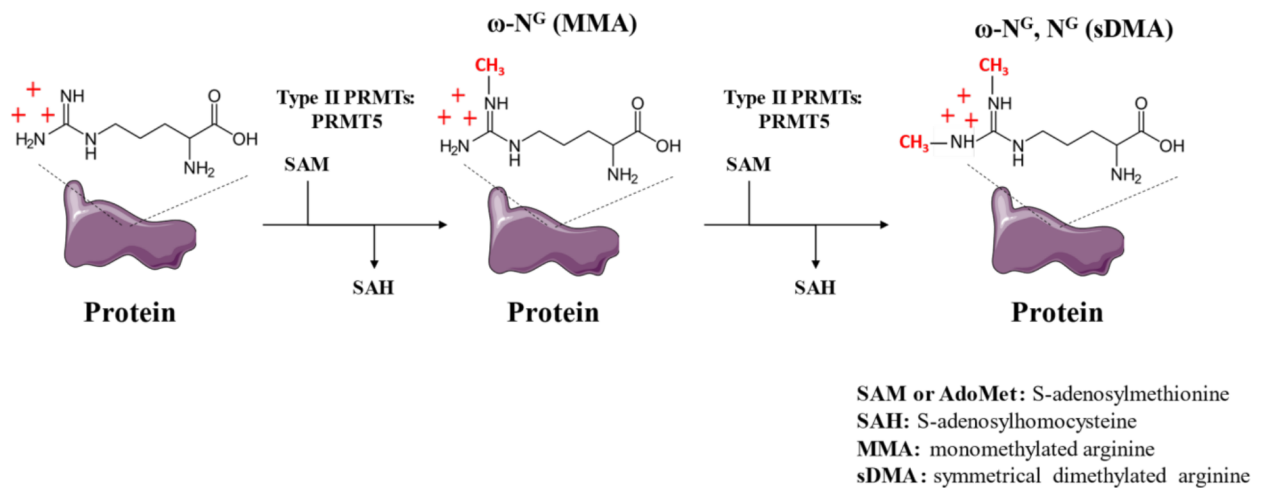


Figure 6. Schematic illustration of the PRMT5 catalytic action of arginine residues mono and di-methylation. Figure elaborated by the author.

Therefore, as PRMT5 was proven in this study co-immunoprecipitating with BICC1 and regulates important processes in the cell, such as splicing and stress granules assembly, PRMT5 was selected to investigate the interaction with BICC1 further, aiming to understand better the cellular mechanisms behind this protein-protein interaction.

## **2. OBJECTIVES**

### **2.1. GENERAL OBJECTIVE**

The present study aimed to characterize the protein interactome of the RNA-binding protein BICC1 to identify new biological processes associated with its expression.

### **2.2. SPECIFIC OBJECTIVES**

- A.** To characterize the BICC1 interactome in dependence on bound mRNAs and in dependence on the protein domain SAM;
- B.** To identify potential biological processes to which BICC1 is associated;
- C.** To select potential BICC1 protein interactors, based on their Gene Ontology (GO) annotation, PPIN analysis, and biological importance;
- D.** To validate BICC1 protein interactors through two different approaches than co-immunoprecipitation followed by mass spectrometry (Co-IP-MS): western blotting and immunofluorescence.

### 3. DETAILED METHODOLOGIES

#### 3.1. CELL CULTURE

The human kidney embryonic cell line HEK293T was chosen as a model for the assays due to its easier manipulation and transfection. The cells were cultured in Dulbecco's Modified Eagle's Media (Thermo Scientific, #11965092) supplemented with 10 % fetal bovine serum (Cultilab, #F063), and 1 % penicillin-streptomycin (Sigma, #P4333). Cells were grown in an incubator with 5 % CO<sub>2</sub> at 37 °C. Subculturing was performed using 0.25 % trypsin-EDTA (Thermo Scientific, #25200-072) with media replacement every two days.

#### 3.2. PLASMID CONSTRUCTS AND DNA PURIFICATION

The vector pcDNA3.1 containing the corresponding sequence of BICC1 (Full-Length sequence of BICC1 – FL) was received from our collaborator Prof. Dr. Opher Gilead, Structural Genomics Consortium (SGC) from Oxford. This plasmid was generated by cloning the human BICC1 CDS (NM\_001080512.3) in a frame with the 3x Flag tag at the C-terminal position. To delete the SAM domain ( $\Delta$ SAM) of BICC1 we used the site-directed mutagenesis technique with the following sequences of primers: Forward 5'-gctgtaacttaaataagctctcgaagaaagcttttgaatc-3'; Reverse 5'-gattcaaaaagctttcttcgagagctatttaagttacag-3'. The FL construct was used for the generation of the deletion construct ( $\Delta$ SAM), both constructs were in the pcDNA3.1 vector backbone. The PRMT5 construct, also in pcDNA3.1 vector, was received from our collaborator Prof. Dr. Panagiotis (Takis) Prinos, Structural Genomics Consortium (SGC) in Toronto. This plasmid was generated by cloning the human PRMT5 CDS (NM\_006109.5) in frame with the Flag tag at the C-terminal position. The construct of pcDNA3-GFP-Flag was used as transfection control and as a negative control for Flag tag immunoprecipitation.

After the constructs were checked by Sanger sequencing, the vectors were transformed in *E.coli* cells Mach1 by heat shock transformation, and the bacterial growth was performed in a bacterial growth medium with the respective antibiotic of resistance. Plasmid DNA was obtained from midipreps using the PureLink™ HiPure Plasmid kit (Invitrogen, #K210005), which consists of extracting plasmid DNA by alkaline lysis, purification in a column, washing, and elution of plasmid DNA from the column. Then the DNA is precipitated with isopropanol, washed with ethanol, and, after drying, resuspended in molecular biology-grade water deionized, and stored at -20 °C freezer.

### 3.3. PLASMID DNA TRANSIENT TRANSFECTION

Transfection of plasmid DNA was executed using Lipofectamine™ 3000 transfection reagent (Thermo Scientific, #L3000001), according to the experiment, following the manufacturer's protocol and optimizing the protocol according to the cell line used at the laboratory. Briefly, the DNA was incubated for 15 min with P300 reagent in a proportion of 1:2 and with Lipofectamine 3000 reagent in a proportion of 1:3, using Opti-MEM for complexing. The default transfection time was 48 h.

### 3.4. WESTERN BLOTTING

Protein samples were obtained from cell lysate with no denaturing lysis buffer (50 mM Tris-HCl pH 7.4, 1 mM EDTA, 150 mM NaCl, 0.5 % Triton X-100, 10 % Glycerol, 1 mM PMSF, all in DEPC treated water) or denaturing lysis buffer RIPA 1X (50 mM Tris-HCl, pH 7.4, 150 mM NaCl, 0.25 % deoxycholic acid, 1 % NP-40, 1 mM EDTA), both containing protease inhibitor cocktail (Roche, #04693159001), and incubated for 15 min on ice, and centrifuged at 20,000 g for 20 min at 4 °C. The supernatants were collected and saved at -20 °C for posterior use. Proteins were separated according to the molecular weight through an SDS-PAGE (sodium dodecyl sulfate-polyacrylamide) gel electrophoresis with running buffer (25 mM Tris, 190 mM glycine and 0.1 % SDS) and semi-dried transferred to PVDF (polyvinylidene difluoride) membrane for 60 min at constant 0.5 A with transfer buffer (25 mM Tris, 19, mM glycine and 20 % methanol (vol/vol)). The membrane was stained with Ponceau, washed with ddH<sub>2</sub>O, and blocked on BSA 5 % in Tris-buffered saline solution plus tween 20 (TBS-t solution; 20 mM Tris-Base, 150 mM NaCl and 0.1 % Tween-20) for 1 h, and incubated with primary antibodies, according to Table 1 dilutions and incubation time conditions. Next, the membrane was incubated with the correspondent secondary antibodies for 1 h at RT and the immune complexes were detected through fluorescence using specific secondary antibodies. The blots were obtained by fluorescence exposure (Li-cor Odyssey CLX scanner). The markers used were the Odyssey® One-Color Protein Molecular Weight Marker (10-250 kDa) (Licor, #928-40000) or Color Prestained Protein Standard, Broad Range (NEB, #P7719S). The following table describes the primary and secondary antibodies used in the western blotting assays for this study:



Table 1. Description of antibodies used in western blotting assays.

Antibody	Host/Isotype	Dilution	Time of incubation	Immunogen	MW (kDa)	Catalog
Anti-BICC1 polyclonal Antibody	Rabbit	1:1,000	Overnight (4 °C)	Amino acids 75-107 mapping at the N-terminal region of human BICC1	104	#PA5-116342
Anti-PRMT5 monoclonal antibody	Rabbit	1:1,000	Overnight (4 °C)	Synthetic peptide. This information is proprietary to Abcam and/or its suppliers	72	#ab109451
Anti-IGF2BP1 polyclonal antibody	Mouse	1:1,000	Overnight (4 °C)	Recombinant full-length IGF2BP1	63	#RN001M
Anti-CCT2 antibody	Rabbit	1:10,000	Overnight (4 °C)	Synthetic peptide. This information is proprietary to Abcam and/or its suppliers.	57	#ab109184
Anti-PARP1 monoclonal antibody	Rabbit	1:2,000	Overnight (4 °C)	Synthetic peptide corresponding to residues surrounding Gly623 of human PARP-1	116	#9532
Anti-HNRNPA1 polyclonal antibody	Rabbit	1:1,000	Overnight (4 °C)	HNRNPA1 fusion protein Ag1656	34	#11176-1-AP
Anti-PABP polyclonal antibody	Rabbit	1:1,000	Overnight (4 °C)	Synthetic peptide conjugated to KLH derived from within residues 600 to the C-terminus of Human PABP	75	#ab21060
Anti-cyclin D1 monoclonal antibody	Rabbit	1:750	Overnight (4 °C)	Synthetic peptide from C-terminus of human cyclin D1	34	#MA5-16356
Anti-GFP monoclonal antibody	Mouse	1:10,000	1 h (RT)	Raised against amino acids 1-238 representing full-length GFP (green fluorescent protein) of <i>Aequorea victoria</i> origin	27	#sc-9996
Anti-GAPDH polyclonal antibody	Mouse	1:10,000	1 h (RT)	GAPDH fusion protein Ag0766	36	#60004-1
Anti-GAPDH polyclonal antibody	Rabbit	1:10,000	1 h (RT)	Synthetic peptide corresponding to residues surrounding Lys260 of human GAPDH protein.	37	#2118
Anti-β actin	Mouse	1:20,000	1 h (RT)	Not Found	43	#sc-47778
Anti-Flag® M2 monoclonal antibody	Mouse	1:10,000	1 h (RT)	Flag peptide sequence: DYKDDDDK	Diverse	#F1804
Anti-Flag polyclonal antibody	Rabbit	1:10,000	1 h (RT)	Flag peptide sequence: DYKDDDDK	Diverse	#F7425

Anti-NanoLuc® monoclonal Antibody	Mouse	1:10,000	1 h (RT)	NanoLuc® luciferase	Diverse	#9PIN7000
IRDye® 680RD antibody	Goat anti- Mouse	1:10,000	1 h (RT)	-		#926-68070
IRDye® 680RD antibody	Goat anti- Rabbit	1:10,000	1 h (RT)	-		#926-68071
IRDye® 800CW antibody	Goat anti- Mouse	1:10,000	1 h (RT)	-		#926-32210
IRDye® 800CW antibody	Goat anti- Rabbit	1:10,000	1 h (RT)	-		#926-32211

### 3.5. SILVER NITRATE IMPREGNATION OF PROTEINS IN POLYACRYLAMIDE GELS

For gel impregnation with silver nitrate, the gels were first fixed with a fixative solution (50 % methanol, 12 % acetic acid, and 0.2 % formaldehyde) for 30 sec in the microwave (maximum power) and incubated for 5 min at RT in a shaker. Then the gels were incubated with a solution of 30 % ethanol for 30 sec in the microwave (maximum power) and incubated for 5 min at RT in a shaker and after that, the gels were treated with a solution of reducing agent sodium thiosulphate (1.265 mM sodium thiosulphate) for 30 sec in the microwave (maximum power) and incubated for 2 min at RT in a shaker. Gels were then washed twice with distilled water for 30 sec in the microwave (maximum power) and incubated for 2 min at RT in a shaker, immediately after they were submitted to silver nitrate treatment protected from light (11 mM silver nitrate and 0.075 % formaldehyde) for 30 sec in the microwave (maximum power) and incubated for 5 min at RT in a shaker. Then the gels were washed with distilled water for 20 sec at RT in a shaker and incubated with a revealing solution (599 mM calcium carbonate, 0.05 % formaldehyde, and 25 µM sodium thiosulphate). The stop solution (50 % methanol and 12 % acetic acid) was added immediately after the appearance of the bands at the desired intensity.

### 3.6. PROTEOMIC ANALYSIS

#### 3.6.1. CO-IMMUNOPRECIPITATION FOR MASS SPECTROMETRY (MS) ANALYSES AND WESTERN BLOTTING

The interactome determination was performed by co-immunoprecipitation assays followed by mass spectrometry and western blotting analyses, see experimental scheme in Figure 7. The HEK293T cells were seeded in 100 mm plates for each experimental condition,

*Characterizing the Interactome of the RNA-binding Protein BICC1*

in triplicates. HEK293T cells were submitted for expression of BICC1 constructs (FL and  $\Delta$ SAM) and control with GFP construct. After 48 h of plasmids transfection, the cells were washed twice with cold PBS 1X and lysed with 1 mL of no-denaturing lysis buffer (50 mM Tris-HCl pH 7.4, 1 mM EDTA, 150 mM NaCl, 0.5 % Triton X-100, 10 % Glycerol, 1 mM PMSF, all in DEPC Treated water) containing phosphatase inhibitor cocktail (Roche, #04906837001) and protease inhibitor cocktail (Roche, #04693159001). The lysates of protein complexes were incubated on ice for 15 min and centrifuged at 20,000x g for 20 min at 4 °C. Protein was quantified using bicinchoninic acid (BCA) kit for protein determination (CYANAGEN, #PRTD1). For IP, each experimental condition and replicate used 1 mg of protein completed for a final volume of 1 mL with equilibration buffer (50 mM Tris-HCl pH 7.4, 1 mM EDTA, 150 mM NaCl, 0.5 % (w/v) Triton X-100, 10 % Glycerol, all in DEPC Treated water) for incubation with 20  $\mu$ L of anti-flag M2 magnetic beads (Sigma, #M8823) and immunoprecipitation during an overnight at 4 °C, under constant rotation. For +/- RNase A treatment each 1 mg of protein was incubated with 15  $\mu$ g of recombinant RNase A (Merckerey-Nagel, # 740505) (+ condition) and with 150 U of Recombinant Ribonuclease Inhibitor, RNaseOUT™ (Thermo Scientific, #10777-019) (– condition). After IP, small volumes of supernatants were reserved for western blotting analysis, and the beads were washed three times with wash buffer (50 mM Tris-HCl pH 7.4, 150 mM NaCl, all in DEPC-treated water) for 1 min. The wash buffer was removed and the immunoprecipitated complexes were eluted in Laemmli buffer 1X at 95 °C for 10 min. The eluates were applied in SDS-Page separation in a 10 % acrylamide/bis-acrylamide gel until achieving the resolving gel. After the electrophoresis, the gels were stained with 0.1 % Coomassie Blue (R-250) in 45 % Methanol and 30 % Acetic acid for 20 min, and destained with 30 % Methanol, 10 % Acetic acid overnight at 4 °C, and each band was excised and sent to the mass spectrometry analysis (in-gel digestion).

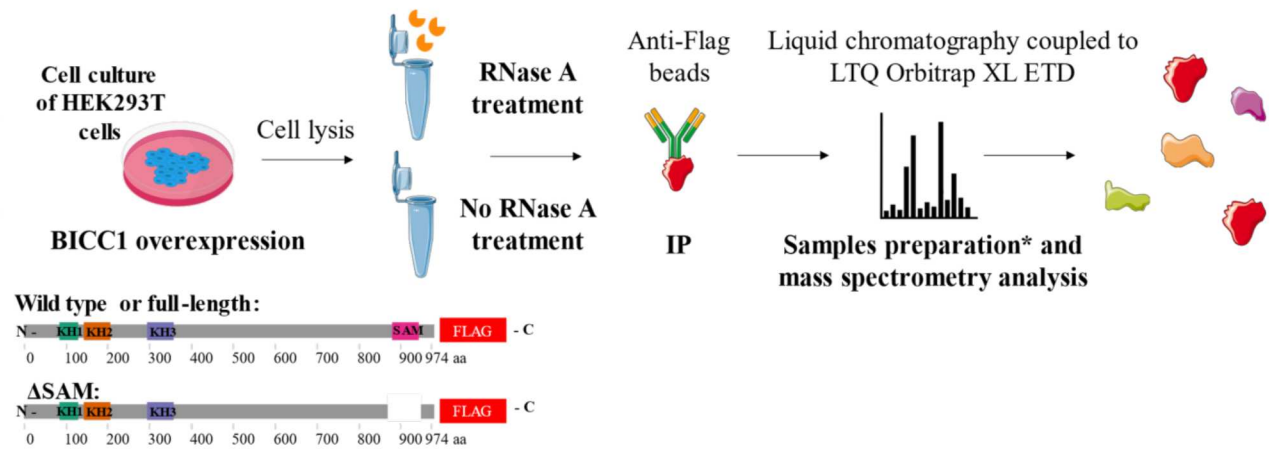


Figure 7. Schematic illustration of the co-immunoprecipitation of BICC1 constructs for mass spectrometry analyses and identification of peptides immunoprecipitated with BICC1. \*In-gel digestion.

### 3.6.2. SAMPLES DIGESTION WITH TRYPSIN

The excised gel pieces were submitted to dehydration with 100 % Ethanol and mixed in the thermomixer for 10 min at 25 °C (800 rpm). The supernatant was removed and the samples were dried in a Speed-vac for 7 min (vacuum pressure = 0.1). The samples were reduced with DTT 10 mmol/L solution in ABC (Ammonium Bicarbonate Buffer) 50 mmol/L for 60 min at 56 °C (800 rpm) and alkylated with 55 mmol/L Iodoacetamide solution in ABC 50 mmol/L for 45 min at 25 °C (800 rpm) protected from light. Next, the gel pieces were resubmitted to the dehydration steps and 12.5 ng/μL of diluted trypsin solution was added to the dried gel pieces with 50 mmol/L ABC solution for 20 min at 4 °C. Then the samples were incubated at 37 °C for 16-18 h and the peptides extraction was performed using extraction solution with 3 % TFA and 30 % acetonitrile in thermomixer for 10 min at 25 °C (800 rpm), twice. Acetonitrile was added for 10 min at 25 °C (800 rpm), twice, and the samples were dried in speed-vac to 10 to 20 % of the original volume to remove acetonitrile. Finally, the dried peptides were stocked at -20 °C for posterior desalting and purification.

### 3.6.3. SAMPLES DESALTING AND PEPTIDES PURIFICATION

The peptides were desalted and purified using StageTip-C18 pre-treated with 100 % Methanol and equilibrated with 0.1 % Formic acid solution. Elution of peptides was performed using 20 μL of 0.1 % Formic acid and 40 % in a refrigerator, twice (final volume = 40 μL). The eluates were dried in Speed-vac for 30 min without heating (vacuum pressure =

0.1) to remove ACN and just before the mass spectrometry injection, the samples were diluted in 0.1 % formic acid, 5 % DMSO, 5 % ACN solution, according to the total mass that was injected into the mass spectrometer.

#### 3.6.4. LIQUID CHROMATOGRAPHY AND MASS SPECTROMETRY ANALYSES (LC-MS/MS)

The peptides were separated by a 2 % to 40 % acetonitrile gradient in 0.1 % formic acid using an analytical PicoFrit column (15 cm × ID75 µm, 3 µm particle size C18), at a flow of 250 nL/min over 60 min acquisition mode. An LTQ Orbitrap XL ETD Mass Spectrometer (Thermo Scientific) coupled with nanoLC-1D plus liquid chromatograph and as-2 autosampler (Eksigent), and electrospray ionization were used for the identification of the peptides. Three technical replicates of each experimental condition were analyzed. All instrument methods for the LTQ Orbitrap were set up in the data-dependent mode (DDA). The initial MS scan recorded the mass range of  $m/z$  300–1800, and the most ten intense peaks were automatically selected for Collision-induced dissociation (CID). The spray voltage was set as 2.7 kV. The raw data from LTQ was searched against the human reference proteome sequence database (UniProt) using Max Quant v2.2.0.0 software and the Andromeda algorithm. The following parameters were set for the database search: **1)** 0.5 Da ion trap mass spectrometry tolerance (ITMS); **2)** 0.15 Da MS/MS deisotoping tolerance (ITMS); **3)** variable Oxidation (M), Acetyl (Protein N-term), Methyl (E), and Methyl (KR) modifications, and **4)** Fixed Carbamidomethyl (C) modifications. Protein FDR and Site FDR values were 0.01. The raw data of mass spectrometry was deposited in the Research Data Repository of the University of Campinas (Unicamp) – REDU. The following link can be accessed to visualize the raw data: <https://redu.unicamp.br/>.

#### 3.7. BIOINFORMATIC ANALYSES

The proteins identified immunoprecipitating with BICC1 by mass spectrometry were submitted to a bioinformatic pipeline for elucidation of GO terms enrichment (molecular functions, biological processes, and cellular components) in the BICC1 interactome and the building of PPIN (see Figure 8). Proteins found with a threshold of two unique peptides in at least two replicates (total of three replicates per experimental condition) and excluded from GFP controls were considered as truly co-immunoprecipitated with BICC1. BioGRID database was accessed for the identification of already reported protein interactors of BICC1. The GO

*Characterizing the Interactome of the RNA-binding Protein BICC1*

annotation of the proteins identified was accessed through the UniProt IDs that were submitted to the PPIN creation, using the STRING database search and Cytoscape software v3.10.0 for building the networks. Scripts using R and Python language were performed for GO annotation and classification of protein domains. The scripts used can be accessed at the GitHub repository through the following link: [https://github.com/HeloisaMonteiroAP/Master\\_BICC1\\_Project](https://github.com/HeloisaMonteiroAP/Master_BICC1_Project)

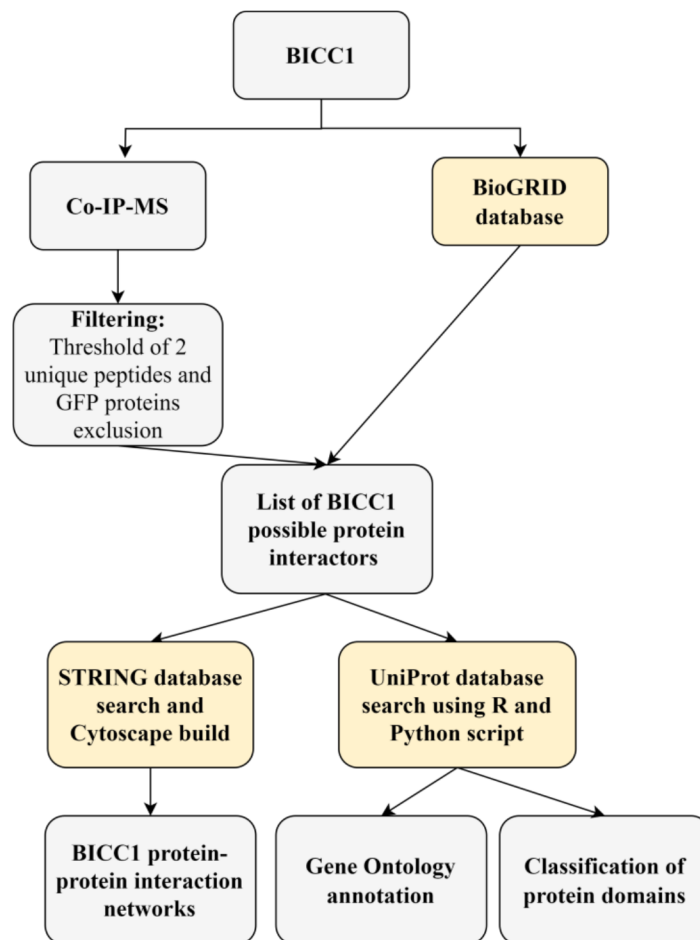


Figure 8. Bioinformatic pipeline followed for mass spectrometry data interpretation. After the selection of proteins listed with a threshold of two unique peptides in at least two replicates, the observed proteins were searched in the BioGRID database for the identification of already reported protein partners. The protein-protein interaction networks were obtained using STRING database search and Cytoscape for building the networks. The UniProt IDs were searched on the UniProt database through R script for gene ontology annotation and a Python script was used for protein domains classification.

### 3.8. IMMUNOFLUORESCENCE

Cells were plated ( $8 \times 10^4$  cells/mL) in a 24-well plate and incubated for 24 h with 5 % CO<sub>2</sub> at 37 °C before the beginning of treatments. Each well contained a previously autoclaved circular slide, pre-treated with Poly-D-Lysine. At 48 hours after transfections, cells

were fixed in 4 % paraformaldehyde in PBS 1X for 20 min. Next, cells were washed three times with PBS 1X and permeabilized with PBS-t (0.1 % Triton X-100 in PBS 1X) for 1 h at RT. Afterward, the cells were incubated with primary antibodies diluted in PBS-t, according to the conditions described in Table 2. After the primary incubation, the cells were washed with PBS 1X five times for 5 min. The secondary antibody was diluted in PBS 1X with DAPI (4',6-diamidino-2-phenylindole) solution (1 mg/mL) added at a final concentration of 1:1,000 (1µg/mg), and the cells were incubated with it for 1 h at RT, and protected from light. After that, the cells were washed with PBS 1X five times for 5 min. The treated cell slides were assembled using ProLong™ Gold Antifade Mountant with DAPI (Thermo, #P36941). The images from immunofluorescence were taken at a magnification of 630X with an Elyra PS.1 Inverted Microscopy (Purple) (super-resolution structured illumination - SR-SIM) and the Numerical Aperture (NA) of the objective was 1.4. The resolution of the images was 31.0154 pixels per micron (Width: 78.3482 microns (2430) x Height: 78.3482 microns (2430)).

Table 2. Description of antibodies used in immunofluorescence assays.

Antibody	Host/Isotype	Dilution	Time of incubation	Immunogen	Catalog
Anti-BICC1 polyclonal antibody	Rabbit	1:100	1 h (RT)	Amino acids 75-107 mapping at the N-terminal region of human BICC1	#PA5-116342
Anti-PRMT5 monoclonal antibody	Mouse	1:100	1 h (RT)	Amino acids 338-637 mapping at the C-terminus region of human PRMT5	#sc-376937
Anti-PARP1 monoclonal antibody	Rabbit	1:50	Overnight (4 °C)	Synthetic peptide corresponding to residues surrounding Gly623 of human PARP-1	#95323
Anti-Flag M2 monoclonal antibody	Mouse	1:500	1 h (RT)	Flag peptide sequence: DYKDDDDK	#F1804
Anti-Flag polyclonal antibody	Rabbit	1:500	1 h (RT)	Flag peptide sequence: DYKDDDDK	#F7425

*Characterizing the Interactome of the RNA-binding Protein BICC1*

Alexa Fluor™ 488 antibody	Goat anti-Mouse	1:500	1 h (RT)	#A-11001
Alexa Fluor™ 555 antibody	Goat anti-Rabbit	1:500	1 h (RT)	#A-21428

### 3.9. IMAGES PROCESSING AND CALCULATION OF CO-LOCALIZATION COEFFICIENT

The figures taken were imported into the free image processing software called ImageJ (Fiji version). Brightness/contrast (linear variations) were adjusted, and the background was subtracted using the plugin “subtract background” and the option “disable smoothing.” The same setting of minimum and maximum intensities was used in the experimental images and their respective control of conjugated only. Co-localization analysis was performed using correlation analysis based on Pearson’s coefficient (PC) from the ImageJ plugin JACoP (Just Another Colocalization Plugin), as previously described (BOLTE; CORDELIÈRES, 2006). PCs can range from 1 to -1, with a score of 1 indicating a complete positive correlation, while a score of -1 representing a complete negative correlation.

### 3.10. CELL VIABILITY AND CYTOTOXICITY

Redox indicator assays were performed for the determination of the cell viability and cytotoxicity by chemical compounds. In summary, the alamarBlue™ cell viability reagent (Thermo Scientific, #DAL1100) can monitor the reducing environment of living cells through the changing of the water-soluble blue non-fluorescent dye resorufindye resazurin [7-hydroxy-10-oxidophenoxazin-10-ium-3-one] to a pink color and high fluorescent resorufin.

For our assays, 24 h before the treatment with the compounds, HEK293T cells were plated in cell culture plates of 384 wells with a confluence of 70,000 cells per well. Next, the cells were treated with different concentrations of the compounds and incubated for 48 h in an incubator with 5 % CO<sub>2</sub> at 37 °C. After the treatment, the cells were incubated for 4 h with the alamarBlue™ cell viability reagent in a final concentration of 1X. After 4 h, the cell viability was measured through fluorescence with excitation/emission maxima: 540–570/580–610 nm. The plate was read in this wavelength using the spectrophotometer CLARIOstar Plus equipment (BMG LABTECH). Quadruplicates for each compound were performed.



### 3.11. REPORTER GENE OF WNT- $\beta$ CATENIN SIGNALING PATHWAY

To investigate the Wnt/ $\beta$ -catenin pathway activity, a GFP reporter gene plasmid was transfected in cells. M38 TOP-dGFP was a gift from Randall Moon (Addgene plasmid #17114; <http://n2t.net/addgene:17114>; RRID: Addgene\_17114). As a positive control of the pathway activity, a plasmid in the pcDNA vector with the  $\beta$ -catenin human gene was ectopically expressed in the cell.  $\beta$ -catenin-Flag pcDNA3 was a gift from Eric Fearon (Addgene plasmid #16828; <http://n2t.net/addgene:16828> ; RRID: Addgene\_16828). As a negative control, cells not transfected with the M38 TOP-dGFP construct were used as a baseline of no GFP expression. After 48 h of transfection, the cells were collected for western blotting and flow cytometer to quantify GFP expression.

Cells in each experimental condition were collected and resuspended in PBS 1X. Flow cytometry (FACS Canto II, BD Biosciences) was used to detect GFP, following the experimental procedures at the LaCTAD facility, Campinas-SP, Brazil. The software BD FACS Diva™ was used to analyze the data. Briefly, the GFP rate for each group was calculated as the average of duplicate measurements of the mean of all FITC-A events.

### 3.12. REPLICATES AND STATISTICAL ANALYSIS

All the assays were performed in triplicates or duplicates and the statistical analyses were performed using GraphPad Prism software (version 9). One-way ANOVA followed by Bonferroni test was performed to compare the means of more than two different groups. The acceptance level of significance was set at  $p\text{-value} \leq 0.05$ .

## 4. RESULTS

### 4.1. CONFIRMATION OF THE BICC1 RECOMBINANT VECTORS OVEREXPRESSION IN HEK293T HUMAN CELLS

The BICC1 FL,  $\Delta$ SAM, and the GFP constructs were generated by collaborators and other laboratory members and were confirmed according to the reference map (Figure 9A) by enzymatic restriction digestion and Sanger sequencing (Figures 9B and 9C, respectively). After that, the constructs were transfected in HEK293T cells and validated by western blotting assay. The construct presented the following molecular weight: GFP of 28 kDa, FL of 108 kDa, and  $\Delta$ SAM of 101 kDa (Figure 10).

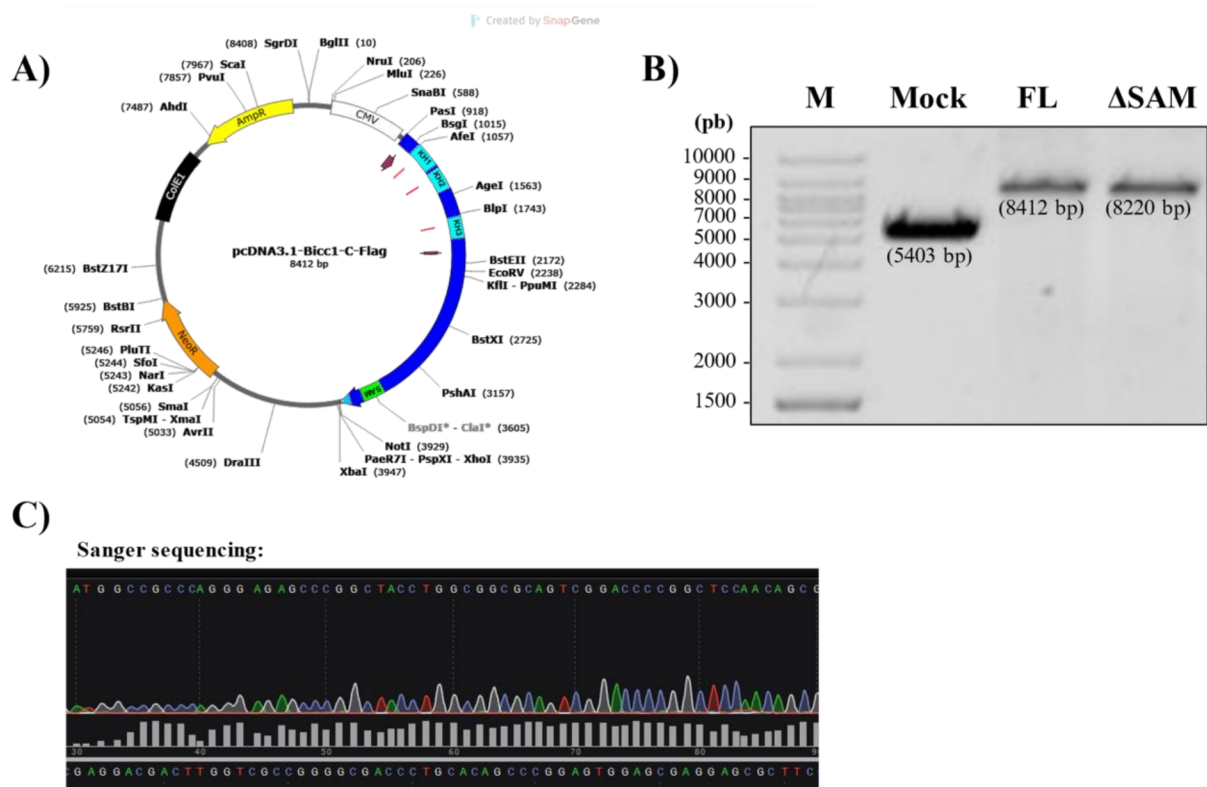


Figure 9. A) Vector map of the construct pcDNA3.1-BICC1-C-3xFlag. The map shows the BICC1 domains highlighted in light blue (KH domains) and green (SAM domain) and was generated using SnapGene software; B) BICC1 constructs (FL and  $\Delta$ SAM) were digested with the restriction enzyme AgeI, resulting in the expected size (8412 and 8220 bp), which only cleaves the BICC1 sequence. Mock (empty vector – pcDNA3.1) was digested with the restriction enzyme EcoRI resulting in the expected size of 5403 bp, as a control of the experiment; C) Snapshot of partial results from Sanger sequencing of BICC1 constructs (FL and  $\Delta$ SAM).

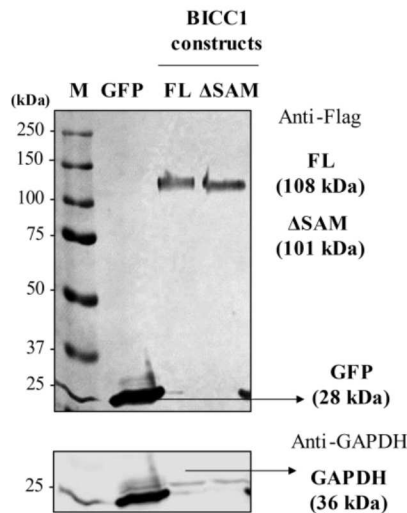


Figure 10. Western blot confirming the overexpression of the constructs. Anti-Flag antibody was used to reveal BICC1 constructs (FL – Full length and  $\Delta$ SAM – Deletion of SAM domain) and the control GFP. The GAPDH housekeeping gene was used as endogenous control. Each well was loaded with 20  $\mu$ g of protein sample. M = marker.

#### 4.2. INTERACTOME DETERMINATION BY CO-IMMUNOPRECIPITATION FOLLOWED BY MASS SPECTROMETRY (CO-IP-MS)

To investigate the interacting proteins, co-immunoprecipitation assays were performed for further determination of BICC1 interactome through mass spectrometry (Co-IP-MS). For the condition with RNase A treatment (+) aiming to evaluate the protein interactors of BICC1 in dependence of RNA, we initially verified the RNase concentration and activity. For that, 1  $\mu$ g of RNA was treated with an increasing concentration of RNase A as a reference, as shown in Figure 11.

Concentrations of RNase A above 2  $\mu$ g could digest the indicated RNA amount. Since we obtained an average of 30  $\mu$ g of total RNA from a 100 mm culture plate with HEK293T cells, we chose to proceed with the experiments using 15  $\mu$ g of RNase A.

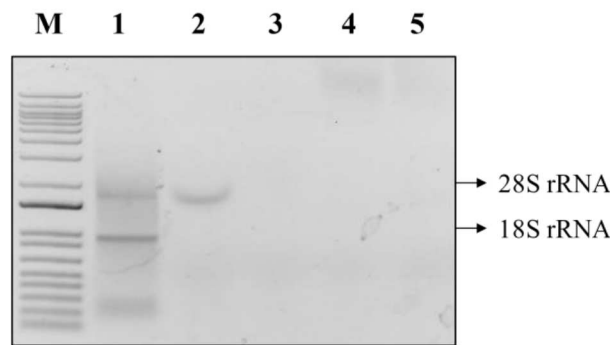


Figure 11. Determination of RNase A concentration for digestion of RNA using purified RNA samples. M = Marker; lane 1 = 1 ug of RNA not treated with RNase A; lane 2 = 1 ug of RNA treated with 2 ug of RNase A; lane 3 = 1 ug of RNA treated with 5 ug of RNase A; lane 4 = 1 ug of RNA treated with 10 ug of RNase A; lane 5 = 1 ug of RNA treated with 15 ug of RNase A.

Before the mass spectrometry analysis, the efficiency and confirmation of the Co-IPs were checked through polyacrylamide gels impregnation with silver nitrate (Figure 12A) and western blotting (Figure 12B). The elution of BICC1 Co-IPs presented a greater number of bands compared to the GFP and the M2-Flag beads Co-IP elutions. Therefore, it was possible to conclude that most of the bands were specific to BICC1 protein Co-IPs, and a few bands corresponded to unspecific interaction between the Flag tag and the beads.

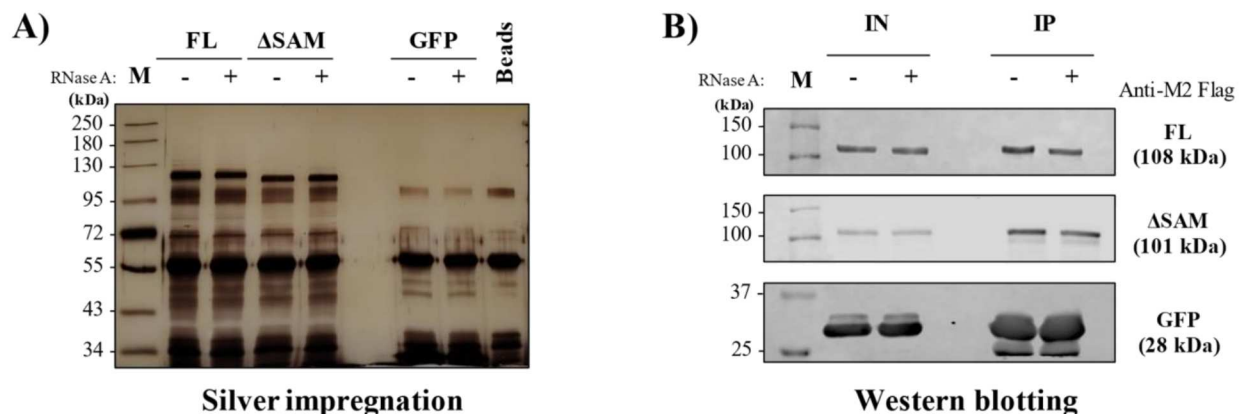


Figure 12. Immunoprecipitation of BICC1 constructs for interactome analyses. A) Silver impregnation of proteins co-immunoprecipitated with BICC1 protein and GFP, followed by Co-IP control using Beads-only, in polyacrylamide gels; B) Immunoblotting of Co-IPs with anti-flag antibody, confirming the Co-IP of BICC1 constructs and GFP. Silver impregnation, Co-IP, and western blot are described in the methods. IN = Input (the sample before immunoprecipitation, qs 20  $\mu$ g BSA-Eq); IP = Immunoprecipitated (20% of the eluate); (-) = addition of recombinant RNAase inhibitor; (+) = addition of 15  $\mu$ g of recombinant RNase A. The marker used for A) was the Color Prestained Protein Standard, Broad Range (NEB, #P7719S) and for B) Odyssey® One-Color Protein Molecular Weight (LI-COR, # 928-40000).

After confirmation of efficient immunoprecipitation, the samples were subjected to mass spectrometry analysis, done by our partners at Fiocruz-Curitiba. We have received the raw and the processed experimental data and we have established our local pipeline (Figure 8). Different numbers of proteins were identified in each experimental condition and the filtered numbers are represented in Figure 13. These filtering steps were performed to exclude potential false positives from the protein lists of BICC1 constructs Co-IPs.

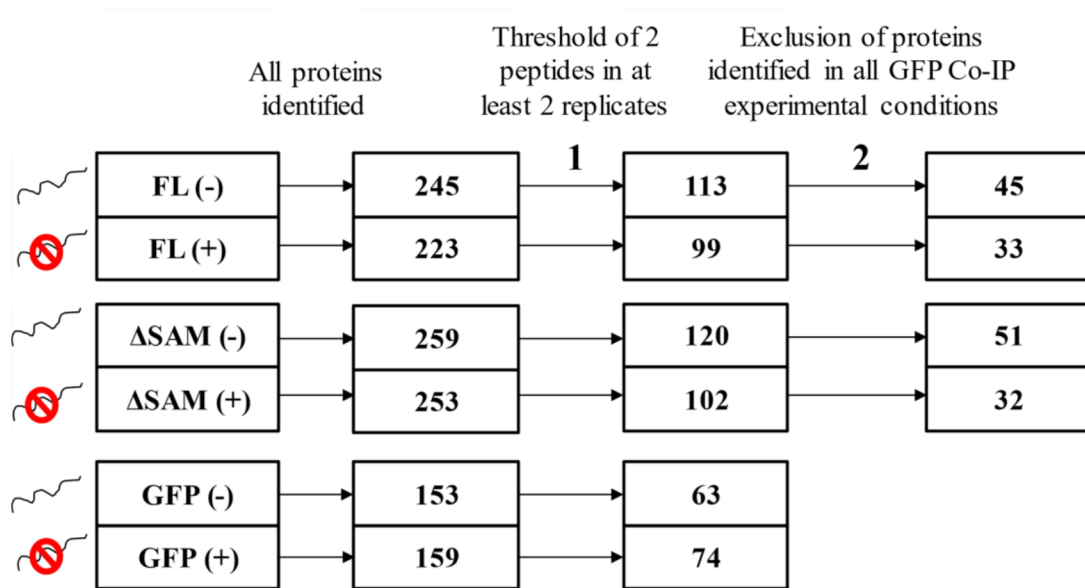


Figure 13. Schematic diagram of the experimental conditions followed by the number of proteins identified in each step of filtering, according to our pipeline (1 and 2).

Next, a Venn diagram was created for the intersection of the proteins identified in each experimental condition. In total 71 proteins were identified in all experiments and in Figure 14A, it is possible to visualize the Venn diagram with the interceptions between the experimental conditions. In Figure 14B, we show a table listing each protein identified in the diagram. A total of 19 proteins were identified in all experimental conditions.

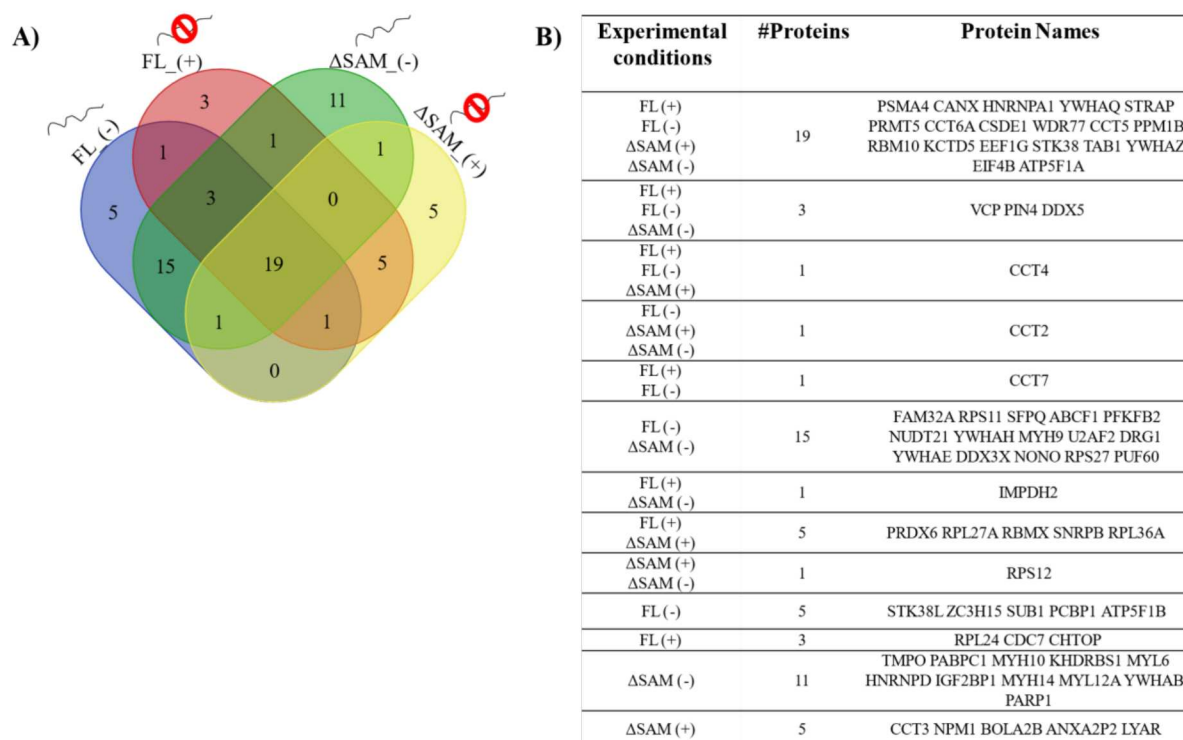


Figure 14. A) Venn diagram of the BICC1 interacting proteins using a threshold of 2 unique peptides present in at least two replicates and exclusion of proteins present in GFP conditions; B) List of the proteins identified in the Venn diagram. The Venn diagram figure was created with the following available webtool: <https://bioinformatics.psb.ugent.be/webtools/Venn/>.

**The lists of the proteins identified in each one of the experimental are in the following attachments:**

- BICC1 Full length (FL) construct Co-IP treated with recombinant RNase inhibitor: FL (-) – MS interacting proteins – [Attachment 2](#);
- BICC1 Full length (FL) construct Co-IP treated with RNase A: FL (+) – MS interacting proteins – [Attachment 3](#);
- BICC1 with the deletion of the SAM domain (ΔSAM) Co-IP treated with RNase inhibitor: ΔSAM (-) – MS interacting proteins – [Attachment 4](#);
- BICC1 with the deletion of the SAM domain (ΔSAM) Co-IP treated with RNase A: ΔSAM (+) – MS interacting proteins – [Attachment 5](#);
- GFP construct Co-IP treated with recombinant RNase inhibitor: GFP (-) – MS interacting proteins – [Attachment 6](#);
- GFP construct Co-IP treated with RNase A: GFP (+) – MS interacting proteins – [Attachment 7](#).

From this initial proteomics analysis, it was possible to observe that when RNase A treatment was executed, the number of identified proteins decreased, suggesting the importance of RNA presence for the whole BICC1 interactome. In comparison, when the SAM domain was absent, there was an increase in the number of proteins, suggesting a possible increase of physical contact with RNAs and more proteins co-immunoprecipitated or a limitation of the technique. Five proteins were enriched exclusively in the FL (-) condition (RNA/ $\Delta$ SAM dependent proteins): STK38L, ZC3H15, SUB1, PCBP1, and ATP5F1B; Three proteins exclusively in the FL (+) condition ( $\Delta$ SAM dependent proteins): RPL24, CDC7, and CHTOP; One protein in the interception FL (-)/FL (+) condition ( $\Delta$ SAM dependent proteins): CCT7; Eleven proteins exclusive of the  $\Delta$ SAM (-) condition (RNA dependent and SAM independent proteins): TMPO, PABPC1, MYH10, KHDRBS1, MYL6, HNRNPD, IGF2BP1, MYH14, MYL12A, YWHAB, and PARP1; and Five proteins exclusive of the  $\Delta$ SAM (+) condition (RNA/ $\Delta$ SAM independent proteins): CCT3, NPM1, BOLA2B, ANXA2P2, and LYAR.

Next, we evaluated the protein domains of all proteins retrieved after the 2 steps of filtering, and, interestingly, the proteins present in the presence of RNA (FL (-) and  $\Delta$ SAM (-)) showed a higher number of proteins with RBDs (KH, RRM, DDX, and CSD). In terms of function, splicing-related proteins were mainly identified in this RNA-dependent experimental condition. The following table shows these proteins identified with RBDs. Table 3 summarizes these proteins listed with RBDs.

When we evaluated the proteins present in GFP Co-IPs we observed more abundant cellular proteins as ribosomal and heat-shock-related proteins. Those were subtracted from the BICC1 Co-IPs.

Table 3. Proteins that were identified with RBDs in each experimental condition.

Experimental conditions	KH domain	RRM domain	DDX domain	CSD domain	Total number of proteins with RBDs
<b>FL (-)</b> (RNA/SAM-dependent)	<b><u>PCBP1</u></b> <sup>#</sup>	PUF60 <sup>#</sup> , NONO <sup>#</sup> , EIF4B, RBM10 <sup>#</sup> , SFPQ <sup>#</sup> , HNRNPA1 <sup>#</sup> , U2AF2 <sup>#</sup>	DDX3X	CSDE1	<b>10</b>
<b>FL (+)</b> (SAM-dependent)	NA	RBM10 <sup>#</sup> , EIF4B, HNRNPA1 <sup>#</sup> , RBMX	NA	CSDE1	<b>5</b>
<b>ΔSAM (-)</b> (RNA dependent and SAM independent)	<b><u>IGF2BP1</u></b> <sup>*</sup> , <b><u>KHDRBS1</u></b> <sup>#</sup>	EIF4B, PUF60 <sup>#</sup> , SFPQ <sup>#</sup> , RBM10 <sup>#</sup> , <b><u>PABPC1</u></b> <sup>#</sup> , <b><u>HNRNPD</u></b> , HNRNPA1 <sup>#</sup> , NONO <sup>#</sup> , U2AF2 <sup>#</sup>	DDX3X	CSDE1	<b>13</b>
<b>ΔSAM (+)</b> (RNA/SAM independent)	NA	EIF4B, RBM10 <sup>#</sup> , HNRNPA1 <sup>#</sup> , RBMX <sup>#</sup>	NA	CSDE1	<b>5</b>

NA = Not appeared; “\*” = IGF2BP1 has also an RRM domain. “#” = splicing-related proteins. **Highlighted proteins** = Proteins that are exclusive of each experimental condition according to the filtering steps that were determined.

#### 4.3. PROTEIN-PROTEIN INTERACTION NETWORKS (PPIN) OF BICC1 INTERACTOME SHOWS ENRICHMENT OF SPLICING, METHYLOSOME AND INTRACELLULAR MEMBRANELLES ORGANELLES PROTEINS

A general PPIN of all proteins identified in the BICC1 Co-IP conditions (n=71) and the proteins present in the BioGRID database (n=23) had an enrichment p-value of 1.0E-16, showing a high significance of the interactions identified (Figure 16A). Some of the enriched functional annotation with FDR (False Discovery Rate) < 0.05 were highlighted on the PPIN (Figure 16B). The FDR scores in Cytoscape are used to measure the p-value enrichment of the network, and an FDR < 0.05 means that less than 5 % of the data is false-positive or false-negative (LI et al., 2012). In this network, we observed biological processes associated with mRNA stability and processing, such as splicing, and cellular components related to methylosome complex and membranelles organelles.

The size of the nodes of these networks was drawn according to the degree of connections. Interestingly, some proteins showed the highest degree of connections (> 25),



HNRNPA1, PABPC1, PCBP1, and EEFIG, and three proteins were also reported in the BioGRID database, CSDE1, YWHAQ, and YWHAH. The HNRNPA1, EEFIG, CSDE1, and YWHAQ were observed in all BICC1 Co-IP-MS conditions, while the PABPC1 and PCBP1 were only observed in conditions without RNase A treatment, that is in Co-IPs with the dependence of RNA presence.

In addition, physical interactions of BICC1 with CSDE1 and ANKS3, already reported according to the STRING database, were highlighted in red in the PPIN. However, from those, just CSDE1 interaction was observed in this Co-IP-MS data.

A classification of the top 10 GO enrichment annotation terms was also performed and we grouped them by general categories (biological processes – BP, cellular component – CC, and molecular functions – MF), as shown in Figure 15. It was possible to observe 34 proteins with RNA-binding molecular function, most of the proteins are present in the cytosol and some are in protein-containing complexes, such as Cajal bodies (n=5: CCT6A, CCT7, CCT4, CCT2, and CCT3), stress granules (n=3: CSDE1, VCP, and IGF2BP1), and P-bodies (n=3: CSDE1, PSMA4, and IGF2BP1).

Proteins annotated as part of stress granules and p-body components were investigated. CSDE1, VCP, and IGF2BP1 were annotated as cytoplasmatic stress granules, while PSMA4 was annotated in P-bodies. CSDE1 and IGF2BP1 were also annotated in P-bodies. Indeed, previous studies are reporting BICC1 presence in P-bodies (TRAN et al., 2010) and stress granules (ESTRADA MALLARINO et al., 2020), however, none of these studies cite CSDE1, VCP, IGF2BP1, and PSMA4 together with BICC1.

The protein-containing complexes (cajal bodies, stress granules and P-bodies) are formed during LLPS, which is an activity in the cell important for survival during stress conditions (LIU et al., 2023). Indeed, the BICC1 protein sequence when submitted to a sequence-based web tool for query and prediction of potential phase separation proteins (PSPredictor) showed a high positive score equal to 0.9919. The PSPredictor uses machine learning to predict the potential phase separation proteins based on curated data from the Liquid-Liquid Phase Separation Database (LLPSDV), and when the scores are closer to 1, the greater the chance of the protein to form liquid condensates structures (CHU et al., 2022).

As a complementary investigation, the overlap of the proteins listed in the RNA granule database (MILLAR et al., 2023) with the 71 proteins identified in all Co-IP conditions was also executed, and, surprisingly, from a total of 71 proteins, 66 were present in this database: PRMT5, STRAP, CSDE1, WDR77, PSMA4, PPM1B, CANX, CCT5, YWHAQ,

YWHAZ, PUF60, NONO, EIF4B, CCT6A, YWHAH, RPS11, RBM10, TAB1, DRG1, MYH9, FAM32A, SFPQ, U2AF2, EEF1G, RPS27, VCP, YWHAH, CCT7, DDX5, DDX3X, ANXA2, HNRNPA1, ABCF1, ATP5F1A, YWHAB, PCBP1, KCTD5, PIN4, PARP1, NPM1, HNRNPD, PABPC1, MYL6, MYL12A, NUDT21, SNRNPB, RPS12, PRDX6, CCT4, SUB1, CCT2, KHDRBS1, ZC3H15, CDC7, RPL24, IMPDH2, RPL27A, TMPO, RPL36A, MYH10, RBMX, CCT3, MYH14, LYAR, IGF2BP1 and CHTOP. The proteins STK38, PFKFB2, ATP5B, STK38L, and BOLA2B were not identified in this database.

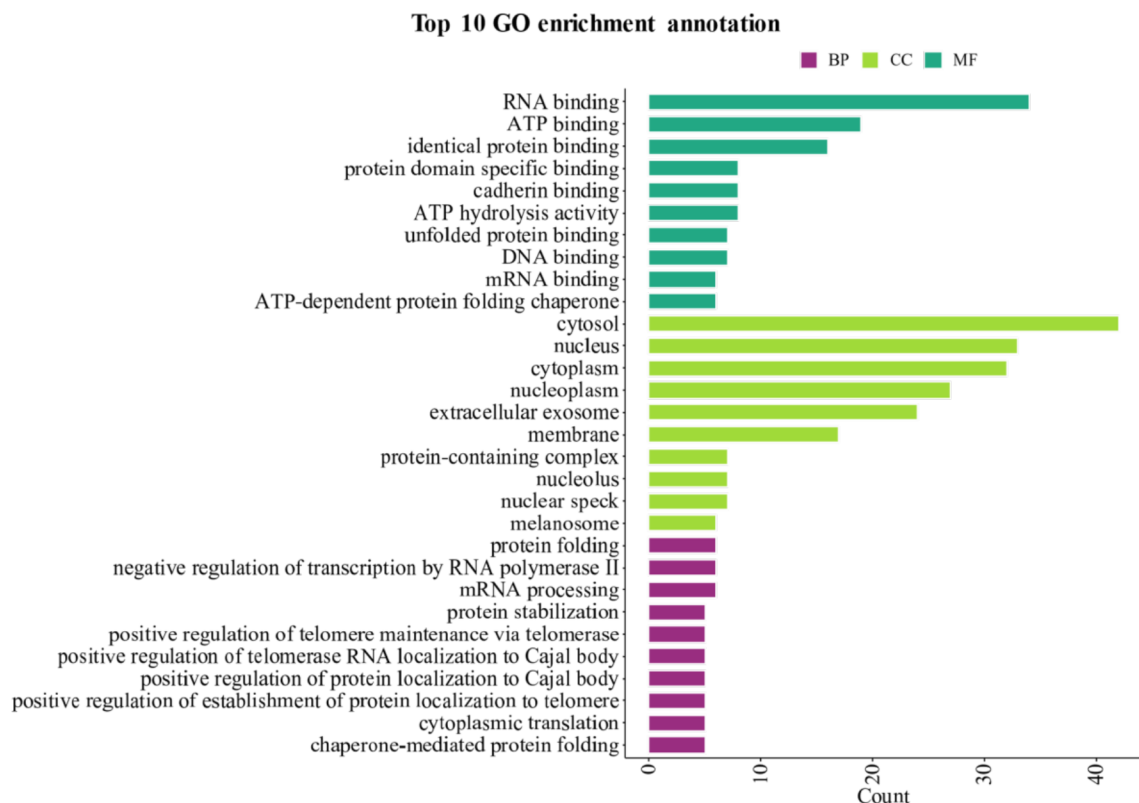


Figure 15. Top 10 GO enrichment annotation of all proteins identified along the BICC1 Co-IP conditions (n=71). This figure was created using R script. Biological processes – BP, cellular component – CC, and molecular functions – MF.

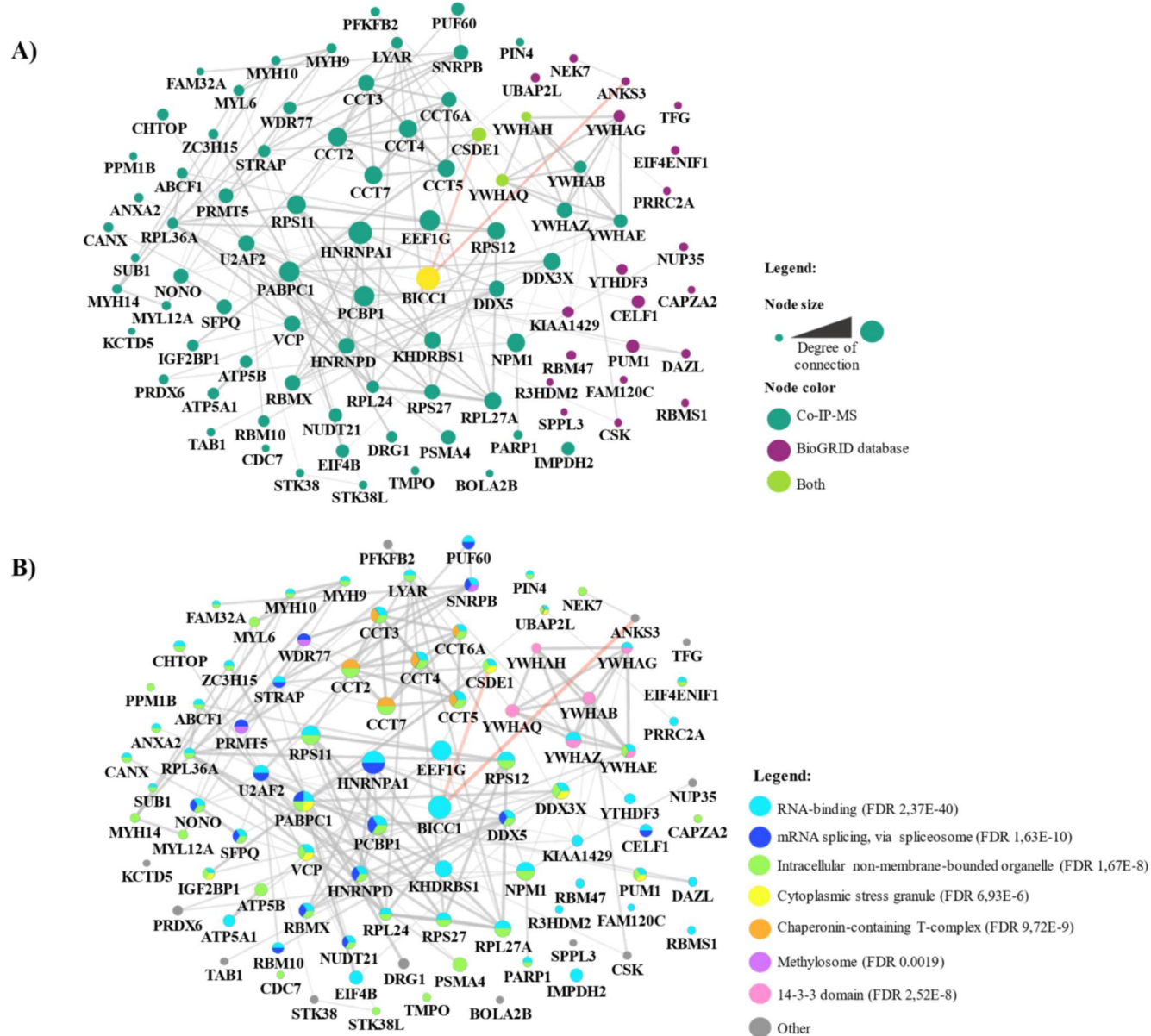


Figure 16. PPIN of all proteins identified in the four different BICC1 Co-IPs experimental conditions (n=71) and proteins present in the BioGRID database. A) PPIN nodes are colored according to proteins identified in this Co-IP-MS study, proteins exclusive of the BioGRID database, and proteins present in both conditions; B) PPIN nodes are colored according to the enriched functional annotation determined by STRING (FDR < 0.05). The network was constructed using Cytoscape and STRING plugin. The node sizes are displayed according to the degree of connections. PPIN was classified according to the physical subnetwork and edges with medium confidence: 0,400. Enrichment p-value = 1.0E-16. The network was constructed using Cytoscape.

Next, the connections between the proteins were identified exclusively in each of the separate Co-IP conditions and identified on the Venn diagram (Figure 14). In Figure 17A, there were analyzed six different conditions: **1) FL (-)/ΔSAM (-)** (probable RNA dependent

proteins); **2) ΔSAM (-)** (probable RNA dependent and SAM domain independent proteins); **3) FL (-)** (probable RNA and SAM domain-dependent proteins); **4) FL (+)/ΔSAM (+)** (probable RNA independent proteins); **5) ΔSAM (+)** (probable RNA and SAM domain independent proteins), and **6) FL (+)** (probable SAM domain-dependent proteins).

The proteins with the highest degree connections (> 10 connections) were PCBP1, U2AF2, and HNRNPD, which are exclusively present in the Co-IP conditions without RNase A treatment. In this PPIN it was also possible to observe that most of the proteins and connections are from Co-IP conditions without RNase A treatment, suggesting the importance of RNA presence for the BICC1 protein interactome. In addition, in the same PPIN, splicing-related proteins were highlighted (Figure 17B). Interestingly, most of them were in the conditions of RNA dependence: PUF60, NUDT21, U2AF2, SFPQ, NONO, PCBP1, PABPC1, and HNRNPD.

In summary, the bioinformatic analysis showed that the Co-IP-MS experiments were consistent and the RNase A digestion was able to decrease the number of proteins related to RNA activity. The results point to new biological processes and cellular components associated with BICC1 (mRNA splicing, methylosome complex, and biomolecular condensates) and new potential protein partners. As a highlight, it was identified a strong enrichment of RNA-granule proteins, which suggests a role of BICC1 in processes of liquid-liquid phase separation in the cell.

Next, we investigated further the interaction of BICC1 with some protein partners using different molecular and cellular biology techniques.

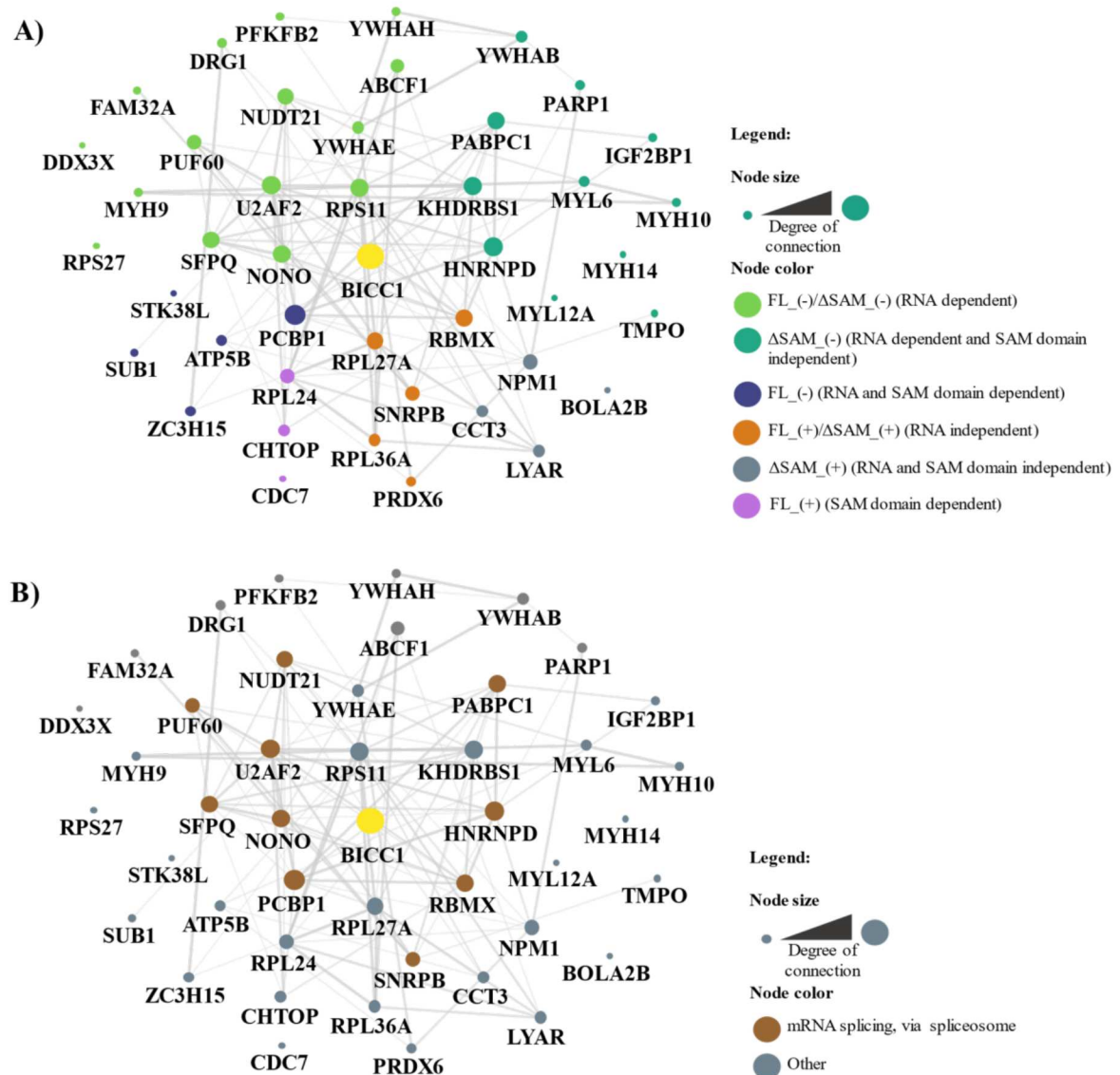


Figure 17. A) PPIN of proteins exclusively identified in each separate BICC1 (FL and ΔSAM) Co-IPs, in the presence or absence of RNase A treatment. B) Splicing-related proteins highlighted in the PPIN. PPINs were classified according to the physical subnetwork and edges with medium confidence: 0,400. Enrichment p-value = 1.0E-16. The node sizes are displayed according to the degree of connections. The networks were constructed using Cytoscape

#### 4.4. CONFIRMATION THAT BICC1-FLAG CO-IMMUNOPRECIPITATES WITH PRMT5, IGF2BP1, PARP1 AND STK38 THROUGH WESTERN BLOTTING

According to the PPIN and GO analysis, some proteins were considered for further investigation of BICC1 interaction: PRMT5, STK38, HNRNPA1, IGF2BP1, PARP1, PABPC1 and CCT2.

The PRMT5 and STK38 were chosen due to their presence in all conditions and importance for biological processes in cells, such as splicing and apoptosis, respectively (JOFFRE et al., 2016; RENGASAMY et al., 2017). Also, these proteins are enzymes with post-translational modifications (PTMs) activity, and there are still no studies reporting enzymes that are post-translationally modifying BICC1 protein. The HNRNPA1 was chosen due to its presence in all conditions, and because it showed the highest degree of connections (total of 34 connections) in the PPIN of Figure 16. PARP1, IGF2BP1 and PABPC1 were selected due to their exclusive presence in the conditions without RNase A treatment, in which the former is also related to RNA-polymerase activity and the latter is a KH domain protein, as BICC1. The availability of reagents and project collaboration in our group were also considered for choosing these protein targets.

PRMT5 was confirmed co-immunoprecipitating with BICC1, and not with GFP, using the western blotting approach (Figure 18A). Besides the methyltransferase PRMT5, Co-IP of BICC1 was also confirmed with other proteins investigated proteins: IGF2BP1 and PARP1 (Figure 18A). IGF2BP1 was observed mainly in the  $\Delta$ SAM (-) Co-IP condition, corroborating with the data obtained in the Co-IP-MS, which showed this protein just in this condition. A slight signal of IGF2BP1 is also observed in the FL (-) Co-IP condition. As already mentioned, IGF2BP1 is an RBP that contains KH domains, thus, its presence just in the condition with RNA dependence and with the KH domains of BICC1 ( $\Delta$ SAM (-) and FL (-)) shows the specificity of this protein to RNA-binding functions in the cell. PARP1 was also observed mainly in the  $\Delta$ SAM (-) Co-IP condition, with a slight signal in the other conditions of BICC1 Co-IPs. This result also corroborates with the Co-IP-MS data, which showed the presence of PARP1 just in the  $\Delta$ SAM (-).

PABPC1, HNRNPA1, and CCT2 did not show specific co-immunoprecipitation with BICC1, in which CCT2 also appeared in IP bands of GFP, as can be observed in Figure 20A. However, many TCP-1 chaperonin families were present in the BICC1 Co-IP lists (as CCT2) in a high number of unique peptides, whereas in the GFP Co-IP lists the number of unique peptides of TCP-1 chaperonin proteins was low and excluded these proteins as potential

false positives after the filtering steps. These results suggested that BICC1 can be physically interacting with CCT2, not through the Flag-tag, and so GFP is interacting with these proteins, as it is a protein with chaperone activity. In addition, CCT2 (and other TCP-1 proteins: CCT5, CCT4, CCT6A, CCT7) plays an important role in the regulation of protein localization to Cajal bodies (MA et al., 2023).

Because we have other lab members researching the kinase STK38, we also investigated this interaction, by using a vector for STK38 (55 kDa) expression, tagged with NanoLuciferase (19,1 kDa). The western blotting shown in Figure 18B also confirmed the BICC1 co-immunoprecipitation (anti-Flag IP) with STK38 (anti-NanoLuc western) (74,1 kDa).

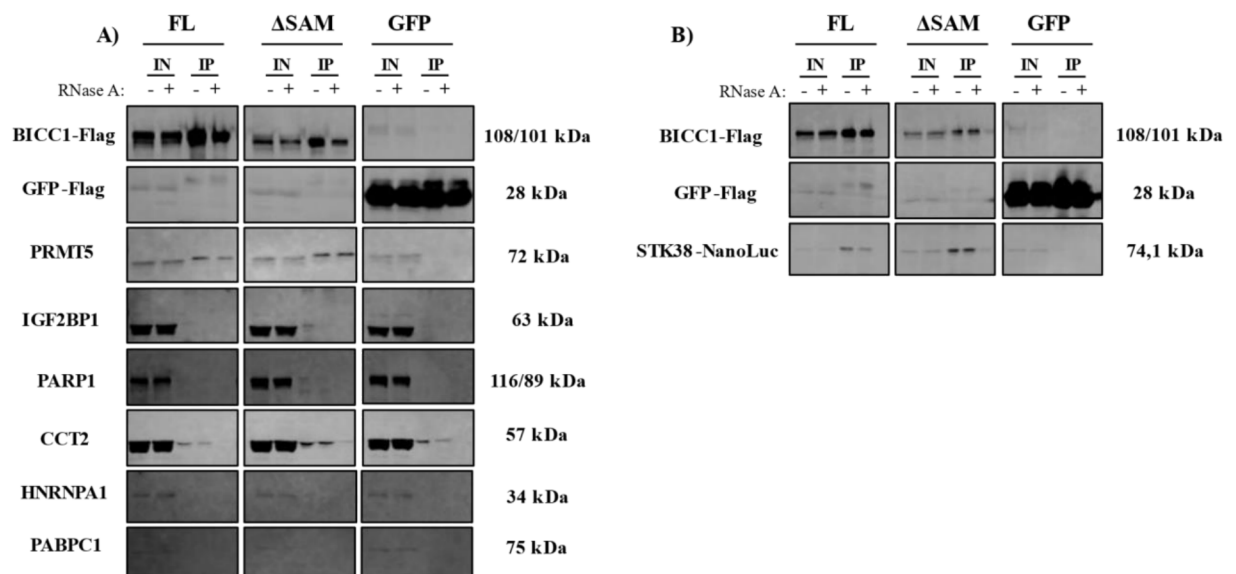


Figure 18. Co-IP of BICC1 followed by western blotting reveals interaction with PRMT5, IGF2BP1, PARP1, and STK38. A) Overexpression of BICC1 constructs (FL and ΔSAM) followed by Co-IP with anti-Flag magnetic beads; B) Overexpression of BICC1 constructs (FL and ΔSAM) and STK38 construct following by Co-IP with anti-Flag magnetic beads. IN = input (20 μg BSA-Eq of total protein); IP = immunoprecipitation; (+) = Condition of RNA presence, in which just before Co-IP, the samples were treated with 150 units of RNaseOUT™ Recombinant Ribonuclease Inhibitor; (-) = Condition of RNA absence, in which just before Co-IP, the samples were treated with 15 μg of RNase A.

In conclusion, BICC1-Flag was confirmed as co-immunoprecipitating with PRMT5 and STK38-NanoLuc, in RNA and SAM domain independence, and with IGF2BP1 and PARP1, more intensely, in RNA dependence. The BICC1 co-immunoprecipitation with CCT2, however, was unspecific.



#### 4.5. INVESTIGATION OF CELLULAR LOCALIZATION OF BICC1 WITH PROTEIN PARTNERS VALIDATED BY CO-IP-MS AND CO-IP-WB

Next, we investigated the cellular localization of BICC1 with the proteins PRMT5 and PARP1 through immunofluorescence (IF) assays. The investigation with IGF2BP1 and STK38 was not possible due to the limitation of antibodies against these proteins. The super-resolution structured illumination microscopy (SIM) was chosen to perform the IF imaging since it can distinguish two different fluorescent points with a higher resolution, due to the moiré pattern and processing of images that overcome the diffraction limitation (WEGEL et al., 2016). Therefore, for assays that aim to determine the co-existence of two proteins, the SIM is an efficient microscopy and can lead to more realistic results, when compared to traditional microscopies, such as confocal microscopy.

##### *4.5.1. BICC1 ANTIBODY EFFICIENCY FOR IF AND IDENTIFICATION OF STRUCTURES LIKE BIOMOLECULAR CONDENSATES WHEN BICC1 WAS OVEREXPRESSED:*

The first step of IF assays was to test the efficiency of the BICC1 antibody. To achieve this goal, cells were overexpressed with BICC1-FL construct, and cells were treated for IF assay, as indicated in the methods. In Figure 19, the cells were double stained with anti-BICC1 (secondary antibody Alexa 555) and anti-Flag (secondary antibody Alexa 488) antibodies, and the merge of these two antibodies can be seen in white color, meaning that the BICC1 antibody also identifies the BICC1-FL construct overexpressed, which contains Flag tag. This also indicated that our commercial anti-BICC antibody was able to detect BICC. The average of Pearson's correlation (PC) of a total of 5 cells analyzed was equal to 0.785, meaning a high colocalization between the fluorophores (see [Attachment 8](#)). Therefore, the efficiency of the anti-BICC1 antibody was successfully confirmed.

In addition, the formation of structures like biomolecular condensates was observed when the FL construct was overexpressed. This agrees with our GO analysis showing the enrichment of interacting proteins associated with protein localization to P-bodies, Cajal bodies, and stress granules.



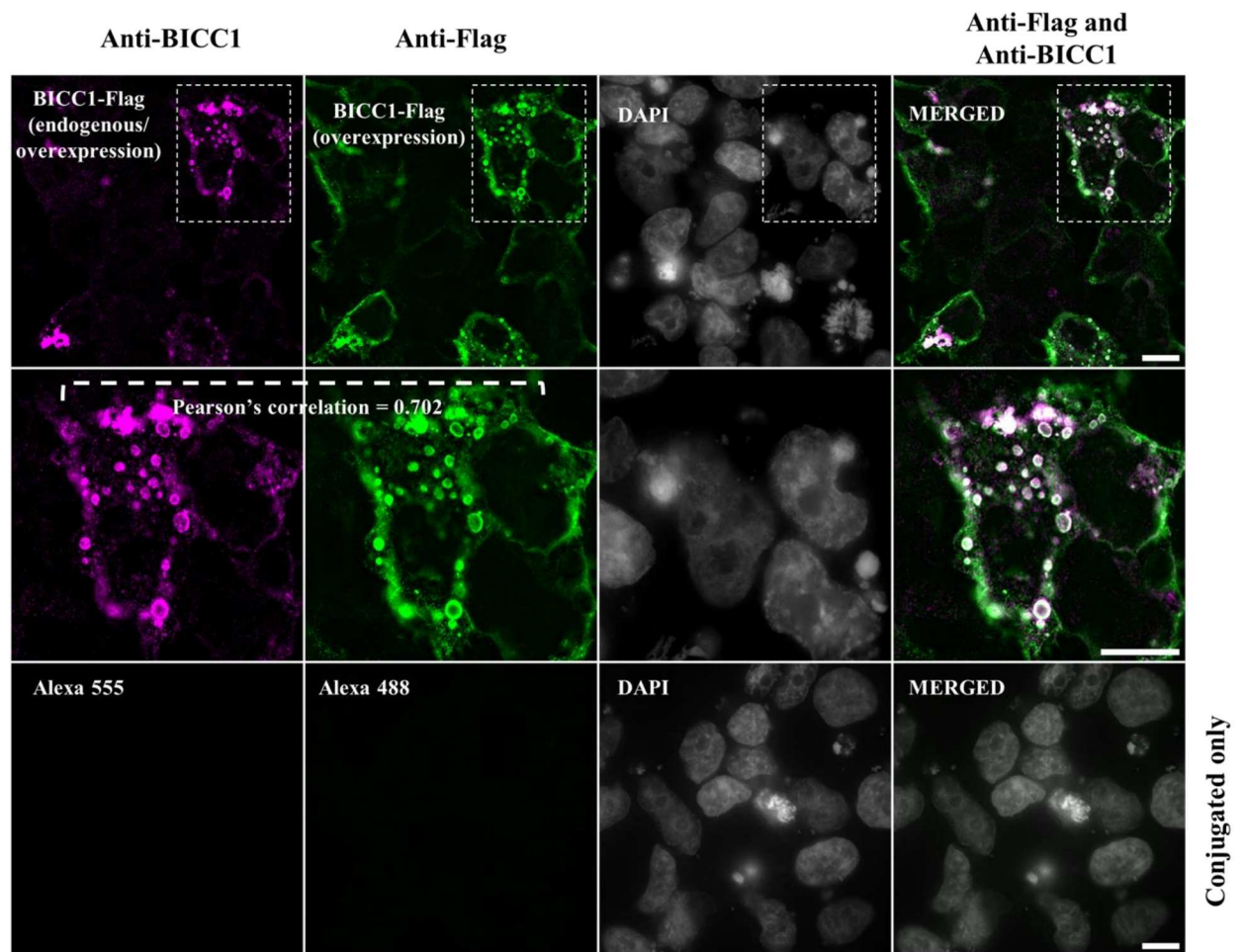


Figure 19. Immunofluorescence using the BICC1 antibody and anti-Flag antibody to detect endogenous and overexpression of BICC in HEK293T. As secondary antibodies, Alexa 555 was used to stain anti-BICC1 and Alexa 488 was used to stain anti-Flag. The nucleus was stained with DAPI. Images were obtained using ImageJ open access software and all pictures were taken at a magnification of 630X with an Elyra PS.1 Inverted Microscopy (Purple) (super-resolution structured illumination). Scale bars are indicated at 10  $\mu$ m.

#### 4.5.2. BICC1 AND PRMT5 CELLULAR LOCALIZATION:

The overexpression of BICC1-FL was performed and the IF of endogenous PRMT5 and BICC1 showed both proteins in the cytoplasm with some points co-localizing (white dots shown in Figure 20). The average of PC of a total of 5 cells analyzed was equal to 0.402 (see [Attachment 8](#)), meaning a positive colocalization between the fluorophores in some points of the cell. Therefore, it is possible to suggest that BICC1 co-localizes with PRMT5 in some regions of the cell, using the immunofluorescence approach.

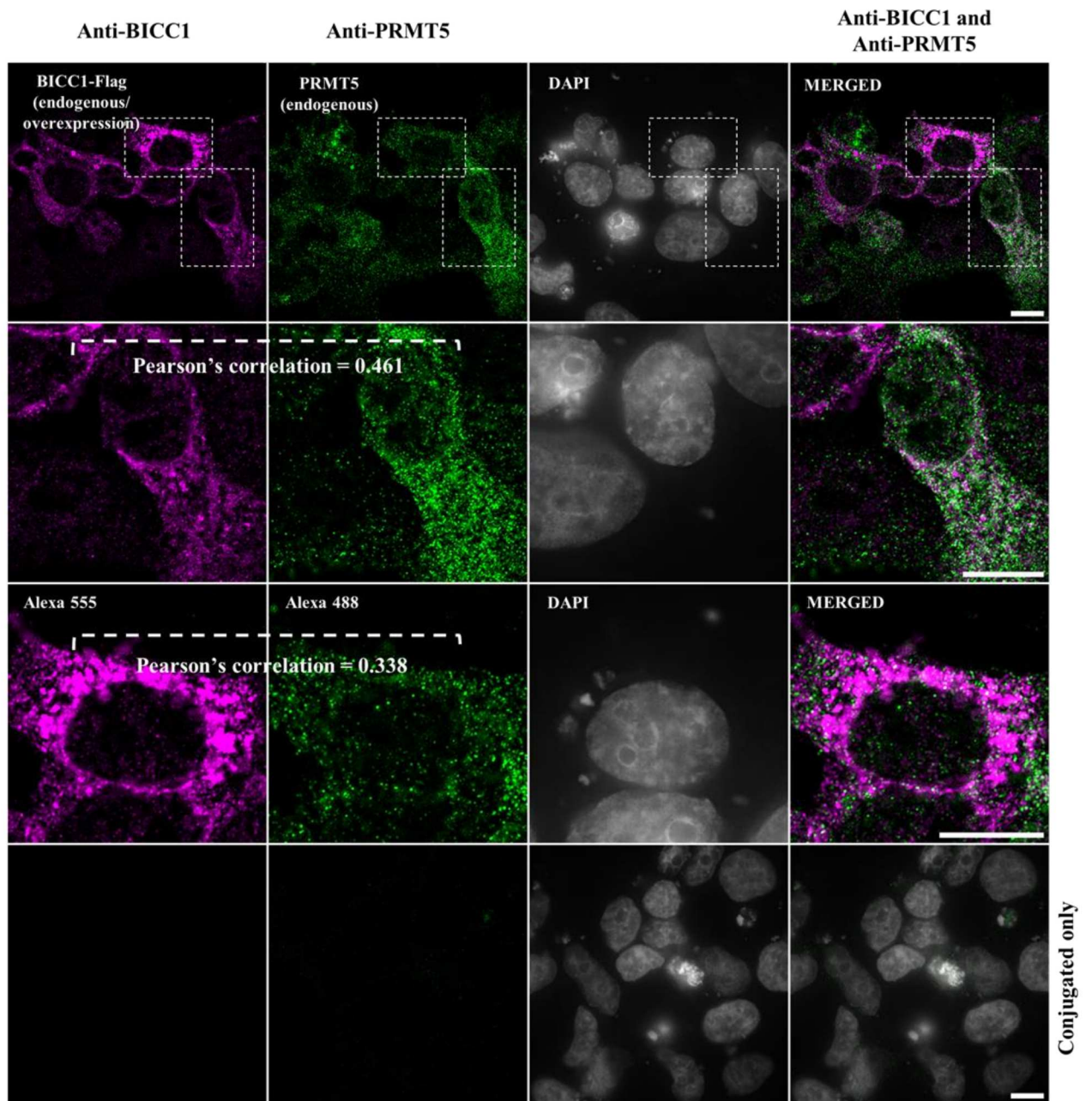


Figure 20. Co-localization of BICC1 and PRMT5. BICC1 was stained with the primary antibody anti-BICC1 and PRMT5 was stained with the primary antibody anti-PRMT5. As secondary antibodies, Alexa 555 was used to stain BICC1, and Alexa 488 was used to stain PRMT5. The nucleus was stained with DAPI. Images were obtained using ImageJ open access software and all pictures were taken at a magnification of 630X with an Elyra PS.1 Inverted Microscopy (Purple) (super-resolution structured illumination). Scale bars are indicated at 10 μm.

#### *4.5.3. BICC1 AND PARP1 CELLULAR LOCALIZATION:*

The overexpression of BICC1 was performed and the IF of endogenous PARP1 and BICC1 overexpressed showed different localization of the proteins, with BICC1 present in the cytoplasm and PARP1 in the nuclei. The co-localization of both proteins was observed in a few cells in one condition of the prophase/metaphase stage of the cell cycle (white dots shown in Figure 22), showing in this condition a positive Pearson's R correlation equal to 0.446, while a negative R score in other conditions of the cell cycle. The average of PC of a total of 5 cells analyzed was equal to -0,0592 (see [Attachment 8](#)). Therefore, it is possible to conclude that these proteins are not co-localizing in most of the cell conditions, with exceptions according to the cell cycle phase, as the prophase stage. So, this would need further studies with synchronized cells.



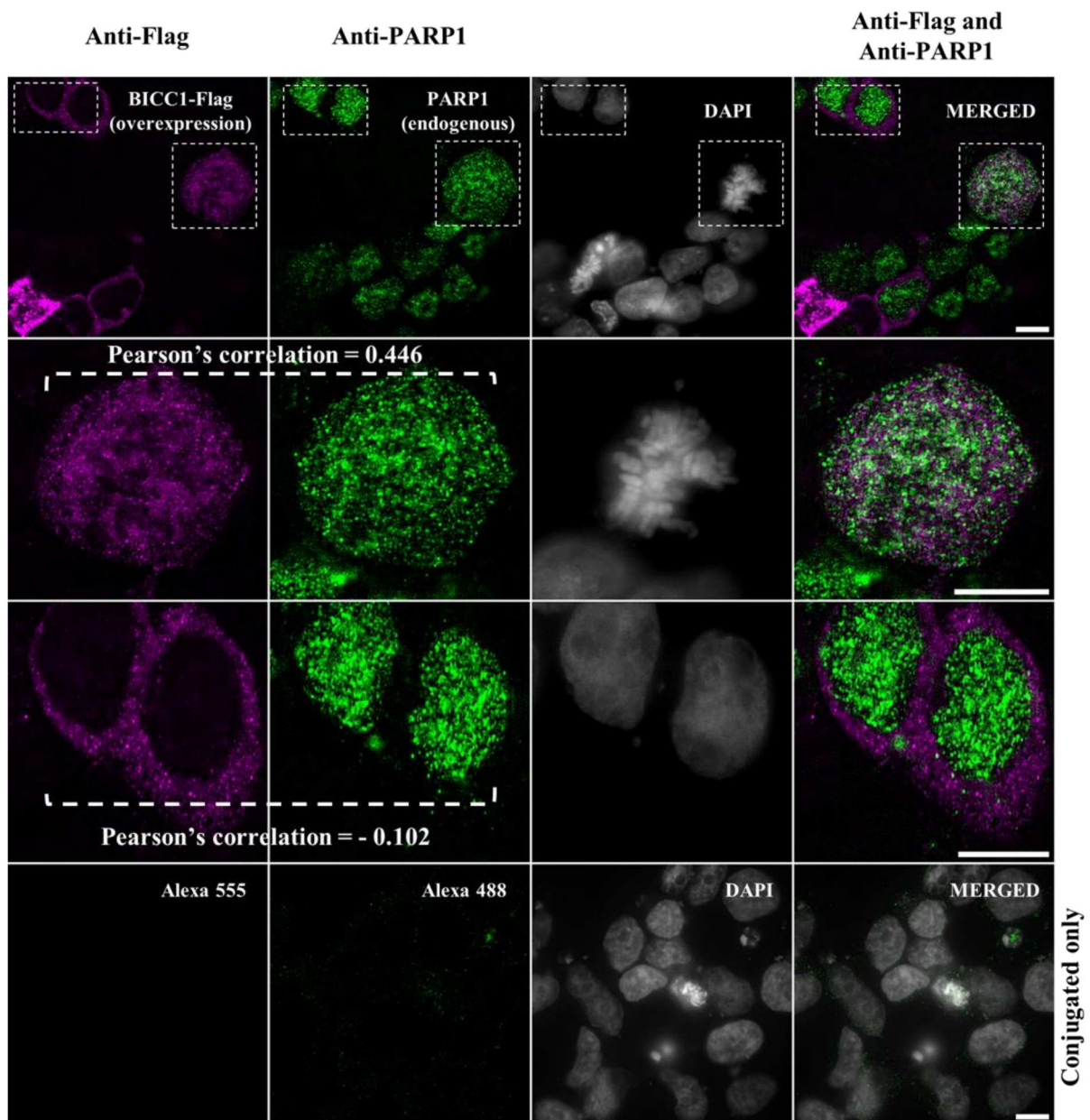


Figure 21. Localization of BICC1 and PARP1. BICC1 was stained with the primary antibody anti-Flag and PARP1 was stained with the primary antibody anti-PARP1. As secondary antibodies, Alexa 555 was used to stain BICC1-Flag, and Alexa 488 was used to stain PARP1. The nucleus was stained with DAPI. Images were obtained using ImageJ open access software and all pictures were taken at a magnification of 630X with an Elyra PS.1 Inverted Microscopy (Purple) (super-resolution structured illumination). Scale bars are indicated at 10  $\mu\text{m}$ .

#### 4.6. CONFIRMATION OF PRMT5 RECOMBINANT VECTOR OVEREXPRESSION AND PRMT5 INHIBITION COMPOUNDS ACTIVITY IN HEK293T CELLS

To expand the investigation of BICC1 and the protein partner PRMT5, a methyltransferase, we investigated possible methylation sites in BICC1 by using a chemical inhibitor of PRMT5 (a chemical probe with high affinity and selectivity).

By contacting a collaborator who studies PRMT5 (Prof. Dr. Panagiotis Prinos, Structural Genomics Consortium (SGC) in Toronto), we obtained the following reagents to investigate the interaction of BICC1-PRMT5: PRMT5-Flag construct and PRMT5 inhibitor compounds. PRMT5-Flag construct was confirmed by western blotting (Figure 23) and sequencing, after HEK293T expression. The PRMT5 construct is also in pcDNA3.1 vector. This plasmid was generated by cloning the human PRMT5 CDS (NM\_00 6109.5) in frame with the Flag tag at the C-terminal position.

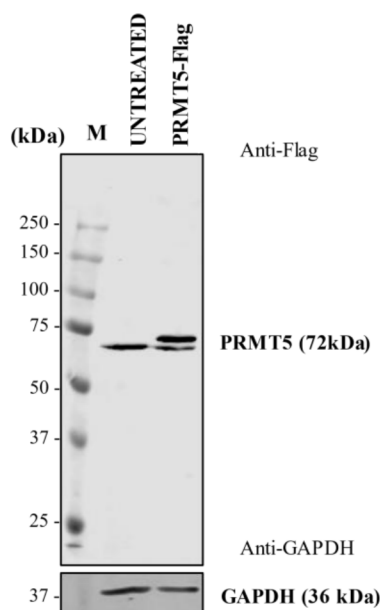


Figure 22. Overexpression of PRMT5-Flag construct in HEK293T cells using a commercial anti-PRMT5 antibody. The GAPDH housekeeping gene was used as endogenous control. Each well was loaded with 20  $\mu$ g of protein sample. M = marker; UNTREATED = Cells not transfected with PRMT5-Flag vector; PRMT5-Flag = Cells transfected with PRMT5-Flag vector.

In parallel to the confirmation of PRMT5 overexpression, the chemical probe GSK591 was tested, this is a substrate-competitive inhibitor of the PRMT5-MEP50 complex and is selective for PRMT5 up to 50  $\mu$ M relative to a panel of other methyltransferases

(“GSK591 | SGC”, [s.d.]; SACHAMITR et al., 2021). The GSK591 inhibitor was initially used and will be followed up to investigate PRMT5's relationship with BICC1 in cells. In addition to this chemical compound, we have obtained the SGC2096 compound, which has a similar structure to GSK591 and is used as a negative PRMT5 control, since it cannot inhibit the PRMT5 activity.

To explore the cellular role of PRMT5 and BICC1, the redox indicator assay was performed for the determination of cell viability and cytotoxicity of the chemical compounds. According to the cell viability results, the compounds were not toxic to cells up to 100  $\mu\text{M}$  (Figure 24), even not achieving a real  $\text{IC}_{50}$  (half-maximal inhibitory concentration) value within the range of 0 up to 100  $\mu\text{M}$ . Therefore, it was only possible to calculate the prediction of the  $\text{IC}_{50}$  (best-fit values of the curve). The  $\text{IC}_{50}$  value was determined by nonlinear regression (curve fit) using log10 (inhibitor) versus response (four parameters) model in GraphPad Prism v9.

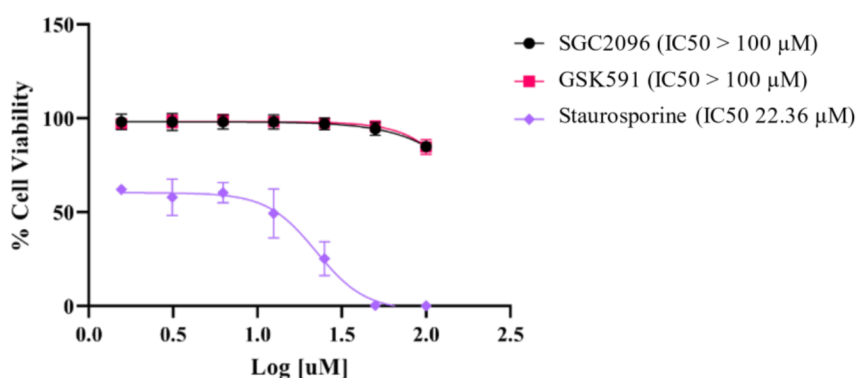


Figure 23. Cell viability assay for the determination of the  $\text{IC}_{50}$  and cytotoxicity of the PRMT5 compound GSK591 and its negative control SGC2096.

It was previously published that the compound GSK591 inhibits the proteins that are symmetrically dimethylated on arginine residues by PRMT5 (meaning the downstream target for PRMT5) (SACHAMITR et al., 2021). To recapitulate (validate) this experimental system in our lab, we used HEK293T cells treated with GSK591 and with the negative control SGC2029 at a final concentration of 6.25  $\mu\text{M}$ , which is in the range of no cytotoxicity. In Figure 25, the treatment with GSK591 inhibited the SDMA proteins (proteins that are symmetrically dimethylated on arginine residues) di-methylated by PRMT5, and no inhibition of di-methylation was observed in the condition of treatment with the negative control compound.

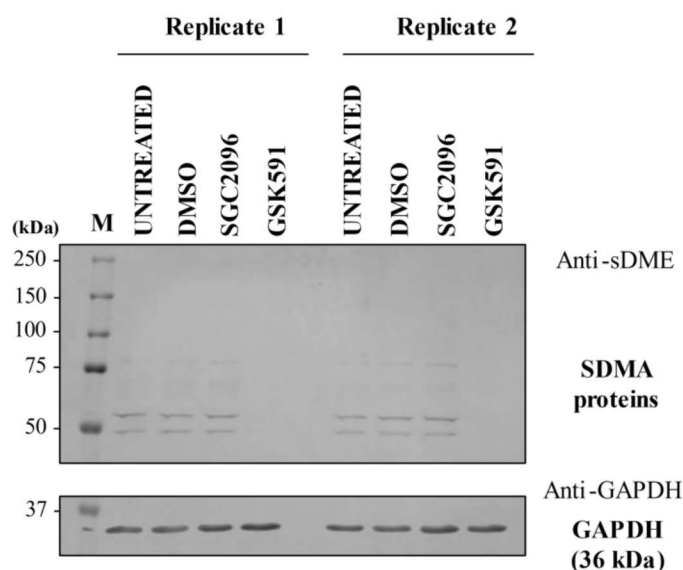


Figure 24. Western blot confirming the inhibition of PRMT5 activity with GSK591 (6.25  $\mu$ M) compound and the absence of inhibition by the negative control SGC2096 (6.25  $\mu$ M), as well as the controls (untreated cells and cells treated with DMSO in an equal volume used as the PRMT5 compounds). The antibody Anti-sDME was used to reveal symmetric di-methyl arginine motifs (SDMA). The GAPDH housekeeping gene was used as endogenous control. Each well was loaded with 20  $\mu$ g of protein samples. M = marker; UNTREATED = Cells not treated with chemical compounds or vehicle; DMSO = Cells treated just with compounds vehicle; SGC2096 = Cell treated with SGC2096 compound; GSK591 = Cells treated with GSK591 compound.

#### 4.7. INVESTIGATION OF METHYLATION SITES IN BICC1 CO-IMMUNOPRECIPITATED IN CONDITIONS OF PRMT5 INHIBITION WITH GSK591

As mentioned in the methods, Methyl (KR) modifications were identified in the MS data. Thus, two additional experimental conditions were sent to the MS after the confirmation of BICC1 Co-IP and PRMT5 activity inhibition, aiming to identify this type of post-translational modifications in BICC1 (Figure 26).

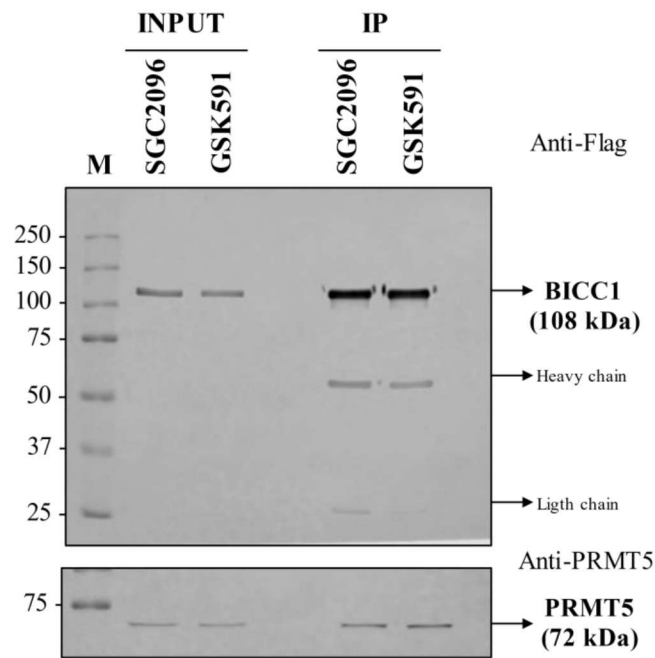


Figure 25. Immunoprecipitation of BICC1 FL protein in cells treated with GSK591 and SGC2096 compounds for evaluation of methylation sites. Western blotting confirming BICC1 Co-IP. IN = Input (the sample before immunoprecipitation, qs 20  $\mu$ g BSA-Eq); IP = Immunoprecipitated (20% of the eluate); SGC2096 = Cell treated with SGC2096 compound; GSK591 = Cells treated with GSK591 compound.

Three methylation sites were identified in BICC1, with two sites located in lysine residues (K592 and K218) and one in arginine residues (R345), as shown in Table 4. The indicated methylation sites were identified according to Posterior Error Probability (PEP) score (lower meaning higher significance). Interestingly, when the post-translational sites were compared to the Phosphosite database, K592 was also identified with a ubiquitination modification, suggesting that this residue site is more susceptible to post-translational modification.

Table 4. Methylation sites were identified in K and R amino acid residues of BICC1 according to the PEP score (Posterior Error Probability of the identification).

UniprotID	Gene Name	Co-IP of BICC1 with GSK591 treatment			Co-IP of BICC1 with SGC2096 treatment			Positions within proteins	Phosphosite database
		#1	#2	#3	#1	#2	#3		
Q9H694; A6NGY7	BICC1	-	-	-	-	0.0229248	-	K592; K218	K592-ub; -
Q9H694	BICC1	3,59E-09	-	2,24E-07	9,43E-04	4,27E+00	0.0110764	R345	-

Ub = Ubiquitination.



From the experiments done so far, it was not possible to correlate the inhibition of PRMT5 activity with a decrease of the methylation sites in R residues of BICC1, since only one site was identified with this type of methylation in both conditions of Co-IP (GSK591 and SGC2096). There were no reported methylation modifications found in the BICC1 protein sequence and so far, this work is the first study that tries to identify methylation sites in BICC1 and to correlate with a methyltransferase, in this case PRMT5. It is important to highlight that the fact that we did not detect more methylation sites does not mean that there is no. Thus, more experiments and replicates would be needed to investigate this PTM in the BICC1 protein sequence.

As a complementation to the investigation of methylation sites in BICC1, a Protein arginine methylation Predictor (PRmePRed) was used to predict potential arginine residue sites that could be methylated in BICC1 protein sequence. In [Attachment 9](#), the peptide sequences are listed with the R site positions. The R345 site was not predicted by the PRmePRed.

#### 4.8. INVESTIGATION OF THE CANONICAL WNT/ $\beta$ -CATENIN SIGNALING ACTIVITY IN CONDITIONS OF PRMT5 INHIBITION WITH GSK591 AND PRMT5 OVEREXPRESSED TOGETHER WITH BICC1 CONSTRUCTS (FL AND $\Delta$ SAM)

Since BICC1 is reported as a modulator of the Wnt/ $\beta$ -catenin pathway (KRAUS et al., 2012), it was also investigated if the modulation of PRMT5 activity in cells can contribute to changes in the activity of this signaling pathway. As described in the methods, a GFP reporter gene assay was used to verify the activity of the Wnt/ $\beta$ -catenin pathway and two controls were used to assess the efficacy of the method: a positive control (CTL +) upon ectopic expression  $\beta$ -catenin-Flag protein, and negative control with cells not treated with the reporter gene vector (NT) that were used as a baseline of “no GFP” detection in the flow cytometer. The normalization of the flow cytometry data, represented in Figure 29A, was performed using 0 % of FITC-A intensity as the mean of GFP events in the NT condition, and 100 % as the mean of GFP events in the FL condition, since it is the condition that was compared with the other.

In Figures 27A and 27B, it is possible to confirm the activity of the pathway and the increase of the  $\beta$ -catenin protein according to the CTL (+), when compared to the condition of the cells that were only treated with the reporter gene (Condition NT+TCF). The condition NT+TCF was important to observe the Wnt/ $\beta$ -catenin pathway activity without ectopic expressing BICC1 (FL and  $\Delta$ SAM) and inhibiting PRMT5 activity.

When BICC1 was expressed in cells (FL and  $\Delta$ SAM), an increase of the pathway activity was observed with the FL, while the  $\Delta$ SAM condition showed a decrease when compared with FL, however, no significance was observed. Intriguingly, the literature points to the opposite, indicating Wnt hyperactivity when the SAM domain is mutated (KRAUS et al., 2012). Next, it was observed with the GSK591 compound treatment (GSK condition) a slight decrease of the Wnt activity (FL+GSK vs FL), while no difference between ( $\Delta$ SAM vs  $\Delta$ SAM+GSK) (Figure 27A). None of these comparisons were statistically significant. The western blotting shown in Figure 27B, nevertheless, did not show a strong difference between the GFP protein intensity. The conditions with the control of the GSK591 compound (SGC conditions) showed a decrease in the GFP expression in Figure 29A, and the conditions just with the PRMT5 compounds (GSK and SGC) showed a strong decrease in the pathway activity when compared to the positive control and the conditions with the BICC1 expression. However, no difference when compared with NT+TCF, suggesting that the transfection with only the reporter gene and the compounds did not up/down-regulate Wnt pathway activity, as observed in the conditions of BICC1 and PRMT5 ectopic expression. Curiously, cells treated only with GSK591 compound (GSK condition) showed lower Wnt pathway activity in Replicate 1 (showed in Figure 27), in both flow cytometry and western blotting assay, however, replicate 2 (showed in [Attachment 10](#)) did not. Therefore, transfection must not have been as efficient in this replicate.

Cyclin D1 is important to the control of the G1 phase of the cell cycle and is also reported as an upregulated target gene of the Wnt/ $\beta$ -catenin pathway in some cancers, such as adenocarcinoma (LECARPENTIER et al., 2019; SHTUTMAN et al., 1999). In addition, studies are reporting the association of PRMT5 expression with Cyclin D1 in some kinds of cancer, such as lymphoma and oropharyngeal squamous cell carcinoma (KARKHANIS et al., 2020; KUMAR et al., 2017a). Therefore, the expression of Cyclin D1 was also investigated, aiming to identify a possible regulation of BICC1 in the expression of this protein and the impact of the PRMT5 activity inhibition in this regulation. We observed a possible decrease in Cyclin D1 protein expression when FL was ectopically expressed and PRMT5 activity was inhibited with the GSK591 compound (Figure 27B). When cells were treated only with GSK591 or ectopically expressed with FL, no difference was observed in the protein expression of Cyclin D1. In [Attachment 10](#), we show the duplicate of the western blotting. Nevertheless, the WB quantification did not show consistency with the replicate 2, with large standard deviation

values. Thus, more experiments and replicates are needed to confirm these results of Wnt/ $\beta$ -catenin activity and its modulation by BICC1 ectopic expression and PRMT5 inhibition.

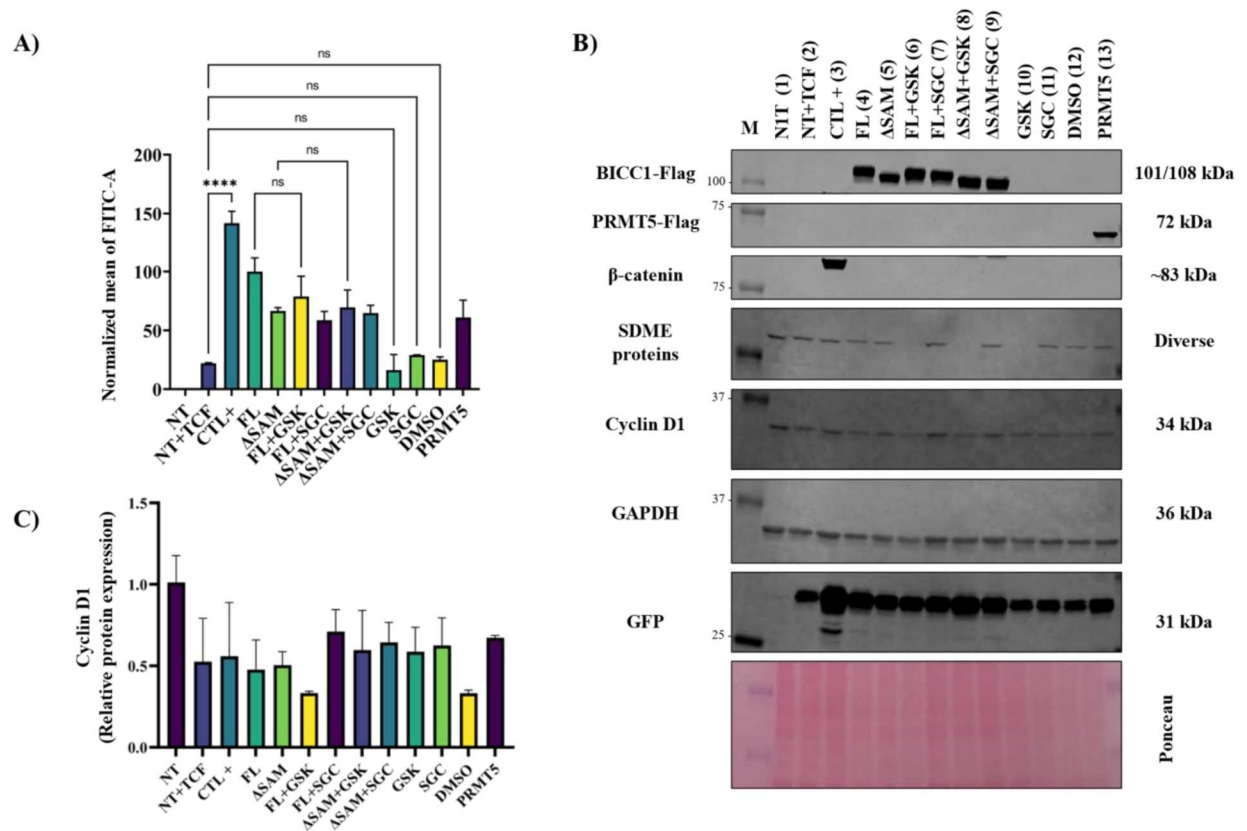


Figure 26. Investigation of Wnt  $\beta$ -catenin activity through reporter gene assay, modulating BICC1 expression and inhibiting PRMT5 activity. A) Measurement of GFP intensity through flow cytometry; B) Representative replicate of Western blotting confirming the efficiency of GSK591 compounds for inhibition of SDMA modifications, BICC1 ectopic expression, GFP expression, and expression of Wnt gene targets (cyclin D1); C) Cyclin D1 relative protein expression quantification using ImageJ software and GAPDH protein expression as control of the protein loading amount in the gel. The data is shown as the normalized mean of duplicates and standard deviation (SD). The GAPDH housekeeping gene was used as endogenous control. Each well was loaded with 40  $\mu$ g of protein sample. M = marker; ns = not significant; \*\*\*\* = p-value < 0.001.

## 5. DISCUSSION AND PERSPECTIVES

In this study, the protein interactome of the Human protein Bicaudal C Homolog 1 (BICC1) was explored through co-immunoprecipitation followed by mass spectrometry (Co-IP-MS) to expand the information on this protein function. In databases of protein-protein interactions, such as BioGRID, most of the interactors reported are still from high-throughput experiments.

The first step of this study was to investigate the proteins identified by Co-IP-MS through the creation of PPIN and GO analysis. To achieve this first objective, a bioinformatic pipeline established in our group was created, as illustrated in Figure 8. According to our bioinformatic analysis, 19 proteins were present in all conditions of Co-IPs, which means proteins that are co-immunoprecipitating with BICC1 in RNA and SAM domain independence, as shown in Figure 14. Besides that, in the conditions of BICC1 Co-IP in the presence of RNA, we obtained a higher number of proteins containing RBDs, which is a result that gives a higher confidence to compare the conditions of Co-IPs in the presence and absence of RNase A treatment (these proteins with RBDs were listed in Table 3).

Regarding the functional annotation, splicing-related proteins were identified with significative enrichment values in the PPIN ( $FDR < 0.05$ ), as shown in Figure 16. Interestingly, many of them were also present in the conditions of RNA dependence, as illustrated in the PPINs of Figures 17A and 17B. According to this analysis at Cytoscape using the STRING plugin, 10 proteins were associated with mRNA splicing, via spliceosome, and 8 of them were exclusive of RNA-dependent Co-IP conditions. There is no study so far pointing to BICC1's association with mRNA splicing in cells. As BICC1 is an RBP, indeed could be possible its role in mRNA processing activities, as splicing, and our study could identify potential protein-partners of BICC1 associated with this important biological process in the cell.

Proteins with cellular localization in biomolecular condensates (E.g., P-bodies, SG, and cajal bodies) were also enriched in the PPINs. These proteins are characterized as membrane-less organelles proteins (MLO), which are a type of pro-survival structures formed when cells are exposed to multiple stresses (FEFILOVA et al., 2022). MLOs do not contain a lipid membrane but rather are assembled from liquid-liquid phase separation (LLPS) of biopolymers and protect cells from genetic damage during stress conditions (FEFILOVA et al., 2022). In total, 52 proteins were classified in this class (as colored in Figure 16B), however, the RNA granule database showed that more proteins from our Co-IP-MS lists are associated with this class of proteins (66 from the total of 71 proteins identified). Indeed, BICC1 associates

with SG when translation is inhibited, and the SAM domain is pointed out as especially important for BICC1 recruitment to RNA-processing bodies (P-bodies) (ESTRADA MALLARINO et al., 2020; JY et al., 2018). CSDE1 was shown in this study co-immunoprecipitating with BICC1 and it is an important protein that participates in the formation of SG (JY et al., 2018) and P-bodies (KAKUMANI et al., 2020). Interestingly, CSDE1 was already identified as co-immunoprecipitating with BICC1 in a high-throughput study (JY et al., 2018). However, there is no study so far investigating this interaction between BICC1-CSDE1 further.

Another interesting example of MLO protein that was identified as co-immunoprecipitating with BICC1 in this study, is the protein PSMA4 (Proteasome subunit alpha type-4). This protein is reported as located in P-bodies (BERCHTOLD; BATTICH; PELKMANS, 2018). Both proteins (CSDE1 and PSMA4) had a relatively high sequence coverage and many unique peptides were identified when compared to other proteins in the Co-IP lists. Unfortunately, our group does not have the antibodies against CSDE1 and PSMA4 to further explore their interaction with BICC1. One alternative strategy for future experiments in our group is cloning these proteins with a different tag than Flag (E.g., His tag) from a cDNA template of HEK293T cells.

Other protein groups were also enriched in the Co-IP-MS lists. TCP-1 chaperonin proteins were identified as co-immunoprecipitating with BICC1 (CCT2, CCT3, CCT4, CCT6A, and CCT7), and these proteins are reported as important to cajal bodies regulations, which are subnuclear structures capable of RNA modification and assembly (FREUND et al., 2014). These structures are membraneless organelles, or biomolecular condensates, as SG and P-bodies, and chaperones are key players in the regulation of condensates (XIA, 2022). Another group of proteins that also drew attention is from the family 14-3-3 since there were five identified in the Co-IP-MS data, and two of them were also reported in the BioGRID database (YWHAH and YWHQ, see Figure 28). These proteins are reported as important players in kidney cells, as a glomerular epithelial cell (YASUDA et al., 2023), similarly with BICC1, which has important roles in kidney development (STAGNER et al., 2009). So far, there is no study relating BICC1 with this protein family and kidney disease development.

After the PPIN and GO analysis, we were able to identify new protein partners of BICC1 through different molecular biology assays, contributing to the validation of the data obtained from the Co-IP-MS. PRMT5, STK38, IGF2BP1, and PARP1 were shown to be new protein partners of BICC1 through different experimental approaches (Co-IP-MS, Co-IP-WB,

and IF), in which IGF2BP1 showed to be an RNA-dependent and SAM domains-independent interaction. CCT2 also appeared in the IP of BICC1, independently of the SAM domain, although it was also present in the IP of GFP, as shown in Figure 20. Thus, this interaction with BICC1 may be unspecific. The IF of BICC1 and IGF2BP1 was not possible to perform due to the lack of antibody availability.

The IF assays showed that BICC1 is predominantly a cytoplasmatic protein and its overexpression produced structures like biomolecular condensates in cells (see Figure 19). Indeed, there are studies about BICC1 indicating its localization in P-bodies and SG, even in the absence of treatments for stress stimulation (ESTRADA MALLARINO et al., 2020). The co-localization of BICC1 with some of its protein partners confirmed through Co-IP-MS and Co-IP-WB was investigated through IF: PRMT5 and PARP1. PRMT5 showed a positive Pearson's correlation, meaning that the fluorophores are probably co-localizing in some regions of the cell. The IF of BICC1 with the PARP1 showed a strong difference between the cellular localization of both proteins, with PARP1 in the nuclei (negative Pearson's correlation).

Interestingly, in this study, PARP1 was observed co-immunoprecipitating with BICC1 strongly in the presence of RNA through both Co-IP-MS and Co-IP-MS. There are studies reporting PARP1 as important to mRNA processing through catalytic activity and direct PPI with RBPs, and modulating the chromatin structure to the splicing activity (KIM et al., 2020). Indeed, in cells identified in the prophase/metaphase cell cycle phase, when the nuclei are disassembled (as shown in Figure 24), we observed the co-localization of BICC1 and PARP1 using the IF approach with SIM microscopy.

It is important to highlight that the MS, WB, and IF techniques were chosen to investigate the PPI in this study since are traditional techniques that are used in studies of PPI (HOU et al., 2018; SIMABUCO et al., 2019). However, other techniques could be performed to verify the physical interaction between the proteins: Two-hybrid screening (ELMORE; VELÁSQUEZ-ZAPATA; WISE, 2023), fluorescence resonance energy transfer (FRET) (TRUONG; IKURA, 2001), and Cross-Linking Mass Spectrometry (XL-MS) (LENZ et al., 2021), are examples of other PPI validation assays.

The interaction of BICC1 with the methyltransferase PRMT5 was chosen for further investigation due to its biological importance as a modulator of splicing, methylating important proteins that form the spliceosome complex, the Sm proteins (STOPA; KREBS; SHECHTER, 2015). Also, PRMT5 is the primary enzyme responsible for the di-methylation of arginine residues, and studies have shown that the loss and inhibition of PRMT5 activity

decreased cell proliferation during cancer development, and PRMT5 is in general upregulated in many types of cancers, such as glioblastoma, breast and lung cancers (JING et al., 2018; RENGASAMY et al., 2017; SACHAMITR et al., 2021). Consistently, the BICC1 interactome data have shown the biological process of mRNA splicing enriched in the PPIN, and 5 of the splicing proteins listed in Figure 16B are reported as PRMT5 protein partners in the BioGRID database: U2AF2, SFPQ, NONO, PABPC1, and SNRNPB. In addition, WDR77 (or MEP50), which is the protein partner of BICC1 in the methylosome complex (ANTONYSAMMY et al., 2012), appeared in Co-IP-MS with a high sequence coverage and number of unique peptides. Thus, we followed up on the investigation of the BICC1-PRMT5 interaction.

We first searched for methylation sites in BICC1 with the modulation of PRMT5 activity through its inhibition with the GSK591 compound, and its control SGC2096. One arginine residue at position 345 (R345) was identified as methylated in the BICC1 protein sequence, however, it was not possible to relate it to the GSK591 treatment, since this modification was also present in the condition of treatment with SGC2096 (see Table 4). The reason that just one R site methylated was found could be explained by the fact that trypsin digestion cleaves the C-terminal of K and R amino acid residues, therefore, this result could be due to a limitation of the technique.

The methylation predictor called PRmePRed was also used to identify if BICC1 can be methylated by PRMTs. This predictor has high accuracy (score of 0.8683) and uses a dataset that contains 6754 methylation sites from 2077 protein sequences, according to Kumar et al. (KUMAR et al., 2017b). A total of 28 sites were predicted and, interestingly, two were predicted in the “GXXG” conserved loop in the KH1 and KH2 domains of BICC1. However, the unique peptides of BICC1 that were identified in the MS were aligned with the BICC1 protein sequence, and the “GXXG” loops of KH1 and KH2 were covered in the MS, and the R methylation was not detected. This result may suggest that the interaction of BICC1 with PRMT5 could be not due to BICC1 methylation but to other reasons, such as protein localization and RNA-protein interaction regulation, since BICC1 is an RBP. However, more studies are needed to investigate BICC1 methylation by PRMT5, one possible experiment is *in vitro* assays with both proteins purified and the substrates for PRMT5 enzymatic activity.

Besides the investigation of BICC1 protein methylation by PRMT5, the activity of the Wnt/ $\beta$ -catenin pathway was also explored, since it is well-established that BICC1 has a negative role in this signaling pathway (KRAUS et al., 2012; ROTHÉ et al., 2015). The results showed an increase in the activity of the pathway with the ectopic expression of the BICC1-FL

construct when compared with the expression of the BICC1- $\Delta$ SAM construct. The literature points out the opposite, that BICC1 negatively regulates the Wnt pathway at the level of the Dishevelled 2 protein (KRAUS et al., 2012; ROTHÉ et al., 2015). Nevertheless, in this study, the cells were not co-transfected with Dvl2 protein as demonstrated in these other two studies that point to the negative role of BICC1 in this pathway. Therefore, it is possible to consider that the reporter gene assay proposed in this study has different conditions than the assays already published in the literature, and without the Dvl2 co-transfection, we are not stimulating the Wnt pathway at the level of Dvl2. Also, the reporter gene used in this present study is with GFP expression, and the other one used in these two studies cited is with luciferase. Indeed, studies are reporting that luciferase is more sensitive in reporter gene assays than GFP reporters, and there are troubleshooting regarding the latter, as background, autofluorescence, and light scattering. In future experiments, our group proposes to investigate the activity of this pathway using a luciferase system of a reporter gene.

Cyclin D1, which is a gene target of the Wnt pathway, seemed to be downregulated in the conditions with GSK591 treatment and FL ectopic expression (see WB of both replicates shown in Figure 27B and Attachment 10, and protein quantification in Figure 27C). Cyclin D1 is an important gene that plays an oncogene function when in general is overexpressed, and studies are pointing that its downregulation is linked with therapeutical improvements against cancer (ALAO et al., 2006; SHTUTMAN et al., 1999). If these results observed are real, we can hypothesize that BICC1-FL modulates the Wnt/ $\beta$ -catenin pathway and the PRMT5 inhibition decreases Cyclin D1 expression. In a disease context, this result could be relevant, since BICC1 is reported as upregulated in some kinds of cancer, such as gastric and pancreatic cancer (MENG et al., 2023; ZHAO et al., 2020), and cyclin D1 is pointed as an oncogene (ALAO et al., 2006; LEHN et al., 2010). Nevertheless, more studies would be needed to prove this.

Besides the investigation between BICC1 and PRMT5 interaction presented in this interactome study, according to the literature, there is a well-established interaction of BICC1 with the proteins ANKS3 and ANKS6 (ankyrin repeat and sterile alpha motif domain containing 3/6), through their SAM domain. These interactions are reported as linked to ciliopathies, such as polycystic kidney disease since many proteins with SAM domain were found mutated in patients with these diseases (BAKEY et al., 2015; ROTHÉ et al., 2018). However, in the protein interactome data generated in this study, these proteins were not identified. This can be due to the difference within the assays, in which ANKS3 and ANKS6



were co-expressed together with BICC1 using different tags for each protein (Flag, GFP, and V5) followed by Co-IP of ANKS6 in HEK293T cells (YAKULOV et al., 2015). Therefore, as in this present study ANKS3/ANKS6 were not ectopically expressed in the cells, it is possible to suggest that the interaction of BICC1-Flag with the endogenous ANKS3/ANKS6 was not strong enough to detect through Co-IP-MS in our samples.

We also searched for protein partners of BICC1 in Interactome databases. The Biological General Repository for Interaction Datasets (BioGRID) is a public database that contains more than 2,650,520 interactions (last search on October 26<sup>th</sup>, 2023) reported in high-throughput studies, as well as individual research (STARK et al., 2006). Furthermore, BioGRID is used to store protein and genetic interaction data from biomedical studies that are focused on humans and other species (OUGHTRED et al., 2019). The BICC1 protein was searched in this database, and within the 23 Human proteins identified (proteins illustrated in the PPIN of Figure 30A), 14 proteins were classified as interactors with physical high-throughput evidence: ANKS3, CAPZA2, CELF1, CSDE1, DAZL, EIF4ENIF1, FAM120C, KIAA1429, NEK7, NUP35, TFG, YWHAG, YWHAH and YWHAQ. Other 7 proteins were classified as interactors with physical low-throughput evidence: PRRC2A, PUM1, R3HDM2, RBM47, RBMS1, UBAP2L, and YTHDF3. Finally, 2 proteins were classified as interactors with genetic high-throughput evidence: CSK and SPPL3. All these works that reported BICC1 as a protein partner are not focused on BICC1 protein interactome, except for ANKS3.

When all these 23 proteins found in BioGRID were searched on the STRING web server (SNEL et al., 2000; SZKLARCZYK et al., 2019) to generate the PPIN, there were few proteins with connection with each other, except for ANKS3 and CSDE1 (Figure 28A). Regarding functional enrichment, the biological process of stress granule assembly (Proteins CSDE1, UBAP2L, YTHDF3, CELF1, and PUM1) was one of the most enriched (Figure 28B).

Our Co-IP-MS data also showed an enriched of biomolecular condensates proteins, such as SG proteins, indicated in Figure 16B. SG structures are mostly composed of RNA (78-95%) (KHONG et al., 2017) and RBPs can form ribonucleoprotein granules (complexes of RNAs and proteins) (CAMPOS-MELO et al., 2021). The assembly of SG occurs during periods of stress in the cells, resulting in the LLPS, which is a process mainly influenced by weak electrostatic, hydrophobic, and PPI between RBPs that have disordered regions in their structure (CAMPOS-MELO et al., 2021; LIN et al., 2015; MOLLIEUX et al., 2015). Interestingly, our *in-silico* prediction of BICC1 to form potential phase separation (PSPredictor (CHU et al., 2022))

showed a high positive score equal to 0.9919, indicating that BICC1 may have disordered regions in its structure.

In summary, we have characterized the BICC1 interactome in RNA and SAM domain dependence, identifying new protein partners of BICC1 never described before (PRMT5, STK38, IGF2BP1, and PARP1) and new biological processes that BICC1 may play a role (mRNA splicing, via spliceosome). In addition, many of the proteins Co-Immunoprecipitated with BICC1 were associated with LLPS processes. The Co-IP of BICC1-FL without the digestion of RNA with RNase A was more enriched in the number of proteins identified when compared to the conditions with RNase A treatment. This result showed that the RNA presence has an impact on the interaction of BICC1 with other proteins, and seems to be important to the formation of a more complete BICC1 protein interactome in the cell.

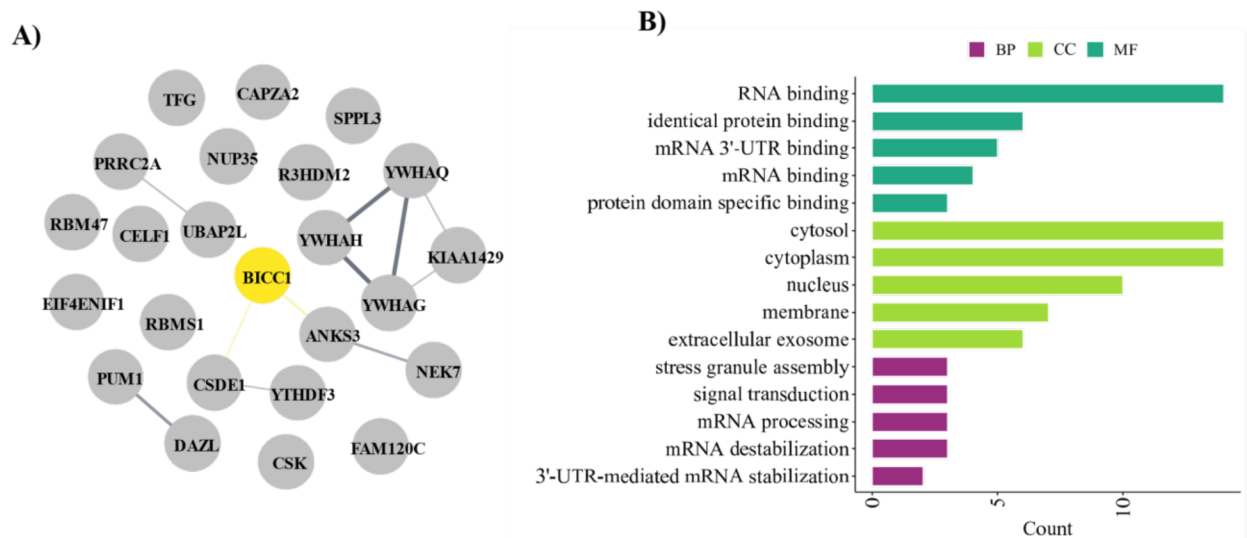


Figure 27. Protein-protein interaction network of protein interactors of BICC1 according to the BioGRID database. The network type was set up for physical interactions and clustered in 3 groups using k means. PPI enrichment p-value: 4.42E-05. Biological processes – BP, cellular component – CC, and molecular functions – MF.

## 6. CONCLUSIONS

The main conclusions of this work can be summarized in the following topics:

- BICC1 interactome shows enrichment of pathways related to biological processes of mRNA splicing and cellular components of methylosome complex and biomolecular condensates (stress granules, P-bodies, and cajal bodies);
- The number of proteins identified in the conditions with RNase A treatment decreased, suggesting the importance of the RNA presence to the protein-protein interaction of BICC1;
- Three proteins identified as protein partners of BICC1 in highthrouput studies (CSDE1, YWHAH, and YWHAQ) are also identified in the interactome data of this present study, suggesting that these proteins are potential protein partners of BICC1 and may be important for biological processes regulated by BICC1;
- BICC1-Flag co-immunoprecipitates with PRMT5, STK38, IGF2BP1 and PARP1 in HEK293T cells though Co-IP-MS and Co-IP-WB;
- The BICC1 interaction with IGF2BP1 shows RNA dependence and SAM domain independence, suggesting that this interaction happens through KH-domain interaction.

## 7. REFERENCES

ALAO, J. P. et al. The cyclin D1 proto-oncogene is sequestered in the cytoplasm of mammalian cancer cell lines. **Molecular Cancer**, v. 5, 2006.

ANTONYSAMY, S. et al. Crystal structure of the human PRMT5:MEP50 complex. **Proceedings of the National Academy of Sciences of the United States of America**, v. 109, n. 44, p. 17960–17965, 30 out. 2012a.

ANTONYSAMY, S. et al. Crystal structure of the human PRMT5:MEP50 complex. **Proceedings of the National Academy of Sciences of the United States of America**, v. 109, n. 44, p. 17960–17965, 30 out. 2012b.

BAKEY, Z. et al. The SAM domain of ANKS6 has different interacting partners and mutations can induce different cystic phenotypes. **Kidney International**, v. 88, n. 2, 2015.

BERCHTOLD, D.; BATTICH, N.; PELKMANS, L. A Systems-Level Study Reveals Regulators of Membrane-less Organelles in Human Cells. **Molecular Cell**, v. 72, n. 6, 2018.

BOLTE, S.; CORDELIÈRES, F. P. **A guided tour into subcellular colocalization analysis in light microscopy.** **Journal of Microscopy**, 2006.

BRANSCOMBE, T. L. et al. PRMT5 (Janus Kinase-binding Protein 1) Catalyzes the Formation of Symmetric Dimethylarginine Residues in Proteins. **Journal of Biological Chemistry**, v. 276, n. 35, 2001.

BULL, A. L. Bicaudal, a genetic factor which affects the polarity of the embryo in *Drosophila melanogaster*. **Journal of Experimental Zoology**, v. 161, n. 2, p. 221–241, 1 mar. 1966.

CAMPOS-MELO, D. et al. **The Integral Role of RNA in Stress Granule Formation and Function.** **Frontiers in Cell and Developmental Biology**, 2021.

CHEN, S. et al. Serum BICCI levels are significantly different in various mood disorders. **Neuropsychiatric Disease and Treatment**, v. 15, p. 259–265, 2019.

CHONG, P. A.; VERNON, R. M.; FORMAN-KAY, J. D. **RGG/RG Motif Regions in RNA Binding and Phase Separation.** **Journal of Molecular Biology**, 2018.

CHU, X. et al. Prediction of liquid–liquid phase separating proteins using machine learning. **BMC Bioinformatics**, v. 23, n. 1, 2022.

CHUA, H. N.; WONG, L. Increasing the reliability of protein interactomes. **Drug Discovery Today**, v. 13, 2008.

CORLEY, M.; BURNS, M. C.; YEO, G. W. **How RNA-Binding Proteins Interact with RNA: Molecules and Mechanisms. Molecular Cell** Mol Cell, , 2 abr. 2020. Disponível em: <<https://pubmed.ncbi.nlm.nih.gov/32243832/>>

DE LAS RIVAS, J.; FONTANILLO, C. Protein-protein interactions essentials: Key concepts to building and analyzing interactome networks. **PLoS Computational Biology**, v. 6, n. 6, 2010.

DOWDLE, M. E. et al. Bicaudal-C Post-transcriptional regulator of cell fates and functions. **Frontiers in Cell and Developmental Biology**, v. 10, 7 set. 2022.

ELMORE, J. M.; VELÁSQUEZ-ZAPATA, V.; WISE, R. P. Next-Generation Yeast Two-Hybrid Screening to Discover Protein–Protein Interactions. Em: **Methods in Molecular Biology**. [s.l: s.n.]. v. 2690.

ESTRADA MALLARINO, L. et al. Nephronophthisis gene products display RNA-binding properties and are recruited to stress granules. **Scientific Reports**, v. 10, n. 1, 2020.

FEFILOVA, A. S. et al. **Stress-Induced Membraneless Organelles in Eukaryotes and Prokaryotes: Bird’s-Eye View. International Journal of Molecular Sciences**, 2022.

FREUND, A. et al. Proteostatic control of telomerase function through TRiC-mediated folding of TCAB1. **Cell**, v. 159, n. 6, 2014.

FU, Y. et al. Loss of Bicc1 impairs tubulomorphogenesis of cultured IMCD cells by disrupting E-cadherin-based cell-cell adhesion. **European Journal of Cell Biology**, v. 89, n. 6, 2010.

GEBAUER, F. et al. **RNA-binding proteins in human genetic disease. Nature Reviews Genetics**, 2021.

**GSK591** | **SGC**. Disponível em: <<https://www.thesgc.org/chemical-probes/GSK591>>. Acesso em: 2 maio. 2023.

*Characterizing the Interactome of the RNA-binding Protein BICC1*

HATEBOER, N. et al. Comparison of phenotypes of polycystic kidney disease types 1 and 2. European PKD1-PKD2 Study Group. **Lancet (London, England)**, v. 353, n. 9147, 1999.

HOU, C. et al. Profiling the interactome of protein kinase C  $\zeta$  by proteomics and bioinformatics. **Proteome Science**, v. 16, n. 1, 2018.

JING, P. et al. **The methylation induced by protein arginine methyltransferase 5 promotes tumorigenesis and progression of lung cancer.** **Journal of Thoracic Disease**, 2018.

JOFFRE, C. et al. **STK38 at the crossroad between autophagy and apoptosis.** **Autophagy**, 2016.

JY, Y. et al. High-Density Proximity Mapping Reveals the Subcellular Organization of mRNA-Associated Granules and Bodies. **Molecular cell**, v. 69, n. 3, p. 517-532.e11, 1 fev. 2018.

KAKUMANI, P. K. et al. CSDE1 controls gene expression through the miRNA-mediated decay machinery. **Life Science Alliance**, v. 3, n. 4, 2020.

KARKHANIS, V. et al. Protein arginine methyltransferase 5 represses tumor suppressor miRNAs that down-regulate CYCLIN D1 and c-MYC expression in aggressive B-cell lymphoma. **Journal of Biological Chemistry**, v. 295, n. 5, 2020.

KHONG, A. et al. The Stress Granule Transcriptome Reveals Principles of mRNA Accumulation in Stress Granules. **Molecular Cell**, v. 68, n. 4, 2017.

KIM, C. A.; BOWIE, J. U. SAM domains: uniform structure, diversity of function. **Trends in biochemical sciences**, v. 28, n. 12, p. 625–628, 2003.

KIM, D. S. et al. **PARPs and ADP-ribosylation in RNA biology: From RNA expression and processing to protein translation and proteostasis.** **Genes and Development**, 2020.

KRAUS, M. R. C. et al. Two mutations in human BICC1 resulting in wnt pathway hyperactivity associated with cystic renal dysplasia. **Human Mutation**, v. 33, n. 1, 2012.

KUMAR, B. et al. Nuclear PRMT5, cyclin D1 and IL-6 are associated with poor outcome in oropharyngeal squamous cell carcinoma patients and is inversely associated with p16-status. **Oncotarget**, v. 8, n. 9, 2017a.

KUMAR, P. et al. PRmePRed: A protein arginine methylation prediction tool. **PLoS ONE**, v. 12, n. 8, 2017b.

KWAK, Y. T. et al. Methylation of SPT5 regulates its interaction with RNA polymerase II and transcriptional elongation properties. **Molecular Cell**, v. 11, n. 4, 2003.

LECARPENTIER, Y. et al. **Multiple Targets of the Canonical WNT/ $\beta$ -Catenin Signaling in Cancers**. **Frontiers in Oncology**, 2019.

LEHN, S. et al. Down-regulation of the oncogene cyclin D1 increases migratory capacity in breast cancer and is linked to unfavorable prognostic features. **American Journal of Pathology**, v. 177, n. 6, 2010.

LENZ, S. et al. Reliable identification of protein-protein interactions by crosslinking mass spectrometry. **Nature Communications**, v. 12, n. 1, 2021.

LI, J. et al. Normalization, testing, and false discovery rate estimation for RNA-sequencing data. **Biostatistics**, v. 13, n. 3, 2012.

LI, W. JUAN et al. Profiling PRMT methylome reveals roles of hnRNPA1 arginine methylation in RNA splicing and cell growth. **Nature Communications**, v. 12, n. 1, 2021.

LIAN, P. et al. Loss of polycystin-1 inhibits Bicc1 expression during mouse development. **PLoS ONE**, v. 9, n. 3, 2014.

LIANG, Z. et al. Protein Arginine Methyltransferase 5 Functions via Interacting Proteins. **Frontiers in Cell and Developmental Biology**, v. 9, 2021.

LIN, Y. et al. Formation and Maturation of Phase-Separated Liquid Droplets by RNA-Binding Proteins. **Molecular Cell**, v. 60, n. 2, 2015.

LIU, Y. et al. **Biomolecular phase separation in stress granule assembly and virus infection**. **Acta Biochimica et Biophysica Sinica**, 2023.

LOVCI, M. T.; BENGTON, M. H.; MASSIRER, K. B. Post-translational modifications and RNA-binding proteins. Em: **Advances in Experimental Medicine and Biology**. [s.l: s.n.]. v. 907.

*Characterizing the Interactome of the RNA-binding Protein BICC1*

MA, X. et al. Multi-omics analysis revealed the role of CCT2 in the induction of autophagy in Alzheimer's disease. **Frontiers in Genetics**, v. 13, 2023.

MAISONNEUVE, C. et al. Bicaudal C, a novel regulator of Dvl signaling abutting RNA-processing bodies, controls cilia orientation and leftward flow. **Development (Cambridge, England)**, v. 136, n. 17, p. 3019–3030, 1 set. 2009.

MENG, F. et al. Lymph node metastasis related gene BICC1 promotes tumor progression by promoting EMT and immune infiltration in pancreatic cancer. **BMC Medical Genomics**, v. 16, n. 1, p. 263, 25 out. 2023.

MILLAR, S. R. et al. **A New Phase of Networking: The Molecular Composition and Regulatory Dynamics of Mammalian Stress Granules**. **Chemical Reviews**, 2023.

MOLLIEX, A. et al. Phase Separation by Low Complexity Domains Promotes Stress Granule Assembly and Drives Pathological Fibrillization. **Cell**, v. 163, n. 1, 2015.

MOTOLANI, A. et al. The Structure and Functions of PRMT5 in Human Diseases. **Life**, v. 11, n. 10, 1 out. 2021.

MULVANEY, K. M. et al. Molecular basis for substrate recruitment to the PRMT5 methylosome. **Molecular Cell**, v. 81, n. 17, 2021.

NUSSE, R.; CLEVERS, H. **Wnt/ $\beta$ -Catenin Signaling, Disease, and Emerging Therapeutic Modalities**. **Cell**, 2017.

OUGHTRED, R. et al. The BioGRID interaction database: 2019 update. **Nucleic Acids Research**, v. 47, n. D1, 2019.

PAL, S.; SIF, S. **Interplay between chromatin remodelers and protein arginine methyltransferases**. **Journal of Cellular Physiology**, 2007.

PESIRIDIS, G. S.; DIAMOND, E.; VAN DUYN, G. D. Role of pICLn in methylation of Sm proteins by PRMT5. **Journal of Biological Chemistry**, v. 284, n. 32, 2009.

PFISTER, A. S.; KÜHL, M. Of Wnts and Ribosomes. **Progress in Molecular Biology and Translational Science**, v. 153, p. 131–155, 1 jan. 2018.

RATOVITSKI, T. et al. PRMT5- mediated symmetric arginine dimethylation is attenuated by mutant huntingtin and is impaired in Huntington's disease (HD). **Cell Cycle**, v. 14, n. 11, 2015.

*Characterizing the Interactome of the RNA-binding Protein BICC1*



RENGASAMY, M. et al. The PRMT5/WDR77 complex regulates alternative splicing through ZNF326 in breast cancer. **Nucleic Acids Research**, v. 45, n. 19, p. 11106, 11 nov. 2017.

ROTHÉ, B. et al. Bicc1 Polymerization Regulates the Localization and Silencing of Bound mRNA. **Molecular and Cellular Biology**, v. 35, n. 19, p. 3339–3353, out. 2015.

ROTHÉ, B. et al. Crystal Structure of Bicc1 SAM Polymer and Mapping of Interactions between the Ciliopathy-Associated Proteins Bicc1, ANKS3, and ANKS6. **Structure**, v. 26, n. 2, p. 209–224.e6, 6 fev. 2018.

SACHAMITR, P. et al. PRMT5 inhibition disrupts splicing and stemness in glioblastoma. **Nature Communications** 2021 **12:1**, v. 12, n. 1, p. 1–17, 12 fev. 2021.

SCHULTZ, J. et al. SMART, a simple modular architecture research tool: Identification of signaling domains. **Proceedings of the National Academy of Sciences of the United States of America**, v. 95, n. 11, 1998.

SEUFERT, L. et al. RNA-binding proteins and their role in kidney disease. **Nature reviews. Nephrology**, 2021.

SHTUTMAN, M. et al. The cyclin D1 gene is a target of the  $\beta$ -catenin/LEF-1 pathway. **Proceedings of the National Academy of Sciences of the United States of America**, v. 96, n. 10, 1999.

SIMABUCO, F. M. et al. Interactome analysis of the human Cap-specific mRNA (nucleoside-2'-O-)-methyltransferase 1 (hMTTr1) protein. **Journal of Cellular Biochemistry**, v. 120, n. 4, 2019.

SNEL, B. et al. String: A web-server to retrieve and display the repeatedly occurring neighbourhood of a gene. **Nucleic Acids Research**, v. 28, n. 18, 2000.

STAGNER, E. E. et al. The polycystic kidney disease-related proteins Bicc1 and SamCystin interact. **Biochemical and Biophysical Research Communications**, v. 383, n. 1, p. 16–21, 2009.

STARK, C. et al. BioGRID: a general repository for interaction datasets. **Nucleic acids research**, v. 34, n. Database issue, 2006.

STERNBURG, E. L.; GRUIJS DA SILVA, L. A.; DORMANN, D. Post-translational modifications on RNA-binding proteins: accelerators, brakes, or passengers in neurodegeneration? **Trends in biochemical sciences**, v. 47, n. 1, p. 6–22, 1 jan. 2022.

STERNBURG, E. L.; KARGINOV, F. V. **Global Approaches in Studying RNA-Binding Protein Interaction Networks. Trends in Biochemical Sciences**, 2020.

STOPA, N.; KREBS, J. E.; SHECHTER, D. The PRMT5 arginine methyltransferase: many roles in development, cancer and beyond. **Cellular and molecular life sciences : CMLS**, v. 72, n. 11, p. 2041–2059, 1 jun. 2015.

SUN, L. et al. Structural insights into protein arginine symmetric dimethylation by PRMT5. **Proceedings of the National Academy of Sciences of the United States of America**, v. 108, n. 51, 2011.

SUN, R. et al. Development of a 3 RNA Binding Protein Signature for Predicting Prognosis and Treatment Response for Glioblastoma Multiforme. **Frontiers in Genetics**, v. 12, 18 out. 2021.

SZKLARCZYK, D. et al. STRING v11: Protein-protein association networks with increased coverage, supporting functional discovery in genome-wide experimental datasets. **Nucleic Acids Research**, v. 47, n. D1, 2019.

TRAN, U. et al. The RNA-binding protein bicaudal C regulates polycystin 2 in the kidney by antagonizing miR-17 activity. **Development**, v. 137, n. 7, 2010.

TRUONG, K.; IKURA, M. **The use of FRET imaging microscopy to detect protein-protein interactions and protein conformational changes in vivo. Current Opinion in Structural Biology**, 2001.

TSAI, W. C. et al. Arginine demethylation of G3BP1 promotes stress granule assembly. **Journal of Biological Chemistry**, v. 291, n. 43, 2016.

TSAI, W. C. et al. Histone arginine demethylase JMJD6 is linked to stress granule assembly through demethylation of the stress granule-nucleating protein G3BP1. **Journal of Biological Chemistry**, v. 292, n. 46, 2017.

VALVERDE, R.; EDWARDS, L.; REGAN, L. Structure and function of KH domains. **The FEBS journal**, v. 275, n. 11, p. 2712–2726, jun. 2008.

WEGEL, E. et al. Imaging cellular structures in super-resolution with SIM, STED and Localisation Microscopy: A practical comparison. **Scientific Reports**, v. 6, 6 jun. 2016.

WOLF, M. T. F.; HILDEBRANDT, F. Nephronophthisis. **Pediatric nephrology**, v. 26, p. 181–194, 2011.

XIA, J. Liquid-liquid phase separation: A new perspective to understanding aging and pathogenesis. **BioScience Trends**, v. 16, n. 5, 2022.

YAKULOV, T. A. et al. Anks3 interacts with nephronophthisis proteins and is required for normal renal development. **Kidney International**, v. 87, n. 6, 2015.

YASUDA, H. et al. 14-3-3 Proteins stabilize actin and vimentin filaments to maintain processes in renal glomerular podocyte. **The FASEB Journal**, v. 37, n. 10, p. e23168, 2023.

ZHAO, R. et al. BICC1 as a novel prognostic biomarker in gastric cancer correlating with immune infiltrates. **International immunopharmacology**, v. 87, 1 out. 2020.

ZHAO, Y. et al. RNA-binding proteins: Underestimated contributors in tumorigenesis. **Seminars in cancer biology**, fev. 2022.

ZHU, F. et al. PRMT5 is upregulated by B-cell receptor signaling and forms a positive-feedback loop with PI3K/AKT in lymphoma cells. **Leukemia**, v. 33, n. 12, 2019.





## ATTACHMENT 2

List of 45 proteins found in the BICC1 full length (FL) immunoprecipitation assays (in triplicates) in the presence of RNA (-), sorted by their number of unique peptides and average of sequence coverage:

UniProtID	Gene Name	Protein Name	#Peptides (1)	#Peptides (2)	#Peptides (3)	Average of Sequence Coverage (%)
<b><u>Q9H694</u></b>	<b><u>BICC1</u></b>	<b><u>Protein bicaudal C homolog 1</u></b>	<b><u>44</u></b>	<b><u>42</u></b>	<b><u>39</u></b>	<b><u>45</u></b>
O14744	PRMT5	Protein arginine N-methyltransferase 5	17	20	17	36
Q9Y3F4	STRAP	Serine-threonine kinase receptor-associated protein	11	9	11	39
O75534	CSDE1	Cold shock domain-containing protein E1	10	16	15	17
Q9BQA1	WDR77	Methylosome protein 50	10	10	10	36
P25789	PSMA4	Proteasome subunit alpha type-4	8	8	7	35
C9JIR6	PPM1B	Protein-serine/threonine phosphatase (Fragment)	7	10	10	32
P27824	CANX	Calnexin	6	2	1	14
E7ENZ3	CCT5	T-complex protein 1 subunit epsilon	5	5	5	8
P27348	YWHAQ	14-3-3 protein theta	5	8	7	14
P63104	YWHAZ	14-3-3 protein zeta/delta	5	4	3	18
Q15208	STK38	Serine/threonine-protein kinase 38	5	9	8	18
A0A0J9YYL3	PUF60	Poly(U)-binding-splicing factor PUF60 (Fragment)	4	5	7	12
A0A7I2V4N2	NONO	Non-POU domain-containing octamer-binding protein	4	4	3	9
E7EX17	EIF4B	Eukaryotic translation initiation factor 4B	4	5	5	10
P40227	CCT6A	T-complex protein 1 subunit zeta	4	3	2	6
P62258	YWHAE	14-3-3 protein epsilon	4	5	6	22
P62280	RPS11	40S ribosomal protein S11	4	4	4	20
P98175	RBM10	RNA-binding protein 10	4	7	5	7
Q15750	TAB1	TGF-beta-activated kinase 1 and MAP3K7-binding protein 1	4	3	3	6
Q9Y295	DRG1	Developmentally-regulated GTP-binding protein 1	4	4	4	13
A0A8I5KWT8	MYH9	Myosin-9	3	13	2	19
K7E1Y1	FAM32A	Protein FAM32A	3	1	3	5
P23246	SFPQ	Splicing factor, proline- and glutamine-rich	3	4	2	14
P26368	U2AF2	Splicing factor U2AF 65 kDa subunit	3	1	3	31
P26641	EEF1G	Elongation factor 1-gamma	3	3	3	27
P42677	RPS27	40S ribosomal protein S27	3	3	3	9
P55072	VCP	Transitional endoplasmic reticulum ATPase	3	3	3	33
Q04917	YWHAH	14-3-3 protein eta	3	3	2	11
Q99832	CCT7	T-complex protein 1 subunit eta	3	2	3	5

A0A0G2JLI4	DDX5	Probable ATP-dependent RNA helicase DDX5	2	3	4	5
A0A2R8YCW1	DDX3X	RNA helicase	2	2	4	6
F8W6I7	HNRNPA1	Heterogeneous nuclear ribonucleoprotein A1	2	3	2	6
H0YGW7	ABCF1	ATP-binding cassette sub-family F member 1 (Fragment)	2	1	3	5
O60825	PFKFB2	6-phosphofructo-2-kinase/fructose-2,6-bisphosphatase 2	2	2	2	4
P25705	ATP5A1	ATP synthase subunit alpha, mitochondrial	2	3	4	4
Q15365	PCBP1	Poly(rC)-binding protein 1	2	1	2	20
Q9NXV2	KCTD5	BTB/POZ domain-containing protein KCTD5	2	4	3	6
Q9Y237	PIN4	Peptidyl-prolyl cis-trans isomerase NIMA-interacting 4	2	2	3	17
O43809	NUDT21	Cleavage and polyadenylation specificity factor subunit 5	1	2	4	1
P06576	ATP5B	ATP synthase subunit beta, mitochondrial	1	2	3	0
P50991	CCT4	T-complex protein 1 subunit delta	1	2	5	10
P53999	SUB1	Activated RNA polymerase II transcriptional coactivator p15	1	2	2	8
P78371	CCT2	T-complex protein 1 subunit beta	1	2	3	1
Q8WU90	ZC3H15	Zinc finger CCH domain-containing protein 15	1	2	2	4
Q9Y2H1	STK38L	Serine/threonine-protein kinase 38-like	1	3	2	5

### ATTACHMENT 3

List of 33 proteins found in the BICC1 full-length (FL) immunoprecipitation assays (in triplicates) in the absence of RNA (+), sorted by their number of unique peptides and average of sequence coverage:

UniProtID	Gene Name	Protein Name	#Peptides (1)	#Peptides (2)	#Peptides (3)	Average of Sequence Coverage (%)
<b><u>Q9H694</u></b>	<b><u>BICC1</u></b>	<b><u>Protein bicaudal C homolog 1</u></b>	<b><u>41</u></b>	<b><u>37</u></b>	<b><u>40</u></b>	<b><u>42</u></b>
O14744	PRMT5	Protein arginine N-methyltransferase 5	15	10	14	24
Q9Y3F4	STRAP	Serine-threonine kinase receptor-associated protein	3	3	4	12
O75534	CSDE1	Cold shock domain-containing protein E1	6	3	6	6
Q9BQA1	WDR77	Methylosome protein 50	7	5	6	23
P25789	PSMA4	Proteasome subunit alpha type-4	5	5	5	18
C9JIR6	PPM1B	Protein-serine/threonine phosphatase (Fragment)	9	6	9	29
P27824	CANX	Calnexin	2	0	2	6
E7ENZ3	CCT5	T-complex protein 1 subunit epsilon	5	2	5	7
P27348	YWHAQ	14-3-3 protein theta	3	2	2	15
P63104	YWHAZ	14-3-3 protein zeta/delta	2	2	2	10
Q15208	STK38	Serine/threonine-protein kinase 38	8	3	5	12
E7EX17	EIF4B	Eukaryotic translation initiation factor 4B	5	3	3	8
P40227	CCT6A	T-complex protein 1 subunit zeta	2	1	5	5
P98175	RBM10	RNA-binding protein 10	6	2	6	7
Q15750	TAB1	TGF-beta-activated kinase 1 and MAP3K7-binding protein 1	3	1	4	5
P26641	EEF1G	Elongation factor 1-gamma	3	0	2	0
P55072	VCP	Transitional endoplasmic reticulum ATPase	4	1	2	0
Q99832	CCT7	T-complex protein 1 subunit eta	4	1	5	6
A0A0G2JLI4	DDX5	Probable ATP-dependent RNA helicase DDX5	4	1	2	0
F8W6I7	HNRNPA1	Heterogeneous nuclear ribonucleoprotein A1	3	3	3	2
P25705	ATP5A1	ATP synthase subunit alpha, mitochondrial	4	2	4	3
Q9NXV2	KCTD5	BTB/POZ domain-containing protein KCTD5	2	2	2	2
Q9Y237	PIN4	Peptidyl-prolyl cis-trans isomerase NIMA-interacting 4	2	2	2	10
P14678	SNRPB	Small nuclear ribonucleoprotein-associated proteins B and B	2	2	2	0
P30041	PRDX6	Peroxiredoxin-6	3	3	3	5
P50991	CCT4	T-complex protein 1 subunit delta	3	2	1	8
B1AMW7	CDC7	Cell division cycle 7-related protein kinase (Fragment)	2	0	2	0
C9JXB8	RPL24	60S ribosomal protein L24	1	2	2	0



E7ETK5	IMPDH2	Inosine-5-monophosphate dehydrogenase	2	0	2	0
E9PJD9	RPL27A	60S ribosomal protein L27a	2	2	2	2
J3KQN4	RPL36A	60S ribosomal protein L36a	3	2	0	2
P38159	RBMX	RNA-binding motif protein, X chromosome	3	1	4	0
X6R700	CHTOP	Chromatin target of PRMT1 protein	1	3	2	0

## ATTACHMENT 4

List of 51 proteins found in the BICC1 deletion of SAM domain ( $\Delta$ SAM) immunoprecipitation assays (in triplicates) in the presence of RNA (-), sorted by their number of unique peptides and average of sequence coverage:

UniProtID	Gene Name	Protein Name	#Peptides (1)	#Peptides (2)	#Peptides (3)	Average of Sequence Coverage (%)
<b><u>Q9H694</u></b>	<b><u>BICC1</u></b>	<b><u>Protein bicaudal C homolog 1</u></b>	<b><u>41</u></b>	<b><u>39</u></b>	<b><u>39</u></b>	<b><u>44</u></b>
O14744	PRMT5	Protein arginine N-methyltransferase 5	20	16	24	45
Q9Y3F4	STRAP	Serine-threonine kinase receptor-associated protein	13	14	12	48
O75534	CSDE1	Cold shock domain-containing protein E1	26	25	24	30
Q9BQA1	WDR77	Methylosome protein 50	8	10	11	39
P25789	PSMA4	Proteasome subunit alpha type-4	4	8	7	31
C9JIR6	PPM1B	Protein-serine/threonine phosphatase (Fragment)	11	11	8	39
P27824	CANX	Calnexin	3	1	2	15
E7ENZ3	CCT5	T-complex protein 1 subunit epsilon	4	5	4	11
P27348	YWHAQ	14-3-3 protein theta	7	8	8	10
P63104	YWHAZ	14-3-3 protein zeta/delta	5	4	5	23
Q15208	STK38	Serine/threonine-protein kinase 38	9	7	7	19
A0A0J9YYL3	PUF60	Poly(U)-binding-splicing factor PUF60 (Fragment)	3	5	6	11
A0A7I2V4N2	NONO	Non-POU domain-containing octamer-binding protein	1	3	3	6
E7EX17	EIF4B	Eukaryotic translation initiation factor 4B	4	5	3	10
P40227	CCT6A	T-complex protein 1 subunit zeta	4	2	6	9
P62258	YWHAE	14-3-3 protein epsilon	7	3	4	21
P62280	RPS11	40S ribosomal protein S11	4	3	5	20
P98175	RBM10	RNA-binding protein 10	2	4	6	7
Q15750	TAB1	TGF-beta-activated kinase 1 and MAP3K7-binding protein 1	3	2	4	6
Q9Y295	DRG1	Developmentally-regulated GTP-binding protein 1	0	4	4	9
A0A8I5KWT8	MYH9	Myosin-9	14	26	0	19
K7E1Y1	FAM32A	Protein FAM32A	2	2	3	4
P23246	SFPQ	Splicing factor, proline- and glutamine-rich	2	2	4	14
P26368	U2AF2	Splicing factor U2AF 65 kDa subunit	0	2	3	34
P26641	EEF1G	Elongation factor 1-gamma	3	2	4	27
P42677	RPS27	40S ribosomal protein S27	3	3	2	8
P55072	VCP	Transitional endoplasmic reticulum ATPase	0	3	2	39
Q04917	YWHAH	14-3-3 protein eta	2	1	3	20

*Characterizing the Interactome of the RNA-binding Protein BICC1*

A0A0G2JLI4	DDX5	Probable ATP-dependent RNA helicase DDX5	2	4	4	3
A0A2R8YCW1	DDX3X	RNA helicase	1	2	3	6
F8W6I7	HNRNPA1	Heterogeneous nuclear ribonucleoprotein A1	2	1	2	6
H0YGW7	ABCF1	ATP-binding cassette sub-family F member 1 (Fragment)	1	2	3	0
O60825	PFKFB2	6-phosphofructo-2-kinase)/fructose-2,6-bisphosphatase 2	2	3	2	4
P25705	ATP5A1	ATP synthase subunit alpha, mitochondrial	5	1	3	5
P31946	YWHAB	14-3-3 protein beta/alpha	2	2	2	10
Q9NXV2	KCTD5	BTB/POZ domain-containing protein KCTD5	3	6	3	3
Q9Y237	PIN4	Peptidyl-prolyl cis-trans isomerase NIMA-interacting 4	1	2	2	26
A0A7I2V3E1	PARP1	Poly [ADP-ribose] polymerase	2	4	1	4
D6RF44	HNRNPD	Heterogeneous nuclear ribonucleoprotein D0 (Fragment)	2	2	1	1
E7EQV3	PABPC1	Polyadenylate-binding protein	3	3	1	0
F8VPF3	MYL6	Myosin light polypeptide 6 (Fragment)	4	4	0	22
J3QRS3	MYL12A	Myosin regulatory light chain 12A	3	5	0	23
O43809	NUDT21	Cleavage and polyadenylation specificity factor subunit 5	3	3	3	1
P25398	RPS12	40S ribosomal protein S12	3	3	3	0
P78371	CCT2	T-complex protein 1 subunit beta	3	2	4	3
Q07666	KHDRBS1	KH domain-containing, RNA-binding, signal transduction-associated protein 1	1	2	2	17
E7ETK5	IMPDH2	Inosine-5-monophosphate dehydrogenase	1	2	2	0
G5E972	TMPO	Lamina-associated polypeptide 2, isoforms beta/gamma	2	1	2	0
P35580	MYH10	Myosin-10	4	8	0	2
Q7Z406	MYH14	Myosin-14	3	3	0	0
Q9NZI8	IGF2BP1	Insulin-like growth factor 2 mRNA-binding protein 1	2	1	2	0

## ATTACHMENT 5

List of 32 proteins found in the BICC1 deletion of SAM domain  $\Delta$ SAM immunoprecipitation assays (in triplicates) in the absence of RNA (+), sorted by their number of unique peptides and average of sequence coverage:

UniProtID	Gene Name	Protein Name	#Peptides (1)	#Peptides (2)	#Peptides (3)	Average of Sequence Coverage (%)
<b><u>Q9H694</u></b>	<b><u>BICC1</u></b>	<b><u>Protein bicaudal C homolog 1</u></b>	<b><u>37</u></b>	<b><u>41</u></b>	<b><u>41</u></b>	<b><u>44</u></b>
O14744	PRMT5	Protein arginine N-methyltransferase 5	16	16	19	38
Q9Y3F4	STRAP	Serine-threonine kinase receptor-associated protein	9	12	10	39
O75534	CSDE1	Cold shock domain-containing protein E1	14	12	15	18
Q9BQA1	WDR77	Methylosome protein 50	7	7	6	25
P25789	PSMA4	Proteasome subunit alpha type-4	6	7	7	31
C9JIR6	PPM1B	protein-serine/threonine phosphatase (Fragment)	9	9	8	32
P27824	CANX	Calnexin	2	1	3	8
E7ENZ3	CCT5	T-complex protein 1 subunit epsilon	5	1	3	13
P27348	YWHAQ	14-3-3 protein theta	2	4	5	13
P63104	YWHAZ	14-3-3 protein zeta/delta	2	3	2	11
Q15208	STK38	Serine/threonine-protein kinase 38	4	6	6	13
E7EX17	EIF4B	Eukaryotic translation initiation factor 4B	4	5	4	10
P40227	CCT6A	T-complex protein 1 subunit zeta	3	2	4	7
P98175	RBM10	RNA-binding protein 10	4	8	5	9
Q15750	TAB1	TGF-beta-activated kinase 1 and MAP3K7-binding protein 1	3	2	3	5
P26641	EEF1G	Elongation factor 1-gamma	3	2	4	0
A6NMY6	ANXA2	Putative annexin A2-like protein	3	2	0	12
F8W6I7	HNRNPA1	Heterogeneous nuclear ribonucleoprotein A1	3	3	3	2
P25705	ATP5A1	ATP synthase subunit alpha, mitochondrial	4	1	3	3
Q9NXV2	KCTD5	BTB/POZ domain-containing protein KCTD5	3	2	3	3
A0A7I2V5J8	NPM1	Nucleophosmin	2	3	2	10
P14678	SNRPB	Small nuclear ribonucleoprotein-associated proteins B and B	2	3	3	0
P25398	RPS12	40S ribosomal protein S12	2	1	2	0
P30041	PRDX6	Peroxiredoxin-6	1	3	2	3
P50991	CCT4	T-complex protein 1 subunit delta	5	2	1	15
P78371	CCT2	T-complex protein 1 subunit beta	5	2	2	0
A0A499FJE1	BOLA2B	BolA-like protein 2	3	2	2	0
E9PJD9	RPL27A	60S ribosomal protein L27a	2	1	2	0
J3KQN4	RPL36A	60S ribosomal protein L36a	3	0	2	5

P38159	RBMX	RNA-binding motif protein, X chromosome	3	2	4	0
P49368	CCT3	T-complex protein 1 subunit gamma	4	0	2	3
Q9NX58	LYAR	Cell growth-regulating nucleolar protein	2	0	2	0

## ATTACHMENT 6

List of 63 proteins found in the control green fluorescent protein (GFP) immunoprecipitation assays (in triplicates) in the presence of RNA (-), sorted by their number of unique peptides and average of sequence coverage:

UniProtID	Gene Name	Protein Name	#Peptides (1)	#Peptides (2)	#Peptides (3)	Average of Sequence Coverage (%)
A0A8I5KVB5	GTF2I	General transcription factor II-I	19	18	15	18
A0A0G2JIW1	HSPA1A	Heat shock 70 kDa protein 1B	17	20	20	35
P11021	HSPA5	Endoplasmic reticulum chaperone BiP	16	13	12	26
P11142	HSPA8	Heat shock cognate 71 kDa protein	15	16	17	28
P68371	TUBB4B	Tubulin beta-4B chain	12	12	12	37
A0A7I2V659	EEF1A1	Elongation factor 1-alpha	11	11	10	34
P07437	TUBB	Tubulin beta chain	10	11	12	34
A0A7I2V2G2	HSPA9	Stress-70 protein, mitochondrial	9	7	11	20
P05141	SLC25A5	ADP/ATP translocase 2	8	7	7	25
P17066	HSPA6	Heat shock 70 kDa protein 6	8	8	8	13
P62249	RPS16	40S ribosomal protein S16	8	5	6	45
P12236	SLC25A6	ADP/ATP translocase 3	8	6	6	3
P04259	KRT6B	Keratin, type II cytoskeletal 6B	7	11	9	13
P62269	RPS18	40S ribosomal protein S18	7	8	10	44
P23396	RPS3	40S ribosomal protein S3	7	9	8	36
P68363	TUBA1B	Tubulin alpha-1B chain	6	9	13	28
Q06830	PRDX1	Peroxiredoxin-1	6	4	6	30
P62263	RPS14	40S ribosomal protein S14	6	6	6	15
P62829	RPL23	60S ribosomal protein L23	6	5	5	49
A0A7P0Z497	PPIB	Peptidyl-prolyl cis-trans isomerase	5	9	8	37
P39019	RPS19	40S ribosomal protein S19	5	6	5	29
P46783	RPS10	40S ribosomal protein S10	5	5	5	33
P63173	RPL38	60S ribosomal protein L38	5	5	5	50
P62851	RPS25	40S ribosomal protein S25	5	5	5	30
P61978	HNRNPK	Heterogeneous nuclear ribonucleoprotein K	4	3	5	11
Q8NC51	SERBP1	Plasminogen activator inhibitor 1 RNA-binding protein	4	5	6	16
P62081	RPS7	40S ribosomal protein S7	4	2	2	20
Q14331	FRG1	Protein FRG1	4	3	5	19
A2NJV5	IGKV2-29	Immunoglobulin kappa variable 2-29	4	3	4	0
P47813	EIF1AX	Eukaryotic translation initiation factor 1A, X-chromosomal	4	4	4	8
P62318	SNRPD3	Small nuclear ribonucleoprotein Sm D3	4	4	4	0
Q86V81	ALYREF	THO complex subunit 4	4	2	3	15

P60866	RPS20	40S ribosomal protein S20	4	3	3	26
Q14011	CIRBP	Cold-inducible RNA-binding protein	4	4	4	0
P35637	FUS	RNA-binding protein FUS	3	3	3	5
A0A0A0MR02	VDAC2	Voltage-dependent anion-selective channel protein 2 (Fragment)	3	1	2	13
H3BNC9	RS17	40S ribosomal protein S17	3	4	3	9
P19474	TRIM21	E3 ubiquitin-protein ligase TRIM21	3	3	3	7
P62273	RPS29	40S ribosomal protein S29	3	3	3	1
P62701	RPS4X	40S ribosomal protein S4, X isoform	3	3	5	48
C9JYQ9	RPL22L1	60S ribosomal protein L22-like 1	3	3	2	0
P07900	HSP90AA1	Heat shock protein HSP 90-alpha	2	2	3	3
F6VRR5	POLDIP3	Polymerase delta-interacting protein 3	2	3	3	1
P48047	ATP5PO	ATP synthase subunit O, mitochondrial	2	3	2	5
Q9Y383	LUC7L2	Putative RNA-binding protein Luc7-like 2	2	2	5	10
A0A075B6R9	IGKV2D-24	Probable non-functional immunoglobulin kappa variable 2D-24	2	2	3	13
P36542	ATP5C1	ATP synthase subunit gamma, mitochondrial	2	1	4	4
Q5T7C4	HMGB1	High mobility group protein B1	2	2	3	5
Q96CT7	CCDC124	Coiled-coil domain-containing protein 124	2	1	5	13
B0QYK0	EWSR1	RNA-binding protein EWS	2	2	1	3
P35268	RPL22	60S ribosomal protein L22	2	3	2	1
P62913	RPL11	60S ribosomal protein L11	2	2	2	0
P62979	RPS27A	Ubiquitin-40S ribosomal protein S27a	2	2	2	13
P32119	PRDX2	Peroxiredoxin-2	2	1	2	0
Q07021	C1QBP	Complement component 1 Q subcomponent-binding protein, mitochondrial	2	2	1	0
P08238	HSP90AB1	Heat shock protein HSP 90-beta	1	2	3	3
A0A7I2V599	HSPD1	60 kDa heat shock protein, mitochondrial	1	2	3	38
Q96AG4	LRRC59	Leucine-rich repeat-containing protein 59	1	2	3	8
P49411	TUFM	Elongation factor Tu, mitochondrial	1	2	2	14
Q14498	RBM39	RNA-binding protein 39	1	4	2	1
B5MDF5	RAN	GTP-binding nuclear protein Ran	1	2	3	11
P98179	RBM3	RNA-binding protein 3	1	2	2	0
P12273	PIP	Prolactin-inducible protein	1	2	2	0

## ATTACHMENT 7

List of 74 proteins found in the control green fluorescent protein (GFP) immunoprecipitation assays (in triplicates) in the absence of RNA (+), sorted by their number of unique peptides and average of sequence coverage:

UniProtID	Gene Name	Protein Name	#Peptides (1)	#Peptides (2)	#Peptides (3)	Average of Sequence Coverage (%)
P62701	RPS4X	40S ribosomal protein S4, X isoform	15	13	13	32
H7BY10	RPL23A	60S ribosomal protein L23a (Fragment)	12	10	11	5
P68371	TUBB4B	Tubulin beta-4B chain	9	8	13	28
A0A7I2V659	EEF1A1	Elongation factor 1-alpha	9	8	7	25
P11021	HSPA5	Endoplasmic reticulum chaperone BiP	8	12	13	21
P07437	TUBB	Tubulin beta chain	8	7	13	26
A0A7I2V2G2	HSPA9	Stress-70 protein, mitochondrial	8	10	10	20
P68363	TUBA1B	Tubulin alpha-1B chain	8	8	7	22
P60709	ACTB	Actin, cytoplasmic I	7	5	6	20
P04259	KRT6B	Keratin, type II cytoskeletal 6B	7	10	8	14
Q06830	PRDX1	Peroxiredoxin-1	7	6	6	35
P39019	RPS19	40S ribosomal protein S19	7	6	5	31
P61247	RPS3A	40S ribosomal protein S3a	7	7	5	0
A0A1W2PPS1	HNRNPU	Heterogeneous nuclear ribonucleoprotein U	6	8	10	12
P62277	RPS13	40S ribosomal protein S13	6	5	5	13
A0A0G2JIW1	HSPA1A	Heat shock 70 kDa protein 1B	5	9	10	16
P62851	RPS25	40S ribosomal protein S25	5	4	3	23
Q86V81	ALYREF	THO complex subunit 4	5	5	5	26
P60866	RPS20	40S ribosomal protein S20	5	4	5	29
P30050	RPL12	60S ribosomal protein L12	5	4	4	0
P10412	H1-4	Histone H1.4	5	4	4	4
A0A8I5KVB5	GTF2I	General transcription factor II-I	4	7	9	8
P05141	SLC25A5	ADP/ATP translocase 2	4	5	3	14
P62269	RPS18	40S ribosomal protein S18	4	2	4	21
P62263	RPS14	40S ribosomal protein S14	4	3	2	3
P63173	RPL38	60S ribosomal protein L38	4	3	2	44
A2NJV5	IGKV2-29	Immunoglobulin kappa variable 2-29	4	3	4	0
H3BNC9	RS17	40S ribosomal protein S17	4	4	4	11
P62316	SNRPD2	Small nuclear ribonucleoprotein Sm D2	4	3	3	46
P62979	RPS27A	Ubiquitin-40S ribosomal protein S27a	4	4	3	3
P08238	HSP90AB1	Heat shock protein HSP 90-beta	4	3	3	5
F8VU65	RPLP0	60S acidic ribosomal protein P0 (Fragment)	4	2	3	0



P11142	HSPA8	Heat shock cognate 71 kDa protein	3	6	8	11
P17066	HSPA6	Heat shock 70 kDa protein 6	3	6	7	10
P12236	SLC25A6	ADP/ATP translocase 3	3	3	1	3
P23396	RPS3	40S ribosomal protein S3	3	6	2	15
P62829	RPL23	60S ribosomal protein L23	3	2	3	25
A0A7P0Z497	PPIB	Peptidyl-prolyl cis-trans isomerase	3	3	5	20
P46783	RPS10	40S ribosomal protein S10	3	5	2	25
P62318	SNRPD3	Small nuclear ribonucleoprotein Sm D3	3	3	3	28
P19474	TRIM21	E3 ubiquitin-protein ligase TRIM21	3	1	2	5
P62273	RPS29	40S ribosomal protein S29	3	3	3	0
A0A075B6R9	IGKV2D-24	Probable non-functional immunoglobulin kappa variable 2D-24	3	2	2	13
P62899	RPL31	60S ribosomal protein L31	3	5	7	28
B5MDF5	RAN	GTP-binding nuclear protein Ran	3	2	1	11
E9PR30	FAU	FAU ubiquitin-like and ribosomal protein S30	3	3	3	0
P12273	PIP	Prolactin-inducible protein	3	2	0	0
Q9BRT6	LLPH	Protein LLP homolog	3	2	2	0
P61978	HNRNPK	Heterogeneous nuclear ribonucleoprotein K	2	1	3	5
P62081	RPS7	40S ribosomal protein S7	2	3	4	25
I3L3P7	RPS15A	40S ribosomal protein S15a	2	2	2	0
P07900	HSP90AA1	Heat shock protein HSP 90-alpha	2	2	3	3
F6VRR5	POLDIP3	Polymerase delta-interacting protein 3	2	2	4	1
P35268	RPL22	60S ribosomal protein L22	2	3	2	0
P32119	PRDX2	Peroxisedoxin-2	2	1	2	4
P61204	ARF3	ADP-ribosylation factor 3	2	2	0	0
A0A7I2V599	HSPD1	60 kDa heat shock protein, mitochondrial	2	3	3	30
P84090	ERH	Enhancer of rudimentary homolog	2	3	3	33
A0A087X2D0	SRSF3	Serine/arginine-rich-splicing factor 3	2	3	3	0
P49411	TUFM	Elongation factor Tu, mitochondrial	2	1	2	0
P04908	H2AC8	Histone H2A type 1-B/E	2	2	2	0
D6RAN4	RPL9	60S ribosomal protein L9 (Fragment)	2	3	2	0
E5RIT6	RPL26L1	60S ribosomal protein L26-like 1 (Fragment)	2	0	2	0
E7ETK0	RPS24	40S ribosomal protein S24	2	2	2	1
P05109	S100A8	Protein S100-A8	2	2	0	11
P62266	RPS23	40S ribosomal protein S23	2	2	1	0
Q92522	H1-10	Histone H1.10	2	2	2	0
Q8NC51	SERBP1	Plasminogen activator inhibitor 1 RNA-binding protein	1	3	2	7
P47813	EIF1AX	Eukaryotic translation initiation factor 1A, X-chromosomal	1	3	3	1

Q14011	CIRBP	Cold-inducible RNA-binding protein	1	2	3	34
P31943	HNRNPH1	Heterogeneous nuclear ribonucleoprotein H	1	2	2	9
P42766	RPL35	60S ribosomal protein L35	1	2	2	0
P50990	CCT8	T-complex protein 1 subunit theta	0	2	2	3
A0A286YF22	PHGDH	D-3-phosphoglycerate dehydrogenase	0	2	2	0

## ATTACHMENT 8

Table of the respective Pearson's correlation obtained from each cell analyzed of immunofluorescence assays:

<b>BICC1 overexpression (Anti-Flag and anti-BICC1)</b>	Cell 1	0,702
	Cell 2	0,779
	Cell 3	0,773
	Cell 4	0,671
	Cell 5	1
	<b>Average</b>	<b>0,785</b>
<b>BICC1 overexpression (Anti-BICC1 and anti-PRMT5)</b>	Cell 1	0,461
	Cell 2	0,338
	Cell 3	0,64
	Cell 4	0,155
	Cell 5	0,416
	<b>Average</b>	<b>0,402</b>
<b>BICC1 overexpression (Anti-Flag and anti-PARP1)</b>	Cell 1	0,446
	Cell 2	-0,102
	Cell 3	-0,207
	Cell 4	-0,188
	Cell 5	-0,245
	<b>Average</b>	<b>-0,0592</b>

## ATTACHMENT 9

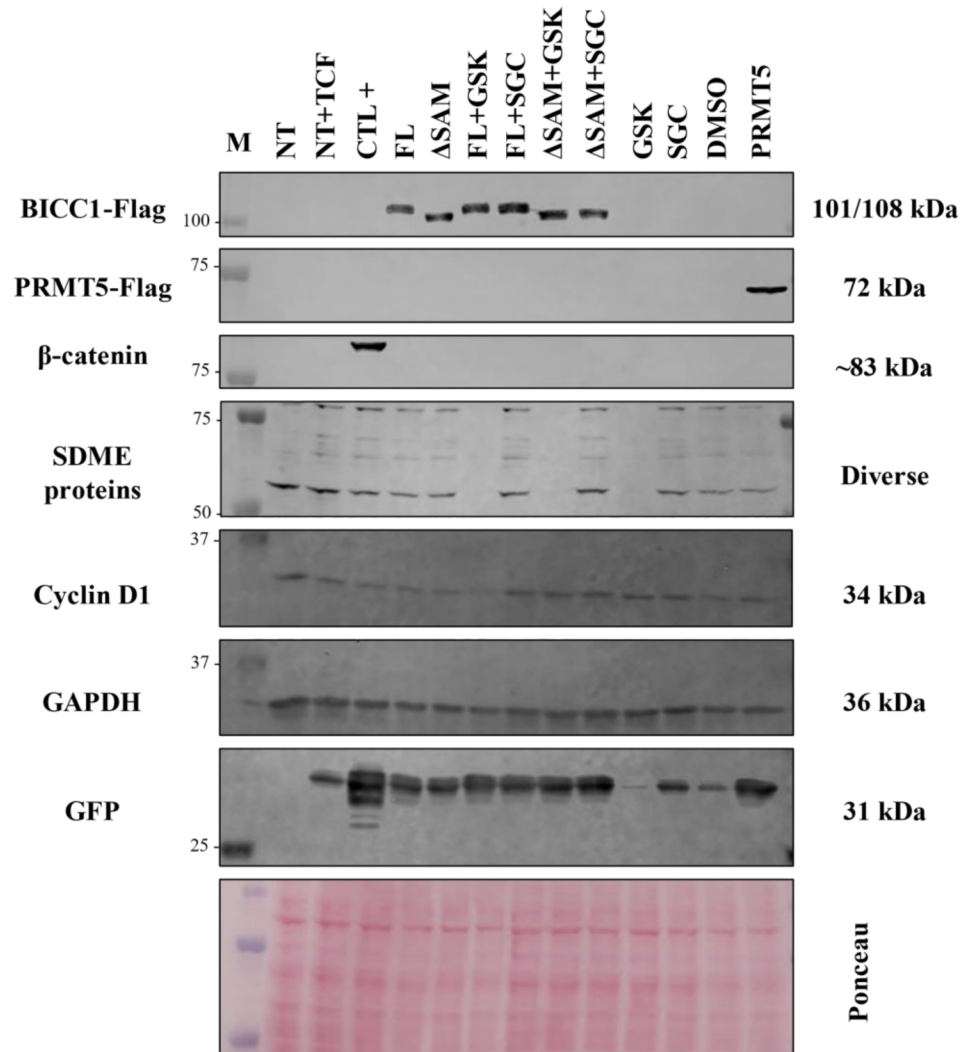
Post-translational modification of BICC1. Protein arginine methylation Predictor (PRmePRed) reveals potential methylation sites in R residues of BICC1:

SeqId	R site	Peptides	Prediction Score
sp Q9H694 BICC1_HUMAN	22	QSDPGSNSERSTDSPVPGS	0.921453
sp Q9H694 BICC1_HUMAN	50	LHSPFWSEERFRVDRKKLE	0.668266
sp Q9H694 BICC1_HUMAN	71	LQAAAEGKGRSGEDFFQKI	0.928475
sp Q9H694 BICC1_HUMAN	132	MSVLDTKSNRVTLKMDVSH	0.595454
sp Q9H694 BICC1_HUMAN	196	GQPAGVESARVIRELLPL	0.889252
sp Q9H694 BICC1_HUMAN	198	PAGVESARVIRELLPLVL	0.705324
sp Q9H694 BICC1_HUMAN	200	GVESARVIRELLPLVLMF	0.70388
sp Q9H694 BICC1_HUMAN	246	ISVSFKQRSRMYGATVIVR	0.542792
sp Q9H694 BICC1_HUMAN	255	RMYGATVIVRGSQNNTSAV	0.935395
sp Q9H694 BICC1_HUMAN	302	AQHHLFMMGRNGSNIKHIM	0.574023
sp Q9H694 BICC1_HUMAN	402	KSVIVKSVERNALNMYEAR	0.518931
sp Q9H694 BICC1_HUMAN	411	RNALNMYEARCKLLGLESS	0.558421
sp Q9H694 BICC1_HUMAN	632	DAFVEVGMPRSPSHSGNAG	0.922339
sp Q9H694 BICC1_HUMAN	657	CPSKVSACAKRQTVELLQGT	0.587174
sp Q9H694 BICC1_HUMAN	676	KNSHLHSTDRLSDPELSA	0.761591
sp Q9H694 BICC1_HUMAN	700	ADKKAPGSEAAERAAAAAQ	0.963761
sp Q9H694 BICC1_HUMAN	704	APGSEAAERAAAAAQNSE	0.821386
sp Q9H694 BICC1_HUMAN	714	AAAAQQNSERAHLAPRSSY	0.773881
sp Q9H694 BICC1_HUMAN	720	NSERAHLAPRSSYVNMQAF	0.724691
sp Q9H694 BICC1_HUMAN	752	LKKPVVTEVRTPTNTWSGL	0.73573
sp Q9H694 BICC1_HUMAN	800	YEGSSMSLSRSNSREHLGG	0.97676
sp Q9H694 BICC1_HUMAN	804	SMSLSRSNSREHLGGGSES	0.964192
sp Q9H694 BICC1_HUMAN	817	GGGSESDNWRDRNGIGPGS	0.79224
sp Q9H694 BICC1_HUMAN	819	GSESDNWRDRNGIGPGSHS	0.774481
sp Q9H694 BICC1_HUMAN	924	LGITTFGARRKMLLAISEL	0.622859
sp Q9H694 BICC1_HUMAN	947	RKLFESPNARTSFLEGGAS	0.858773
sp Q9H694 BICC1_HUMAN	958	SFLEGGASGRLPRQYHSDI	0.960709
sp Q9H694 BICC1_HUMAN	961	EGGASGRLPRQYHSDIASV	0.820884

**Highlighted residues** = conserved hallmark “GXXG” loop in KH domains of BICC1.

## ATTACHMENT 10

Investigation of Wnt  $\beta$ -catenin activity through reporter gene assay, modulating BICC1 expression and inhibiting PRMT5 activity. Replicate 2 of the Western blotting confirming the efficiency of GSK591 compounds for inhibition of SDMA modifications, BICC1 ectopic expression, GFP expression, and expression of Wnt gene targets (cyclin D1). The GAPDH housekeeping gene was used as endogenous control. Each well was loaded with 40  $\mu$ g of protein sample:



## ATTACHMENT 11

Statements regarding bioethics and/or biosafety:

DECLARAÇÃO CBMEG nº 31/2022



### DECLARAÇÃO

A Comissão Interna de Biossegurança (CIBio) do Centro de Biologia Molecular e Engenharia Genética da Unicamp, declara que o projeto "Superexpressão e imunoprecipitação de complexos de ligação a RNA em cultura de células HEK293 e posterior validação em células tronco embrionárias", sob responsabilidade da Dra. Katlin Brauer Massirer, foi aprovado em janeiro de 2013, sob o número CIBio 01/2013.

Ademais, a CIBio-CBMEG declara que a aluna de mestrado Heloisa Monteiro do Amaral Prado foi incluída neste projeto por meio do relatório anual de 2021.

Campinas, 21 de novembro de 2022.

Profa. Dra. Edi Lúcia Sartorato  
Membro Titular da Comissão de Biossegurança  
CBMEG - UNICAMP

UNIVERSIDADE ESTADUAL DE CAMPINAS - CENTRO DE BIOLOGIA MOLECULAR E ENGENHARIA GENÉTICA  
CIDADE UNIVERSITÁRIA "ZEFERINO VAZ" - BARÃO GERALDO - CEP 13083-875 - CAMPINAS - SP - BRASIL  
FONE: (19) 3521-1134, 3521-1130 ou 3521-1131

Documento assinado. Verificar autenticidade em [sigad.unicamp.br/verifica](https://sigad.unicamp.br/verifica)  
Informar código 0A048C5B 0C3B4623 B5757BCA F7ED75F4

---

Documento assinado eletronicamente por **Edi Lúcia Sartorato**, **MEMBRO DA CIBIO/CBMEG**, em 22/11/2022, às 09:31 horas, conforme Art. 10 § 2º da MP 2.200/2001 e Art. 1º da Resolução GR 54/2017.

---



A autenticidade do documento pode ser conferida no site:  
[sigad.unicamp.br/verifica](http://sigad.unicamp.br/verifica), informando o código verificador:  
**0A048C5B 0C3B4623 B5757BCA F7ED75F4**




## ATTACHMENT 12

Statement regarding copyright:

### Declaração

As cópias de artigos de minha autoria ou de minha co-autoria, já publicados ou submetidos para publicação em revistas científicas ou anais de congressos sujeitos a arbitragem, que constam da minha Dissertação/Tese de Mestrado/Doutorado, intitulada **CARACTERIZAÇÃO DO INTERACTOMA DA PROTEÍNA DE LIGAÇÃO A RNA BICC1**, não infringem os dispositivos da Lei n.º 9.610/98, nem o direito autoral de qualquer editora.

Campinas, 01 de dezembro de 2023

 Documento assinado digitalmente  
HELOISA MONTEIRO DO AMARAL PRADO  
Data: 01/12/2023 10:35:58-0300  
Verifique em <https://validar.it.gov.br>

Assinatura : \_\_\_\_\_

Nome do(a) autor(a): **Heloisa Monteiro do Amaral Prado**

RG n.º 39.755.323-7

KATLIN BRAUER

Assinatura : **MASSIRER:64925323091**

Nome do(a) orientador(a):

RG n.º

Digitally signed by KATLIN BRAUER  
MASSIRER:64925323091  
Date: 2023.12.07 21:43:10 -03'00'